THE EFFECT OF ELEVATED TEMPERATURE ON THE FRETTING FATIGUE BEHAVIOR OF NICKEL ALLOY IN-100

THESIS

John F. Ownby, Captain, USAF

AFIT/GA/ENY/08-M04

DEPARTMENT OF THE AIR FORCE
AIR UNIVERSITY

AIR FORCE INSTITUTE OF TECHNOLOGY

Wright-Patterson Air Force Base, Ohio

The views expressed in this thesis are those of the author and do not reflect the official policy or position of the United States Air Force, Department of Defense, or the United States Government.

AFIT/GA/ENY/08-M04

The Effect of Elevated Temperature on Fretting Fatigue Behavior of Nickel Alloy IN-100

Thesis

Presented to the Faculty

Department of Aeronautics and Astronautics

Graduate School of Engineering and Management

Air Force Institute of Technology

Air University

Air Education and Training Command

In Partial Fulfillment of the Requirements for the

Degree of Master of Science in Astronautical Engineering

John Ownby AFIT, BS

Captain, USAF

April 2008

AFIT/GA/ENY/08-M04

The Effect of Elevated Temperature on Fretting Fatigue Behavior of Nickel Alloy IN-100

John Ownby AFIT, BS

Captain, USAF

Approved: Date:

Shankar Mall — 4/18/08

Dr. Shankar Mall (Chairman)

Som Soni — 4/18/08

Dr. Som Soni (Member)

Vinod K Jain — 4/18/08

Dr. Vinod K. Jain (Member)

Abstract

This thesis studied the effect of elevated temperature (600 C) on the fretting fatigue behavior of IN-100. First, fretting and plain fatigue S-N curves were determined over a large range of applied stress at an identical stress ratio of 0.03 at 600 C and for fretting tests, with a constant contact load. The partial slip condition was verified by using hysteresis between shear force and axial stress techniques. The contact width and the crack initiation location were observed for all of the fretting specimens. The contact widths were consistent with expected values and the crack initiation location was at the trailing edge of contact for all fretting specimens. This study compared its high temperature results to room temperature testing accomplished by this study as well as room temperature data from a previous study using IN-100 with an identical microstructure and another room temperature study of IN-100 with a coarser microstructure. It was found that fretting fatigue reduces the cycles to failure compared to plain fatigue at elevated temperature but a more pronounced reduction was noticed than with room temperature. It was also found that the elevated temperature environment increased the both the plain and fretting fatigue life as compared to similar stress levels at room temperature. The study found that elevated temperature does have an effect on crack initiation and crack propagation as compared to room temperature environment. The higher temperature allowed a longer initiation and crack propagation time which strongly suggests the fatigue life increases with temperature up to 600C. The creation of oxide films and temperature induced softening or plasticity were both found to act as crack closure mechanisms in another nickel based superalloy, IN-718, when fatigued in the high temperature environment. It is therefore likely that these oxidation and plasticity crack closure mechanisms are the reasons for the improved performance at elevated temperatures. These findings were different than in titanium alloys, where elevated temperatures allowed a shorter crack initiation time by greater stress relaxation thus hastening crack development.

Acknowledgements

I would like to thank my thesis advisor, Dr. Mall for his patience and guidance in completing this thesis. I would like to thank both of my parents and my sisters for believing in me and supporting my efforts to see my master's degree through to the end. I would also like to thank Dr. Kim for his assistance with the microscopy of my specimens. I would especially like to thank Barry Page for his immeasurable help in the laboratory and with the numerous modifications to the testing machine without which this study certainly would not have been possible. Finally, I would like to thank the Air Force for extending me the opportunity to attend AFIT.

John Ownby, Capt, USAF

Table of Contents

List of Figures

List of Tables

List of Symbols

a	Half contact width
b	Specimen half thickness
c	Stick zone boundary
d	Tensile bar thickness
E	Modulus of elasticity
f	Coefficient of friction
K_1	First Ruiz parameter
K_2	Second Ruiz parameter
N	Number of cycles
N_f	Number of cycles to failure
P	Normal load
p_o	Maximum pressure in the contact zone
Q	Shear load
Q_{max}	Maximum shear load
Q_{min}	Minimum shear load
r	Radius of curvature
R	Stress ratio
σ	Stress
δ	Slip at interface
σ_{axial}	Axial stress applied to tensile bar
σ_{max}	Maximum applied axial stress
σ_{min}	Minimum applied axial stress

σ_{xx}	Axial stress in the contact zone
σ_{yy}	Transverse stress in the contact zone
$\Delta\sigma$	Stress range
τ	Surface shear stress
$\tau_{\max}$	Maximum shear
$\tau_{\min}$	Minimum shear
τ_{xy}	Shear stress in contact zone
$\Delta\tau$	Shear stress range
$\Delta\tau_{crit}$	Shear range in the critical range
υ	Possion's ratio

I. Introduction

1.1 Fretting Fatigue

Fretting is the physical phenomenon in which two surfaces in contact with one another, though not rigidly attached, rub against one another to the point that material is damaged. Although these surfaces are not rigidly attached they are also not free to move large distances as they are constrained to remain in constant contact. It is this condition that allows for a tiny amount of lateral movement between these two surfaces. This motion is of a very small magnitude, usually between 5 and 50 microns, and is referred to as micro slip [1] indicating that the two surfaces are in fact slipping but the displacements are microscopic as they are prevented from slipping further by the surrounding environment. This condition of micro slip and therefore fretting is localized to where these two surfaces are in contact and subject to elevated stress conditions.

Fretting begins when this micro slip begins to damage the outermost region of the two surfaces. It is this fretting damage that creates a stress concentration factor on the affected surface near the edge of the fretting zone. This fretting induced stress concentration factor in turn yields crack initiation originating somewhere near the edge of the fretting region which then may propagate through the material in four distinct stages. The first stage is that of crack initiation (also known as nucleation) which occurs relatively soon after the fretting condition is established. The second stage is the crack propagation due to the combination of the bulk and contact stresses. The third stage is crack propagation due to just the bulk stress. The fourth and final stage is fracture which occurs when either the crack propagates all the way to the edge of the affected part or when the critical stress intensity factor, K_{Ic}, is reached. When the stress conditions are high enough to permit these cracks to propagate beyond the initial stage of crack

formation, the conditions then constitute fretting fatigue as the cracks will hasten the destruction of the material. These types of conditions of micro slip and high stress loads are commonly found in mechanical joints such as surfaces near bolt and rivet connections and in geometrically locking joints such as dove tail connections found in modern turbine engines.

In the case of dovetail connections found in modern turbine engines the surface to surface interface is found between the numerous individual turbine blades and the collar that is mounted around the rotor that constitutes the centerline of the entire engine (Figure 1.1). These connections, blade and collar shapes and materials have all been optimized for various engineering and operational concerns. Due to the intricate way in which modern engines are assembled it is extremely difficult and time consuming to routinely inspect and repair or replace broken components. As such it is highly desirable to design components that are more resistant to fretting damage and thus could serve for longer periods of time between inspections. To accomplish this objective the fundamentals of the fretting phenomenon need to be better understood and, to the extent possible, predicted before an engine is ever put into service. This study will attempt to further the fundamental knowledge of the fretting fatigue phenomenon so that future efforts may employ this knowledge to improve the design and maintenance schedules of modern turbine engines.

1.2 Relevance of Nickel Alloys

As mentioned above the one common application for knowledge of the fretting phenomenon is turbine engines. The turbine blade and collar interface depicted (Figure 1.2) is located well within the hot zone of a turbine engine. The temperatures in this

portion of the engine vary greatly depending on location but all areas are routinely exposed to temperatures greatly in excess of room temperature. To accommodate this extreme temperature environment many materials and high temperature alloys have been developed. While Nickel has been a common constituent used in a variety of alloys it can also be used to constitute the majority of an alloy. These alloys containing a majority of nickel have been observed to provide a great deal of strength at elevated temperatures while also demonstrating relatively small thermal coefficients of expansion [2] and as such are ideally suited for the high temperature environment described [3].

Previous work on fretting fatigue has been done on a variety of materials such as titanium alloys, steel alloys and aluminum alloys [4]; [5]; [6]; [7]; [8]; [9]. Although some fretting analysis has been done of nickel based alloys, it has seldom been studied at temperatures higher than room temperature. It is important to study the fretting phenomenon in environments that more closely represent the applications where it is commonly found. For this reason this study has endeavored to study the fretting fatigue behavior and characteristics of a particular nickel super-alloy, IN-100, at a temperature of 600 ºC. This study will reference previous fretting research work done on this same alloy at room temperatures [10]; [11] for a basis of comparison.

1.3 Factors Affecting Fretting

There are many factors that affect fretting fatigue; far more than would be practical to list here, but the most important factors are: contact conditions such as contact loads and shapes, surface treatments such as shot peening, and the applied cyclic stress conditions [12]; [13]; [14]; [15]. Each of these factors influences the overall fretting fatigue crack initiation, crack propagation and ultimately fracture methodology of

the component. Previous studies done on IN-100 and other nickel based super alloys have examined the influence of contact geometry and the microstructure of the material grains each under a variety of loading conditions [11]; [10]; [16]; [17, 18]; [19]; [20]; [21]; [22]. Unfortunately, the majority of these studies did not take temperature in to account and the experiments that were conducted were often only done at room temperatures. As previously mentioned, the room temperature environment does not replicate the environment inside of a turbine engine. Considering how high temperature environments have been proven to alter the way in which materials fatigue [23]; [24], it seems that temperature is one of the factors that could affect the fretting fatigue of IN-100. This study will attempt to characterize the effect that elevated temperature, 600 ºC, has on fretting fatigue of IN-100. As many of the other factors known to affect fretting fatigue (i.e. contact geometry and loading conditions) will be similar to the previous fretting fatigue studies of IN-100 done by Madhi [11] and Saladin [10]. These previous studies, and the room temperature data they provided, will be the control set for a proper comparison of the different temperature conditions and subsequent effects on fretting fatigue.

1.4 Purpose and Objectives

The ultimate purpose of this study is to determine the extent to which elevated temperatures has an impact on fretting fatigue behavior of IN-100. To accomplish this several experiments will be conducted to establish the applied stress vs. number of cycles curve (S-N curve) for both fretting and plain fatigue. The plain fatigue data will be used to compare the extent to which the fretting fatigue conditions shortened the operational life of the specimens. Each specimen will be analyzed by optical and scanning electron

microscopy to determine crack initiation points, fretting contact area and the micro-slip regions and crack propagation regions and mechanisms. These observations will then be compared to fretting experiments done at room temperature to determine the likely causes for differences in fretting fatigue behavior.

1.5 Methodology

Recreating a comprehensive model of the exact turbine dovetail joint geometry, loading conditions and operational high temperature environment in the laboratory would be extraordinarily difficult and extremely cumbersome to operate consistently and successfully. Fortunately this is not necessary because the fretting phenomenon can be successfully modeled with a much simpler and experimentally convenient set up. The details of this set up will be discussed in detail in Chapter III but it is essentially a greatly simplified geometric contact surface model simulating a simple cylinder on flat surface. Fretting pads with a curved surface that imitates a cylinder are applied to both sides of a flat dog bone shaped specimen that is loaded with a known cyclic axial load. The pads are applied to the specimen with a known force and the contact area is predicted by way of a known Hertzian geometric condition. The axial loading of the specimen provides the frictional motion required to produce the fretting phenomenon. The testing environment is heated by four electric resistance heating elements configured near the contact region. The temperature of the contact region of the specimen and fretting pads is controlled by an elaborate thermocouple feedback design. Experimental data is gathered throughout the course of the experiment until the specimen finally fractures. This data is then analyzed and the results are presented in Chapter IV.

Figure 1.1 - Photograph of a typical dovetail joint [10]

Figure 1.2 - Photograph of turbine collar and turbine blade

II. Background

This chapter will expand on the details of fretting fatigue introduced in the previous chapter. First this chapter begins with an introduction to the fundamentals of contact mechanics as they apply to the fretting fatigue conditions utilized in this study's experiments followed by a brief discussion of the Ruiz analytical model. Next, the mechanisms of crack nucleation and crack growth are discussed in more detail followed by an explanation of both gross and partial slip. Then several parameters that have been developed to predict fretting fatigue life are introduced. Finally, this chapter ends with a brief survey of previous fretting fatigue studies that have been done on both titanium and nickel alloys at both room and elevated temperatures.

2.1 Contact Mechanics

This study utilizes a cylindrical on flat contact configuration. This configuration is derived from the classic Hertzian contact problem of contact between two infinite cylinders which has a well defined and exact solution. Figure 2.1 is a two dimensional depiction of this configuration, where σ_{axial} is the applied stress, P is the applied contact load, Q is the tangential load, A is the cross sectional area of the specimen, a is the contact half-width, b is the specimen's half thickness and r is the fretting pad radius. Hills and Nowell [25] and Fellows, Nowell and Hills [26] have studied this particular configuration in great detail and have provided a detailed analytical solution to this contact scenario. The analytical solution for this type of fretting condition comes from solving the displacements of the two contacting bodies. The following equation governs the contact region:

$$\frac{1}{A^*}\frac{\delta h(x)}{\delta x} = \frac{1}{\pi}\int \frac{p(\varsigma)}{x-\varsigma} d\varsigma - \beta q(x) \qquad (2.1)$$

where $h(x) = v_1(x) - v_2(x)$ represents the displacements in the y direction if the two surfaces could penetrate each other freely, p is the pressure in the contact zone and q is the surface shear stress. The two other parameters are defined as:

$$A^* = 2\left(\frac{1-\upsilon_1^2}{E_1} + \frac{1-\upsilon_2^2}{E_2}\right) \qquad (2.2)$$

$$\beta = \frac{1}{2A^*}\left(\frac{1-2\upsilon_1}{E_1} - \frac{1-2\upsilon_2}{E_2}\right) \qquad (2.3)$$

where E_i and υ_i are the modulus of elasticity and Poisson's ratio of the two contact bodies respectively. Similarly, if the tangential displacement is defined as $g(x) = u_1(x) - u_2(x)$, then the following equation complements equation 2.1.

$$\frac{1}{A^*}\frac{\delta g(x)}{\delta x} = \frac{1}{\pi}\int \frac{q(\varsigma)}{x-\varsigma} d\varsigma - \beta p(x) \qquad (2.4)$$

Note that if the two contact bodies have the same material properties, as is the case in this study, then $\upsilon_1 = \upsilon_2$ and $E_1 = E_2$; therefore equations 2.2 and 2.3 then reduce to:

$$A^* = 4\left(\frac{1-\upsilon_1^2}{E_1}\right) \qquad (2.2a)$$

$$\beta = 0 \qquad (2.3a)$$

which then further simplifies equations 2.1 and 2.4 such that the displacements in the stick zone will be exactly the same. Once the contact load, P, is applied the pressure distribution, p(x,y), in the stick zone can be represented by:

$$p(x) = p_o\sqrt{1-\left(\frac{x}{a}\right)^2} \qquad (2.5)$$

where p_o is the peak pressure which is given by either of the following equations:

$$p_o = \frac{2P}{\pi a} \tag{2.6}$$

$$p_o = \sqrt{\frac{PE}{2\pi(1-\upsilon^2)R}} \tag{2.7}$$

In equation 2.8, R is defined as:

$$R = \frac{\sigma_{\min}}{\sigma_{\max}} \tag{2.7a}$$

To calculate the half-width of the contact zone, a, the following equation is used:

$$P = \frac{(\pi k a^2)}{2A^*} \tag{2.8}$$

which, when rearranged, becomes:

$$a = \sqrt{\frac{2PA^*}{\pi k}} \tag{2.8a}$$

where the parameter k, the radius of curvature, is defined as:

$$k = \frac{1}{R_1} + \frac{1}{R_2} \tag{2.9}$$

where R_1 and R_2 are the radii of the fretting pad and the specimen, respectively. Note that the radius of the specimen is essentially infinite and so the second term reduces to zero.

Now the axial stress, σ_{xx}, can be defined in terms of x, a, and peak pressure, p_o:

$$\sigma_{xx} = -p_o\left(\frac{\sqrt{a^2 - x^2}}{a}\right) \tag{2.10}$$

The shear stress distribution along the contact surface can now be expressed in terms of x, a and Q:

$$q(x) = \frac{Q}{\pi\sqrt{a^2 - x^2}} \qquad (2.11)$$

The total shear stress along the contact length, Q, can be defined in terms of a, c, and p_o by integrating the shear stress distribution:

$$Q = \frac{fp_o\pi}{2a}\left(a^2 - c^2\right) \qquad (2.12)$$

Finally, the stick zone size, shown in terms of the fraction $\frac{c}{a}$, can be calculated in terms of Q and P and the coefficient of friction, f :

$$\frac{c}{a} = \sqrt{\left(1 - \left|\frac{Q}{fP}\right|\right)} \qquad (2.13)$$

2.2 Analytical Model

To compute the values of the variables such as the Hertzian Peak Pressure, p_o, in equation 2.6, the contact half-width, a, in Equation 2.8a, the axial stress, σ_{xx}, in equation 2.10, etc. Chan and Lee [27] wrote a FORTRAN program titled the "Ruiz Program" that can generate values of the stress state anywhere along the contact length. The solutions generated by the Ruiz program are valid for fretting conditions provided that the following condition is satisfied:

$$\frac{b}{a} \geq 10 \qquad (2.14)$$

If the ratio of specimen half thickness, b, to contact half width, a, is less than 10 the Ruiz program's values are no longer valid but may still be considered as approximations of the true values. In this scenario, as would be the case with this study, one should use Finite

Element Analysis (FEA) to model the contact problem and obtain stress, strain and displacement information from the FEA output.

The Ruiz program uses two parameters, K_1 and K_2, to predict the crack initiation location while the other predicts the crack opening and propagation behavior.

$$K_1 = (\sigma_T)_{\max}(\tau\delta)_{\max} \qquad (2.15)$$

$$K_2 = (\sigma_T \tau\delta)_{\max} \qquad (2.16)$$

K_1 uses the maximum surface tangential stress, $(\sigma_T)_{\max}$, and the maximum value of shear stress and interface slip, $(\tau\delta)_{\max}$, to predict the frictional work that nucleates the crack. K_2 combines the effects of surface tangential stress, σ_T, shear stress, τ, and the relative slip at the interface, δ, to predict crack opening and propagation. When these two parameters are combined they yield one criterion to describe both the crack's initiation and its growth characteristics.

2.3 Crack Nucleation and Growth

The first stage in fretting fatigue is the crack initiation or nucleation stage in which the very beginnings of the crack that will ultimately lead to the final fracture and failure of the specimen or component originate. This stage is not understood as well as the subsequent stages of crack propagation and fracture and yet it is known that the majority of fretting fatigue life is spent in this stage. It is therefore important to study crack initiation not only because it constitutes the majority of fretting fatigue life but also because it appears to be influenced by so many factors. The term initiation itself can be misleading if one takes its meaning to be a singular event. In fact, crack initiation is a process and not a discrete event. Under plain fatigue conditions cracks emerge from

inherent flaws such as voids or inclusions that exist naturally within the material or from other external flaws which become stress concentration factors. These nascent cracks are known to exist but can not be detected because they are too small. It is not until these cracks begin to grow that they even become observable. Under fretting fatigue conditions however cracks do not just originate from random internal flaws alone. They are created near the edges of the contact region by the local stresses and the microscopic conditions of the material. One of the more promising theories in explaining this stage is the Persistent Slip Band theory offered by Venkataraman et al. [28].

In the Persistent Slip Band model, slip planes develop from several adjacent dislocations which form slip planes. These slip planes are subjected to the repeated loading and unloading which causes them to pile up around obstacles such as inclusions and grain boundaries. Over time these slip bands lead to the creation of extrusions and intrusions of material. These extrusions are smeared by the slip from contacting surfaces. Eventually, after enough cycles it becomes energetically favorable to form embryonic cracks, about the size of one grain but potentially up to two or three grain sizes long. The model has even been developed enough to predict, in a general sense, how long initiation should take based on three main parameters: slip amplitude, slip band length and the contact width of the fretting surface. Once these embryonic cracks are established they can begin to propagate or grow until they are large enough to be modeled by other techniques.

Exactly how long or perhaps more appropriately how many cycles are required to transition from the crack initiation or nucleation stage and enter the crack propagation stages is a very difficult problem to address. Occasionally small cracks will develop and grow briefly before their growth is arrested by other effects. This has been observed in

large power generation turbines. Still other factors can exacerbate crack nucleation. Szolwinski and Farris [29] demonstrated that increases in the coefficient of friction and the surface micro slip drastically hasten crack nucleation. In a study by Fellows, Nowell and Hills [30] several experiments involving the frequency of the bulk stress and the frequency of the fretting stress were devised to isolate the effect that different loading conditions had on the initiation of fretting fatigue cracks. Unfortunately their findings were not as conclusive as they had hoped because it is not possible to create loading conditions that impact crack initiation and not propagation and vice versa. In other words, it is not always possible to draw a clear distinction between conditions that favor crack initiation from the beginnings of short crack growth.

Once these cracks are large enough they enter the domain of regular fracture mechanics and can be modeled by several more macroscopic methodologies. Crack tip stress intensity factors can be analyzed with linear elastic fracture mechanics, elastic-plastic fracture mechanics, crack tip opening displacement and J contour integrals just to list a few available techniques. Hattori [31] has made estimations of fretting fatigue strength based on the stress intensity factor at these crack tips. Multiaxial stress states from the bulk stress and the contact stresses will cause these small cracks to grow. In fact, once cracks are established they will grow at ever increasing rates until the critical stress intensity factor is reached and total fracture occurs.

2.4 Gross and Partial Slip

At the beginning of a fretting fatigue process the surfaces in contact will experience a certain amount of slippage. This slippage can be categorized in two different ways; gross slip or partial slip. The first type of slippage, gross slip, is

characterized as when the surfaces are undergoing relatively large displacements with respect to one another during each cycle. This gross slippage leads to the two surfaces wearing upon each other causing damage by an abrasive interaction. This damage process is known as fretting wear.

The second type of slippage is partial slip and it is the opposite of gross slip. Under partial slip conditions the two surfaces will begin to stick to one another and are only under going slip near the edges of the contact zone. There are no large relative displacements between the two contacting surfaces as the substrate and contacting surface are essentially being welded together. In this study the fretting pads and the tensile specimen are initially able to slip against one another freely. This initial gross slip persists until the pads and the specimen begin to stick together thus inhibiting large displacements. This region of the contact zone which is no longer moving with respect to both the pads and the specimen due to the surface welding is called the stick zone. The region immediately outside of the stick zone but still in the contact zone is called the slip zone (Figure 2.2). Under ideal fretting conditions the stick zone will form exactly in the center of the contact zone and the slip zone on each side will be symmetrical.

2.5 Predictive Fretting Fatigue Parameters

The ability to reliably predict in advance if a fretting fatigue crack will form as well as when and where it might develop would be a tremendous breakthrough in the field of fretting fatigue. If such cracks could be predicted early in the design phase of aircraft structures and engines then engineers could take these hazards into account when designing structures and components and in turn greatly reduce the chances of an unexpected and catastrophic failure. Even if fretting fatigue cracks could not be

eliminated, better predictions of fretting fatigue cracks would still afford maintainers and inspectors a much greater means by which to detect and repair or replace parts in time to prevent such catastrophes.

Ever since fretting fatigue was discovered researchers have been searching for better ways to analyze fretting fatigue data and develop better models for fretting fatigue cracks. Plain fatigue offers a wonderful starting point for developing fretting fatigue predictive models and parameters. Over time several methods and parameters have been developed and evaluated for their applicability in predicting plain fatigue life. Efforts are currently underway to modify these predictive capabilities and extend them into fretting fatigue conditions.

Some predictive methods that have been shown to be useful thus far are the Critical Plane parameter, the Smith-Watson-Topper (SWT) parameter and the Shear Stress Range (SSR) and Modified Sheer Stress Range (MSSR) parameters. While these parameters have been shown to be useful thus far in some materials, such as titanium alloys, very little work has been done to evaluate these parameters for suitability in nickel-based super alloys. The following sections will introduce three of these parameters: Critical Plane, Shear Stress Range and Modified Shear Stress Range.

2.5.1 Critical Plane

In fretting fatigue cracks initiate and grow in the contact region. In this region the state of stress is multi-axial in nature due to the combination of the bulk stress and the applied contact load. One of the predictive parameters is the notion of a critical plane. The critical plane is the plane where the maximum shear stress is located and this occurs at some angle between the contact line of the fretting pad and the specimen's surface. In

this plane it is theorized that the maximum normal stresses work to open the cracks and in do so reduce the friction between surfaces and the shear stresses induce dislocation movement along slip lines. The critical plane model seeks to find the maximum shear strain amplitude and the plane on which it acts. The normal stress associated with this plane is then used to determine the effect of mean stress. The shear and normal stress can be determined for any plane if the state of stress, $\sigma_{xx}, \sigma_{yy}, \tau_{xy}$, is known for that point. Shear stress can be found from:

$$\tau = -\frac{\sigma_{xx} + \sigma_{yy}}{2}\sin(2\theta) + \tau_{xy}\cos(2\theta) \qquad (2.17)$$

and the normal stress can be found from:

$$\sigma = \frac{\sigma_{xx} + \sigma_{yy}}{2} + \frac{\sigma_{xx} - \sigma_{yy}}{2}\cos(2\theta) + \tau_{xy}\cos(2\theta) \qquad (2.18)$$

These equations depend on θ which is evaluated from $-\frac{\pi}{2}$ to $+\frac{\pi}{2}$ (radians) in small intervals. It is very difficult to experimentally measure the state of stress in the fretting fatigue zone. Therefore analytical and finite element simulations are used to determine these values.

The critical plane model is popular among fretting fatigue researchers because of the multi-axial stress state in the contact region. Namjoshi et al. [7] studied the critical plane model and applied it to fretting fatigue tests of a common titanium alloy, Ti-6Al-4V. He demonstrated that the fretting fatigue crack initiation was a function of the shear stress on the critical plane and that the fretting fatigue life is influenced by the normal stress acting on the same plane. The critical plane parameter was able to predict the crack orientation and to a lesser degree of accuracy, the crack size.

2.5.2 Shear Stress Range

The stress range is influenced by mechanistic parameters such as peak contact pressure, local bulk stress, local shear stress, slip amplitude and contact half width. Iyer et al. [32] defined the shear stress range as follows:

$$\Delta\tau = \tau_{\max} - \tau_{\min} \tag{2.18}$$

where $\tau_{\max}$ and $\tau_{\min}$ are the shear values from the maximum and minimum axial loadings respectively. These values are determined from evaluating:

$$\tau\big|_{\theta} = -\frac{(\sigma_{xx} - \sigma_{yy})}{2}\sin(2\theta) + \tau\cos(2\theta) \tag{2.19}$$

for θ ranging from $-\frac{\pi}{2}$ to $+\frac{\pi}{2}$ (radians). However, this takes neither mean stress nor stress ratio into account which have been clearly shown to be relevant to fatigue life. To address this Walker [33] suggests an alternate method, seen below, which does take these factors into consideration.

$$SSR = \Delta\tau_{crit} = \tau_{\max}(1 - R_T)^m \tag{2.20}$$

In this equation m is a fitting parameter that is chosen to collapse plain fatigue initiation data at different strain ratios which Lykins [5, 34] has determined to be 0.45 and R_T is the stress ratio on the critical plane and is evaluated as:

$$R_T = \frac{\tau_{\min}}{\tau_{\max}} \tag{2.21}$$

Madhi [11] calculated the SSR parameter for IN-100 in his study and found that although it could predict crack location and orientation, it did not predict the fatigue life without dependence on pad geometry.

2.5.3 Modified Shear Stress Range

The MSSR parameter is considered by many fretting fatigue researchers to be the premier predictive parameter discovered thus far. As its name suggests it is a modification of the Shear Stress Range parameter that does takes into account the effects of maximum normal stress which generally acts to open the crack surface. MSSR is calculated by the following equation:

$$MSSR = A\Delta\tau_{crit}^{B} + C\sigma_{\max}^{D} \qquad (2.22)$$

where A, B, C and D are constants that vary according to material. Sabelkin et al [35] determined these to be equal to 0.75, 0.5, 0.75 and 0.5 respectively for Ti-6Al-4V. Just as with the SSR, the MSSR is calculated for all planes ranging from using the stress state data provided by an FEA model at every point along the contact length. The critical plane is the orientation where the MSSR value is greatest. Namjoshi [7] notes that MSSR shows little dependence on pad geometry. He attributes the accuracy of MSSR to the inclusion of both the shear and normal stress in its calculation. Madhi [11] analyzed the utility of the MSSR in his study of IN-100 and found that the best agreement came when he used values of 0.5, 0.25, 0.75 and 0.5 respectively for A, B, C and D. Overall, Madhi found that the MSSR parameter was the best predictive parameter for fretting fatigue in IN-100.

2.6 Previous Fretting Fatigue Studies

This section will attempt to briefly summarize some of the fretting fatigue work that has already been done. Extensive literature exists for fretting fatigue in titanium based alloys. Therefore summaries of fatigue and fretting fatigue are a good starting point for understanding what research has already been accomplished. First room

temperature titanium studies are presented followed by high temperature titanium work. Next, fatigue and fretting fatigue in nickel based alloys is discussed. The literature on nickel based alloys is not nearly as extensive as it is for titanium alloys. Nickel based alloys studied at room temperature are presented first followed by high temperature studies of nickel based alloys.

2.6.1 Room Temperature Studies on Titanium alloys

Namjoshi et al [7] investigated the fretting fatigue behavior of Ti-6Al-4V under different pad configurations. Five different pad geometries were used; three cylindrical pads with radii of 50.8 mm, 101.6 mm and 304.8 and two flat pad types with edge radii of 5.08 mm and 2.54 mm. This particular study was referenced earlier in sections 2.5.1 and 2.5.3 for its contributions to the Critical Plane parameter and the Modified Shear Stress Range parameter. The experimental results tended to show that fretting fatigue life was decreased as the cylindrical fretting pads radii was increased and the flat pads edge radii were decreased. Basically as the contact area increased due to the flatter contact surfaces of the fretting pads the fretting fatigue life decreased.

Sabelkin et al [35] investigated the effects of shot-peening intensity on the fretting fatigue behavior of Ti-6Al-4V. The shot-peening intensities employed were 4A, 7A and 10A. The shot-peening was shown to have a beneficial effect on fretting fatigue life with the greater shot-peening intensities having a greater effect. The explanation for this result was that residual stress increases with the increasing shot-peening intensities thus moving the boundary between negative and positive stresses to a greater depth. For the 4A and 7A specimens the crack initiated on the contact surface while the 10A specimens crack's initiated at a depth away from the contact surface.

Yuksel [8] also evaluated the effects of shot-peening on the fretting fatigue behavior of Ti-6Al-4V. His study compared the results of his experiments on thicker specimens (6.35 mm) to earlier results of shot-peening on thinner specimens (3.81mm). While shot-peening proved to be beneficial for fretting fatigue life for both the thick and thin specimens there were differences observed in the crack initiation locations. He found that the cracks initiated at depths of 200 to 300 microns from the contact surface in the thinner specimens while the cracks in the thicker specimens initiated on the contact surface. Furthermore, the crack orientations also differed between the two thicknesses. The thinner specimen's cracks initiated close to the +/- 45 degree angle while the thicker specimen's cracks were oriented at -37 and -28 degrees for primary and secondary cracks respectively.

2.6.2 High Temperature Studies on Titanium alloys

Hamdy and Waterhouse [36] studied the fretting fatigue behavior of Ti-6Al-4V at elevated temperatures ranging from 200 C to 600 C. They determined that the fatigue life decreases, though not dramatically so, as the temperature was increased from 200 C to 400 C to 600 C. They attributed this decrease in fatigue endurance to changes in the fatigue properties of Ti-6Al-4V rather than an aggravation of the fretting damage process. This study further indicated that at higher temperatures the surface damage observed differed greatly from what is observed at room temperature.

Jin, Mall and Sahan [37] evaluated the effect of elevated temperature (260 C) on the fretting fatigue behavior of Ti-6Al-4V. This study confirmed Hamdy and Waterhouse's earlier observation that unlike nickel-based alloys, there was no glaze oxide formation to prolong the fatigue life. Furthermore, this study found that although there

was a significant reduction in the fretting fatigue endurance as compared to plain fatigue endurance at both room temperature and 260 C respectively, there was no significant difference between the room temperature and high temperature endurance of either plain or fretting fatigue tests. This establishes that temperatures up to 260 C do not benefit or detract from the fatigue endurance of Ti-6Al-4V at all.

Albinali [23] evaluated the effects of both temperature and shot-peening intensity on the fretting fatigue behavior of Ti-6Al-4V. His study tested specimens that had received 4A, 7A and 10A shot-peening intensities at both room temperature and at 260 C. His results concluded that while the shot-peening did increase the fretting fatigue endurance of Ti-6Al-4V at room temperature it did not increase at 260 C. Instead he concluded that the elevated temperature environment negated the effects of the shot-peening due to increased stress relaxation.

Gean and Farris [38] studied another titanium alloy, Ti-17, at temperatures of 600 F (316 C) with various surface coatings, lubricants and shot-peening treatments. Ironically they concluded that the shot-peening, even at elevated temperatures, was the only aspect to significantly increase the fretting fatigue life in their testing. It was not made clear how the shot-peening was improving the fretting fatigue endurance only that it was the only aspect of testing to exhibit a difference.

2.6.3 Room Temperature Studies on Nickel alloys

Sondhi, Dyson and McLean [39] discovered the presence of an internal stress field within an as-received IN-100 alloy which was determined to be responsible for an unusual response of low and even negative creep rates in tension. This study compared the as-received alloy to a pre-aged alloy in order to validate the internal stress field

hypothesis. The absolute values of initial creep rates were significantly higher in compression than in tension, resulting in the asymmetric creep response thus proving the presence of the internal stress field. This asymmetry was easily removed by thermal ageing prior to testing.

Madhi [11] studied the fretting fatigue behavior of IN-100 in conditions with two different cylindrical fretting pad radii; 50.8 mm and 304.8 mm. The microstructure of the IN-100 used in his study was a coarse grained alloy with oblong grain dimensions of 10 microns by 50 microns. He investigated the validity of extending predictive parameters such as the Smith-Watson-Topper (SWT), Findley, Shear Stress Range (SSR) and Modified Shear Stress Range (MSSR) parameters. His results indicated that the MSSR parameter was the only parameter to accurate model crack initiation location and orientation and fretting fatigue life. The experimental set-up used by Madhi is substantially similar to this study's experimental set-up except that it was conducted at room temperature and using an IN-100 alloy with a coarse grained microstructure. His results are analyzed and compared to this study's results in Chapter IV as a room temperature reference data set.

Saladin's work [10] evaluated the effect of microstructure on the fretting fatigue behavior of IN-100. His study examined the differences in fretting fatigue crack initiation, location and propagation of fine and coarse grained IN-100. He found that the coarse grained microstructure had a greater resistance to crack initiation and propagation than the fine grained structure due to a higher crack initiation threshold. This difference was greater in the high cycle fatigue region than in the low cycle fatigue region. The experimental set-up used by Saladin is also substantially similar to this study's experimental set-up except that it was conducted at room temperature. The

microstructure of the IN-100 used in Saladin's study is identical to the microstructure used in this study because all of the specimens were taken from the same plate.

2.6.4 High Temperature Studies on Nickel alloys

In a study by Wan and Yue [19] smooth and notched specimens of a single crystal nickel alloy, DD3, were tested at 620 C in air and under load/stress control at a frequency of 0.17 Hz. A relationship between shear stress and cycles to failure in the low cycle fatigue region was developed using resolved shear stress and resolved shear strain of slip systems activated during the fatigue cycles. The resolved shear stress, τ^{α}, corresponding to a particular slip system, α, can be obtained from the following equation.

$$\tau^{\alpha} = \sigma : P(\alpha) \qquad (2.23)$$

where $P(\alpha)$ is defined as:

$$P(\alpha) = 0.5(\hat{m}^{\alpha}\hat{n}^{a^T} + \hat{n}^{\alpha}\hat{m}^{\alpha^T}) \qquad (2.24)$$

In equation 2.24, $\hat{n}^{\alpha}$ and $\hat{m}^{\alpha}$ are the unit vectors that are normal to the slip plane and along the slip direction respectively. To relate shear stress and the number of cycles to failure a power law life model was assumed.

$$\frac{\Delta\tau_{\max}}{2} = AN_f^b \qquad (2.25)$$

In this equation, $\frac{\Delta\tau_{\max}}{2}$ is the maximum resolved shear stress amplitude, A and b are parameters, and N_f is the number of cycles to failure. Equation 2.25 is only valid if the mean stress is zero. If the mean stress is not zero then equation 2.25 can be modified as follows:

$$\frac{\Delta\tau_{\max}}{2} = AN_f^b \left\{ 1 - \left(\frac{\tau_m}{\tau_b} \right)^2 \right\} \qquad (2.26)$$

where τ_m is the mean resolved shear stress on the slip system corresponding to maximum shear stress and τ_b is the resolved shear stress corresponding to the ultimate tensile strength.

In a study by Brien and Decamps [40, 41] the effect of microstructure of another single crystal nickel based super alloy, AM1, was examined under high temperature fatigue at 950 C ($T \cong 0.7\ T_m$). For repeated fatigue ($R_e = 0$), two types of behavior were found depending on N, the number of cycles, and $\Delta\varepsilon^t$, total strain amplitude, allowing a map of microstructures versus the N and $\Delta\varepsilon^t$ to be developed. The first domain, A, shows anisotropic microstructures due either to a partition of the plasticity throughout the γ channels, or to an oriented coarsening of the γ' precipitates of the so called type N (rafts perpendicular to the loading axis). The second domain, H, presents homogenous deformation microstructures. The presence of precipitates significantly affects the usual behavior of monocrystalline alloys under fatigue and localizes the plastic deformation in the channels.

In addition, Brien and Decamps claim that there is a geometrical differentiation of plasticity due to heterogeneity on the local stress resulting from the presence of internal stresses. Further, alternate fatigue ($R_e = -1$) also leads to the same type of coarsening, even for very low cycle numbers. It was shown that alternate fatigue causes a three dimension distribution of the plastics deformation in the γ channels, since tension activates plastic flow in the channels perpendicular to [0 0 1] and compression in the others. One final note with regard to temperature was that at low temperatures it is

expected that precipitate shearing occurs in a significant manner. At very low temperatures ($T \ll 0.6\ T_m$), no coarsening should be observed.

Piard et al [42] concentrated on creep fatigue crack growth in PM Astroloy, a nickel based super alloy, at 750 C and in high vacuum. Various cohesive models and experimental data were used. The study focused on the ΔK range with crack propagation during the reloading phase of creep only. Two simulations were used, one with a hold time of up to 1000 seconds and one without a hold time. The fatigue and creep damage fields were related to the crack opening displacements of the specimens. The predictive crack curves were found to accurately reflect the influence of hold time duration during the reloading phase.

Shyam and Milligan [18] developed a theoretical model for slip irreversibility in a polycrystalline nickel-base super alloy, KM4, which deforms in a planer manner. The slip irreversibility parameter was based on the fraction of dislocations exiting the free surface due to the applied loading. The parameter assigned values ranging from zero, coinciding with reversible slip, to one, coinciding with fully irreversible slip. The experiments conducted where single stroke compression tests at temperatures of 20 C, 550 C and 650 C. When the theoretical calculations were compared to the experiments results it was discovered that slip irreversibility increased with temperature. It was this change in slip irreversibility that was associated with the observed decrease in fatigue crack propagation threshold. Scanning electron microscopy was used to observe that nickel based polycrystalline super alloys deform by slip on crystallographic planes. The fracture surface was found to be on he octahedral slip plane (1 1 1) [0 1 1]. In conclusion, the activation and movement of slip systems are the basic deformation mechanism of notched and round specimens used in testing.

Shyam et al [43] studied the effects of temperature, surface treatments and frequencies of Rene'88DT at both room temperature (20 C) and at elevated temperatures (593 C) under ultrasonic conditions (19.6 kHz). In that study it was discovered first that at 593 C the surface treatments did not have an effect because crack initiations were always below the surface and second, that at ultrasonic frequencies, higher temperatures reduced the fatigue life as compared to room temperatures. However, it was also noted that "[a]s temperature is increased from 20 to 593 C (at 10 Hz) or when frequency is decreased from 19.6 kHz to 10 Hz (at 593 C), the fatigue lives increase." This indicates that although an inverse relationship exists between temperature and fatigue life at ultra sonic frequencies, the opposite is true of the relationship between fatigue life and temperature at lower frequencies, like the frequency utilized in this study (10 Hz).

Golden [44] has also begun studying Rene'88DT at elevated temperatures. His efforts have been focused on creating a fretting fatigue fixture that more closely resembles the dovetail geometry and the elevated temperatures (650 C) of the turbine engine environment. Although only six tests have been completed as of the time the paper was written, his results have already indicated a wide range of scatter (118,000 and 1.38 million cycles to failure) for one particular loading condition that was repeated. This preliminary finding establishes the fact that occasionally a very wide range of scatter can occur when testing the behavior of nickel based alloys at elevated temperatures.

Kawagoishi, Chen and Nisitani [21] studied Inconel 718 under rotary fatigue at elevated temperatures ranging from 300 to 600 C in air and compared its fatigue performance to room temperature. They discovered that in the long-life region, the fatigue strength of a plain specimen is much higher at elevated temperatures than at room temperature, though the static strength decreases with the increase in temperature. The

effect of temperature on the fatigue strength was examined in terms of the initiation and early growth behavior of small cracks. It was determined that initiation and propagation of small cracks, less than 20-30 micrometers is suppressed by oxidation and plasticity induced crack closure. Since most of fatigue life is spent in crack growth stage this is why higher temperatures result in longer life. Ultimately fatigue life increases with increase in temperature, except in short life region and it especially increases over room temperature. This indicates that the crack initiation and propagation suppression characteristics of the high temperature environment are having an impact.

Hamdy and Waterhouse [36] discussed in the previous section also noted that in a previous study [45] they completed on Inconel 718 that:

> As the temperature was increased from 280 to 540 C the fretting fatigue strength was increased by 130% ... This marked improvement was attributed to the formation of the glaze oxide ... which is formed under the conjoint action of oxidation and sliding, appears on this alloy to behave as one would hope an externally applied protective coating would act.

This finding provides an insight into the processes of fretting fatigue wear and how these interactions might be responsible for improving fretting fatigue behavior.

Murthy, Gao and Farris [16, 20, 46, 47] studied the fretting fatigue behavior of single crystal nickel contacting with IN-100 at elevated temperatures (610 C) subjected to a range of loading conditions. Different multi-axial fatigue parameters were investigated for their ability to predict the initiation life of the specimens. Estimations of crack propagation life were made using conventional fracture mechanics approaches, after making certain assumptions to simplify the problem. Total life was predicted using nucleation life from different parameters and propagation life from conventional fracture mechanics approach. The predicted lives were compared with the experimentally

observed failure lives. The quality of the comparison provides confidence in the notion that conventional life prediction tools can be used to assess fretting fatigue at elevated temperatures.

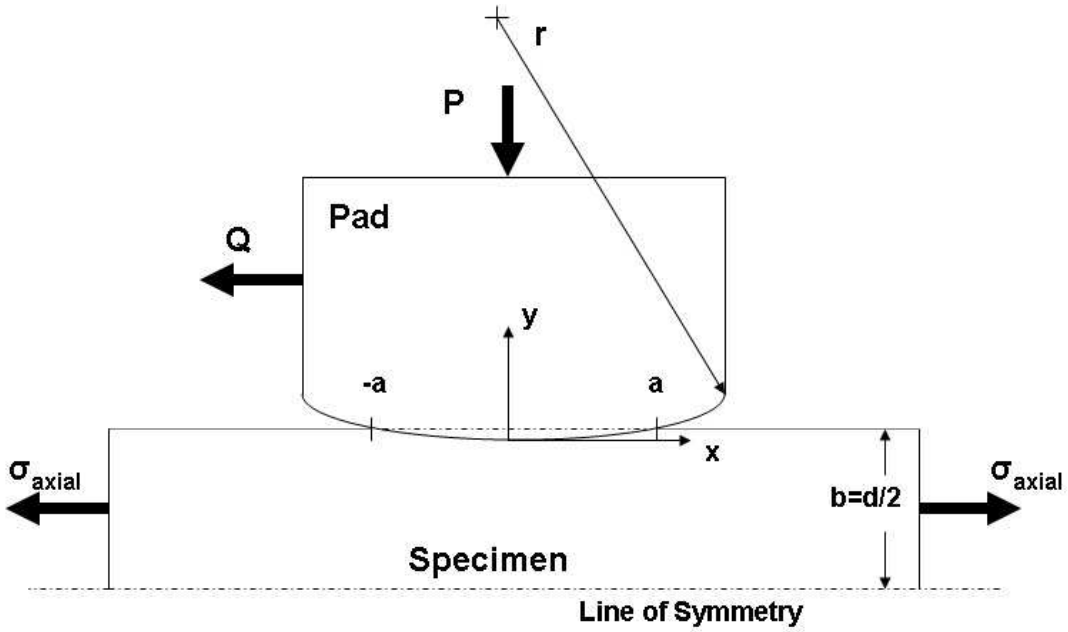

Figure 2.1 Diagram of cylinder on flat fretting fatigue configuration [11]

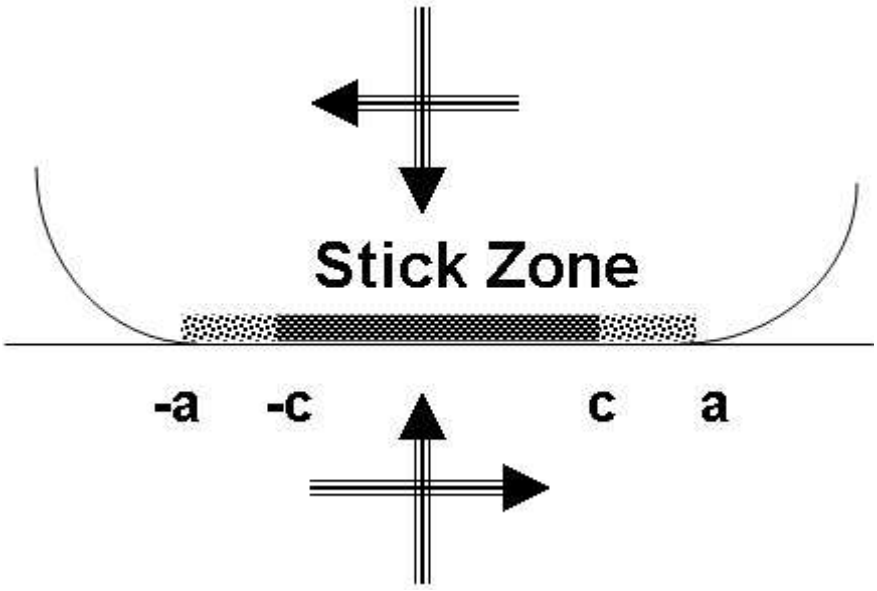

Figure 2.2 Diagram of stick zone [11]

III. Experimental Method

This chapter discusses the test design in detail and the data collected during the test. The experimental method used in this study is substantially similar to the methods used in the Madhi [11] and Saladin [10] studies but has been modified significantly in order to facilitate the testing conditions of elevated temperature. What follows is a brief description of the testing apparatus, the specimens and pads used, and the procedures utilized in executing a proper test. Particular attention is paid to those areas which were developed or modified to accommodate the high temperature aspects of testing.

3.1 Test Set-up

The test set-up in this study was intended to match the conditions of the room temperature version of fretting fatigue testing of previous works but to add the environmental aspect of high temperatures. While making this change may seem simple in principle it has required a great deal of effort to become a reality. The testing machine used for all of the experiments is a first of its kind MTS 22 kip servo-hydraulic axial and a 1 kip servo-hydraulic horizontal test machine (Figure 3.1). The specimen is loaded into the hydraulic grips that are attached to the upper and lower actuators. Unlike the previous test apparatus used by Madhi [11] and Saladin [10], the upper grip is not a stationary cross head but a fully movable actuator that for the purposes of these experiments was programmed to remain in displacement control in order to provide an approximately rigid boundary condition. Both upper and lower grips house load cells which were used to monitor the axial loading conditions of the specimen under test conditions.

The fretting actuator is a simple hydraulic ram that is mounted on a movable sled with a load cell in the receiving end (left side as pictured) that monitors the fretting load applied (Figure 3.2). This constitutes a significant departure from the fretting apparatus used by Madhi [11] and Saladin [10] because the pads are applied by the machine at the appropriate point in the test once the specimen has been brought up to the desired temperature. Furthermore, as will be discussed later in this chapter, the actual applied fretting loads were not constant throughout each fretting test and so the fretting normal load, P, was actually a dynamic load that was slightly out of phase with the axial load. One last characteristic of both the axial and fretting actuators is that they were all actively cooled by chilled water which was pumped through the grips and around the fretting cylinders by a stand alone water chiller and pump located behind the machine. The cooling is necessary because the load cells are only rated to operate in the -40 ºC to 177 ºC temperature range.

The temperature is controlled by an MTS temperature controller with two platinum rhodesium R type thermocouples and two heater boxes mounted in the front and rear sides of the machine each controlling two electric resistance heating elements. The thermocouples are mounted by a custom designed and build thermocouple apparatus that is placed in between the upper and lower grips and around the specimen (Figure 3.3). The thermocouples extend down from the apparatus into the hot zone of the testing area in between the four electric resistance heating elements (Figure 3.4). The thermocouple heads are aligned in the same horizontal plane as the center line of the fretting pads but are removed from the actual fretting pad and specimen interface area by approximately 1.5 cm. The original design had called for the thermocouples to be spot welded to each

specimen on the non-contact front and back sides but this proved problematic as the spot welds introduced surface flaws that become significant stress concentration factors.

The heating elements are attached to the two heater boxes, one front and one rear, that are attached to the same sled as the fretting actuator (Figure 3.5b). The heating elements extend from the interior side of the heater box with one element on the left and one on the right side of the specimen at an angle of approximately 30 degrees from the horizontal (Figure 3.5a). The elements from the front and rear heating boxes are aligned such that one heating element from the front box and one from the rear box are on each side of the specimen and are angled such that the elements avoid touching either the specimen, the fretting pad or each other (Figure 3.5d). The heater boxes are secured to the sled by two screws located on each side of the box through a narrow channel running along the entire side of the heater box that allows them to be slid from the outer edge of the sled towards the specimen and pads once they are installed and aligned (Figure 3.5c).

The thermocouple apparatus is attached to the heater boxes by two screws on the top of the front box and loosely rests on the rear heater box to which it fits snugly over three screw heads. Since the heating elements and the thermocouples are all attached, directly and indirectly respectively, to the heater boxes which are attached to the same sled as the fretting apparatus which is rigidly attached to the frame of the entire machine it is assumed that the thermocouples are therefore located in the same position relative to the specimen, fretting pads and heating elements for each high temperature test. This assumption is critical to the reliability, repeatability, and accuracy of the temperature control of the specimen and fretting pads for each high temperature test as all of this temperature apparatus is exposed to the open air of the laboratory. As such the actual temperature of the specimen and pads in the area of fretting interest is likely to fluctuate

over the course of the test due to the flow of ambient air around the test set-up. Also, because the thermocouples are removed from the specimen the whole temperature controlling environment must be calibrated in order to accurately control the temperature of the specimen during the test.

This calibration was done by mounting a specimen with two thermocouples that had been spot welded on the front and back non-contact sides in the center of a specimen in between the fretting pads contact area and noting the difference in observed temperature from the thermocouples that were attached to the specimen and those suspended from the apparatus attached to the heater boxes. The observed temperature of the suspended thermocouples was used as the feedback value for the commanded temperature of the heater boxes which controlled the electric current going to the heater elements which therefore controlled the temperature of the test environment.

It was determined that for a fretting fatigue test the commanded temperature of 455 ºC was the temperature which best correlated with the desired temperature of 600 ºC on the specimen to within a range of 594 ºC to 608 ºC or to within about ±1% of the desired temperature. For a plain fatigue test the commanded temperature of 370 ºC was best correlated to the desired temperature of 600 ºC again to within a range of about ±6 ºC. The details and data for the thermal calibration can be found in Appendix A. The difference between the commanded temperatures is related to the difference in heat sink placed on the specimen by contact with the fretting pads and thus the fretting actuator which was actively cooled by the chilled water exchanger.

3.2 Experimental Configuration

The chief purpose of the experiments is to load the specimens under fretting or plain fatigue conditions until complete fracture in order to determine the S-N curve for IN-100 at 600 ºC. There are many steps involved in correctly preparing and executing a successful test. The procedure for executing a fretting test is considerably more complicated and requires several additional steps than the procedure for executing a plain fatigue test. For completeness this next section will describe the procedures for executing a fretting test and the reader will understand that all steps pertaining to fretting pads are omitted for executing a plain fatigue test.

The first step is to measure the physical dimensions of the test specimen and the fretting pads. Using an indelible marker and a ruler lines are drawn on the narrow sides of the test specimen in the center of the gage section to indicate where the center of the specimen is located. Lines are also drawn along the length of the top and front sides of the fretting pads in the center to indicate the center line of each pad (Figure 3.6a). These lines will be used later to ensure that the pads are symmetrically aligned on each side of the specimen (Figure 3.6b). The each test specimen's gage section is measured with precision calipers to calculate the cross sectional area of the gage section.

The next and perhaps most important consideration in executing a quality test is properly aligning the specimen and the fretting pads in the grips and the fretting actuators. The specimen must be loaded in the center of the upper and lower grips so as to be correctly placed with respect to the fretting pads. The specimen must also be loaded completely vertically so as not to undergo any longitudinal torsion or bending loads during the test. The fretting pads are loaded in the fretting actuator by way of an intricate ring and four holding pad configuration that is then bolted to the fretting

cylinders (Figure 3.7). Once the fretting pads are attached to the fretting cylinders the only remaining degree of freedom is a rotational movement about the fretting loading direction. The fretting pads can be aligned using a simple leveling technique (Figure 3.8) that results in an estimated error of no more than 0.4 degrees from perfectly horizontal and the curved faces of the fretting pads are aligned such that the front, back, top and bottom surfaces are flush. The center line drawn on each fretting pad should line up exactly with the center line drawn on the other pad and the line drawn on the center of the gage section of the specimen (Figure 3.6b). The proof of good alignment is taken by using pressure sensitive paper inserted between the fretting pads faces and the specimen. The fretting pads are then closed by applying a force using the fretting ram actuator. If the alignment is good the Hertzian shape embossed on the pressure sensitive paper should be a symmetric rectangle on both sides. If this is not the case the pads are adjusted until the alignment is as close to ideal as is possible.

The next step is to tune the servo-hydraulic controller to the desired test axial loads. This is done using the controller's internal auto-tuning procedure. It is important to perform this auto-tuning procedure before each test because the specimens are never exactly identical and the axial loads applied are usually changed from each test case to the next. Furthermore, it is important to tune the machine with the fretting pads applied using the actual testing load. All of this helps to ensure that the machine will function properly during the entire test and that it will accurately follow the desired load profile. The fretting load used for all tests in this study was a constant load of 4003 N while the axial loading was a sinusoidal wave with a frequency of 10 Hz with a stress ratio of minimum to maximum applied stress held constant at a value of 0.03. The actual maximum and minimum applied loads used were calculated before each test using the

cross-sectional area measured from each specimen. The loading and execution of the test is scripted by the Multi Purpose Test (MPT) software developed by MTS and provided with the machine. This allows for the machine to be programmed with the appropriate loading conditions and data collection schemes also known as a test procedure and run independent from constant operator observation and control. Because each test procedure is programmed with specific loading values a separate procedure is programmed for each test.

The test procedure consists of several carefully ordered steps that are executed to control the temperature and loading conditions as well as collect data and shut down the test as soon as the specimen fractures. The first step is to increase the temperature of the specimen in the center of the gage section, and the fretting pads if it is a fretting test, up to the target temperature of 600 ºC. The commanded temperature is ramped up linearly over a fifteen minute period until the target temperature, 455 ºC for fretting tests and 370 ºC for plain fatigue tests, is reached (Figure 3.9a). Once the suspended thermocouples have reached the target temperature the program begins a dwell period where it monitors the temperature feedback. The program will not exit this dwell period until the observed temperatures from both thermocouples indicates that the temperature has remained at the commanded temperature within a range of +/- 15 ºC for at least 15 minutes (Figure 3.9b). The purpose of this hold is to ensure that the specimen has had sufficient time to reach the target temperature of 600 ºC and that the electric heaters and the temperature controller are all functioning properly and are able to maintain the elevated temperature accurately. Also during this time the specimen is being held in load control with a commanded load of 0 N by the lower actuator. This is done so that the specimen is

allowed to thermally expand freely. Generally the thermal expansion of each specimen was less than 0.03 inches.

The next step in the fretting fatigue test is to apply the fretting pads to the specimen. The best way to do this was eventually determined to apply the fretting pads with a small load of about 132 N that allowed the specimen slip easily in between the fretting pads. This became necessary because it was discovered that the fretting pads were a considerable heat sink once applied and would cause the specimen to contract as soon as they were applied. If they were applied with the full testing load it would pinch the specimen and keep the top portion from moving freely as it underwent normal thermal changes. This then lead to the top portion of the specimen being initially held in a compressive load of approximately 300 to 400 N which ultimately biased the shear force data collected. Once the fretting pads were applied and held at the lower load for 10 minutes the temperature throughout the thickness of the specimen and fretting pads would stabilize and the loads detected by the upper and lower load cells were back to zero.

Next the maximum axial load was applied in a ramp function followed by the full fretting load of 4003 N. Once the initial loading conditions were achieved the fatigue loading portion of the test would begin. The fatigue loading step is programmed to apply an axial 10 Hz sinusoidal load using a peak-valley compensator to ensure that the target maximum and minimum axial loads to the specimen are met thus ensuring a constant stress ratio of 0.03 while simultaneously applying a constant fretting load of 4003 N from the fretting actuator.

At the same time as the fatigue loading step began the procedure would also begin collecting data from the test. The data collected included the load cell values of the upper

and lower grips, the applied fretting force, the upper and lower displacements, the running time and cycle count of the experiment and the temperature reading of each thermocouple. Data was collected at a linear interval of every 200 cycles as well as logarithmically every 10, 20, 30, ... 100, 200, 300, ... 1000, 2000, 3000 cycles up to 10,000,000 cycles. The linear spaced data values collected the peak and valley values of each of the signals listed over the course of the next 2 cycles while the logarithmically spaced data points were collected continuously over the next 3 cycles at a time spaced interval of approximately 0.002 seconds or a sample rate of 500 Hz thus approximately 150 data points for each signal were collected for each logarithmic entry. The reason for sampling at this frequency will be explained later. The fatigue loading and data collection steps continue until the machine detects that the specimen has completely fractured and then it shuts down the hydraulics for both the upper and lower axial actuators and the horizontal fretting actuator.

3.3 Specimen and Fretting Pad Geometry

The complete dimensions of the dog bone specimens can be found in Figure 3.10 but the gage section for both the 8 inch long and 7.5 inch long specimens was 3.81 mm thick by 6.35 mm wide yielding a cross sectional area of 24.1935 mm^2. The edges of the specimens were rounded slightly by grinding wheel and then were hand polished along the narrow sides of the gage section and the transition region to remove as many potential stress risers as possible to prevent premature fracturing. The complete dimensions for the fretting pads (Figure 3.11) were 34.925 mm and 38.1 mm long for the left and right side pads respectively. The height and width of each pad was 9.525 mm and the curved circular surface had a radius of 50.8 mm. All of the specimens and fretting pads were cut

from the same plate of stress relieved IN-100 by wire electrical discharge method and then ground to the final dimensions and a smooth surface. As can be inferred from the silhouette of the specimens extracted from the disk material the grain orientations of each specimen were not identical due to the nature of cutting them from the shape of the disk.

3.4 Load Determination

The loading conditions observed by the specimen during the test are determined from each test for later analysis. The bulk stress can be easily inferred as the force measured by the lower load cell applied across the cross sectional area of the gage section. The shear force however is calculated from the data collected by the following equation:

$$Q = \frac{V - W}{2} \qquad (3.1)$$

where V is the force measured by the lower load cell and W the force measured by the upper load cell and Q is the resulting shear force. The shear force, Q, is calculated for all of the data values in the logarithmically spaced data file. These data values can then be plotted on the vertical axis against the corresponding axial stress data on the horizontal axis for each of the 10th cycle, 100th cycle, 1000th cycle and so on up to the last cycle for which data was collected. The resulting hysteresis plot demonstrates how well the fretting condition is being met during the test. The plots should initially form a closed elliptical loop for the earlier cycles but then stabilize to form a much narrower loop that resembles a straight line for the higher cycles. Once the hysteresis plot resembles a straight line it indicates that no mechanical energy in the specimen-fretting pad system is

being lost due to slippage. Consequently this assures that the fretting pads are no longer undergoing any gross slip with the specimen.

One problem with the fretting actuator that was discovered during testing was that the applied contact load appeared to be sinusoidal and slightly out of phase with the applied axial load when it should have been constant at 4003N. Figure 3.12 is a screen capture of a plot produced by the MTS controller software that demonstrates this apparent condition. It depicts the applied contact load in blue with a sinusoidal shape and a frequency of approximately 10 Hz that also appears to be about 8 microseconds behind or 30 degrees out of phase with respect to the axial loading in red. While the mean contact load is approximately 4003N it does appear to have a range of up to 300N above or below that mean level. At first it was thought that this was due to the design of the fretting actuator in that it was behaving like a cantilever beam and exhibiting a relatively large oscillatory up and down motion. Attempts were made to try and arrest this vibration to no effect. Then further analysis of the collected data revealed that the data could be corrected by applying a small phase shift. Once this phase shift was applied the resulting hysteresis plots clearly fell in line with the expected shape and orientation. This phase shift analysis will be discussed in further detail in Chapter IV.

The minimum and maximum shear force values for each of the 10th cycle, 100th cycle, 1000th cycle and so on up to the last cycle for which data was collected were then plotted against the number of cycles on a logarithmic scale. The resulting plot indicates the shear force range as the test progressed. It was expected that the range between the maximum and minimum shear forces would increase as the test progressed until they asymptotically reached a constant range. This again was not the case for all of the tests in this study. Most tests in this study would stabilize initially and then resume gross

slippage yet still maintaining a constant shear stress range. Figure 3.13 depicts a typical shear stress range plot form this study.

3.5 Crack Development

Crack initiation location, orientation and the various stages of its growth are all crucial to understanding fretting fatigue. A fretting fatigue specimen can be analyzed under a microscope after it has failed to determine the manner in which it failed and what was physically occurring during the test. The fretting pads leave clear markings on the specimen that can be observed and measured to determine the actual contact half width and contact shape of the test. These markings are often referred to as fretting scars because the material surface is permanently damaged by the fretting process. Figure 3.14 is an example of such a fretting scar taken by an optical microscope of test #5. One can also examine the fretting scars left on the fretting pads as well (Figure 3.15). From analyzing these fretting scars from each of the tests one can determine where the crack initiated. It is expected that the cracks will initiate near the edge of the contact region. Often the cracks initiate near the longitudinal edges of the specimens but this is not always the case. A Scanning Electron Microscope (SEM) can also be used to observe in great detail the fracture surfaces of the specimens. The images of the fracture surface can then be analyzed for the points where cracks initiate and their orientations as well as the different stages or regions of the cracks growth as discussed earlier in Chapters I and II. Figure 3.16 is an image of a fracture surface taken from test #5.

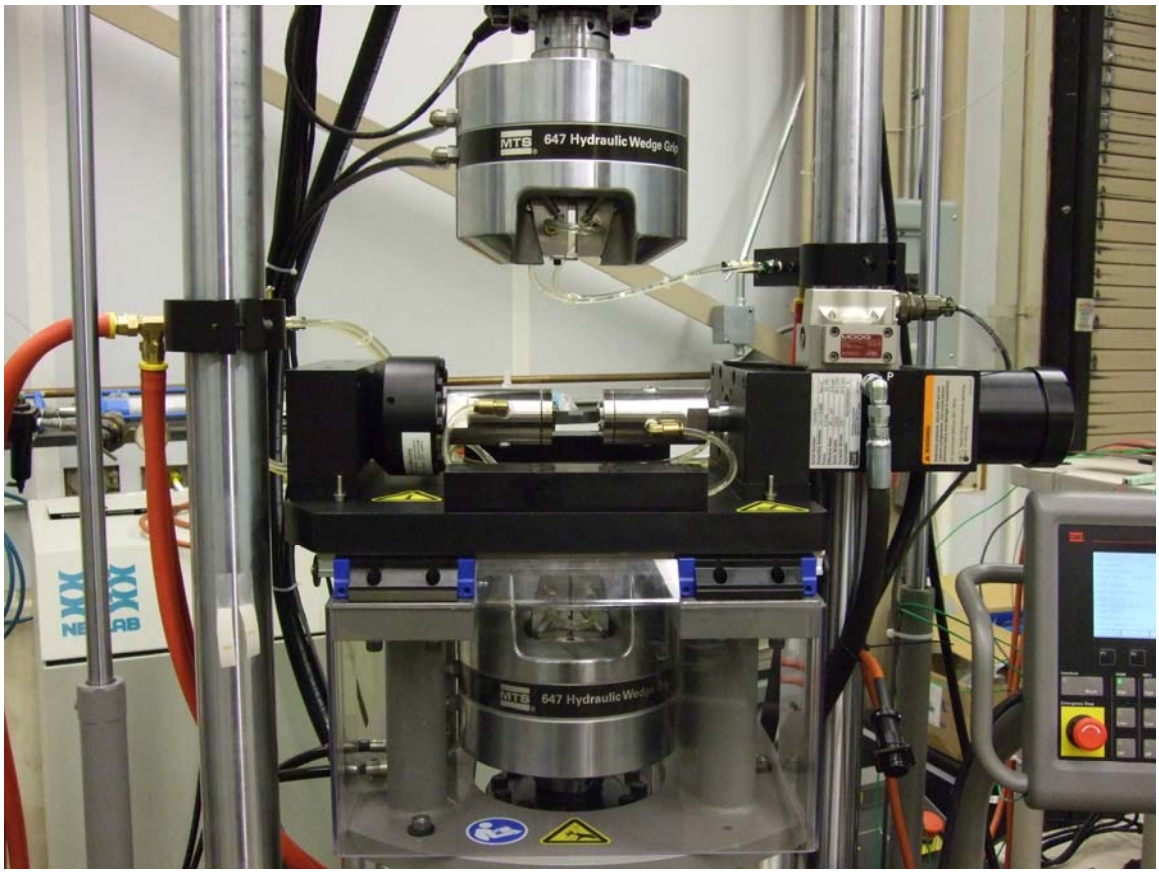

Figure 3.1 - MTS Machine

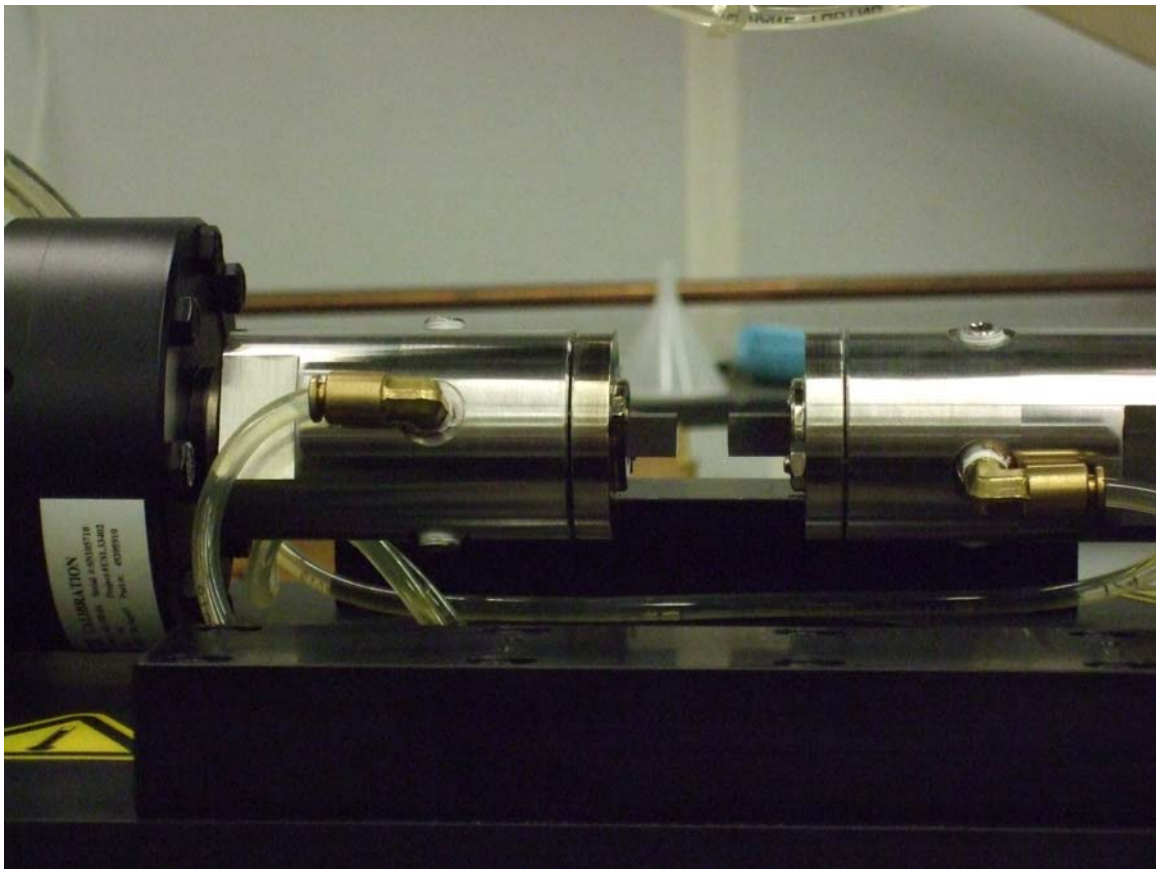

Figure 3.2 - Close up of fretting actuator

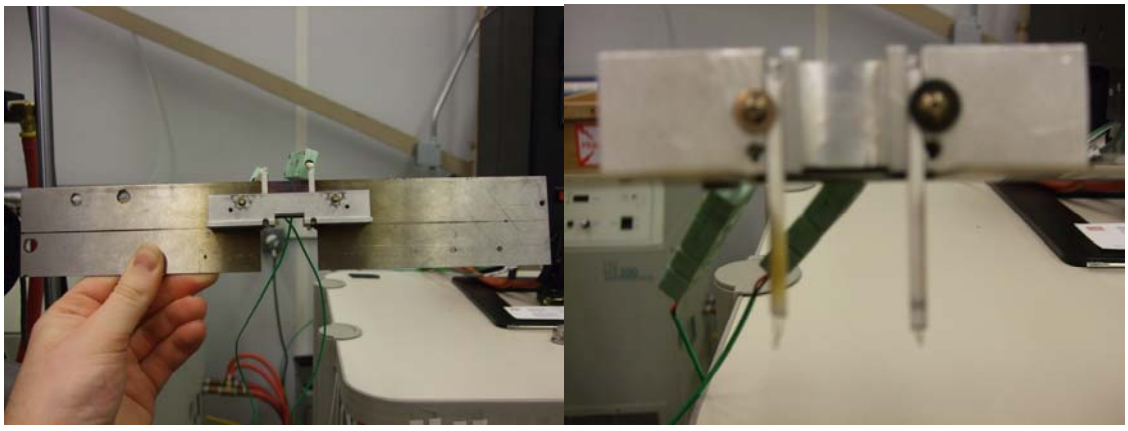

(a) (b)

Figure 3.3 - Thermocouple apparatus

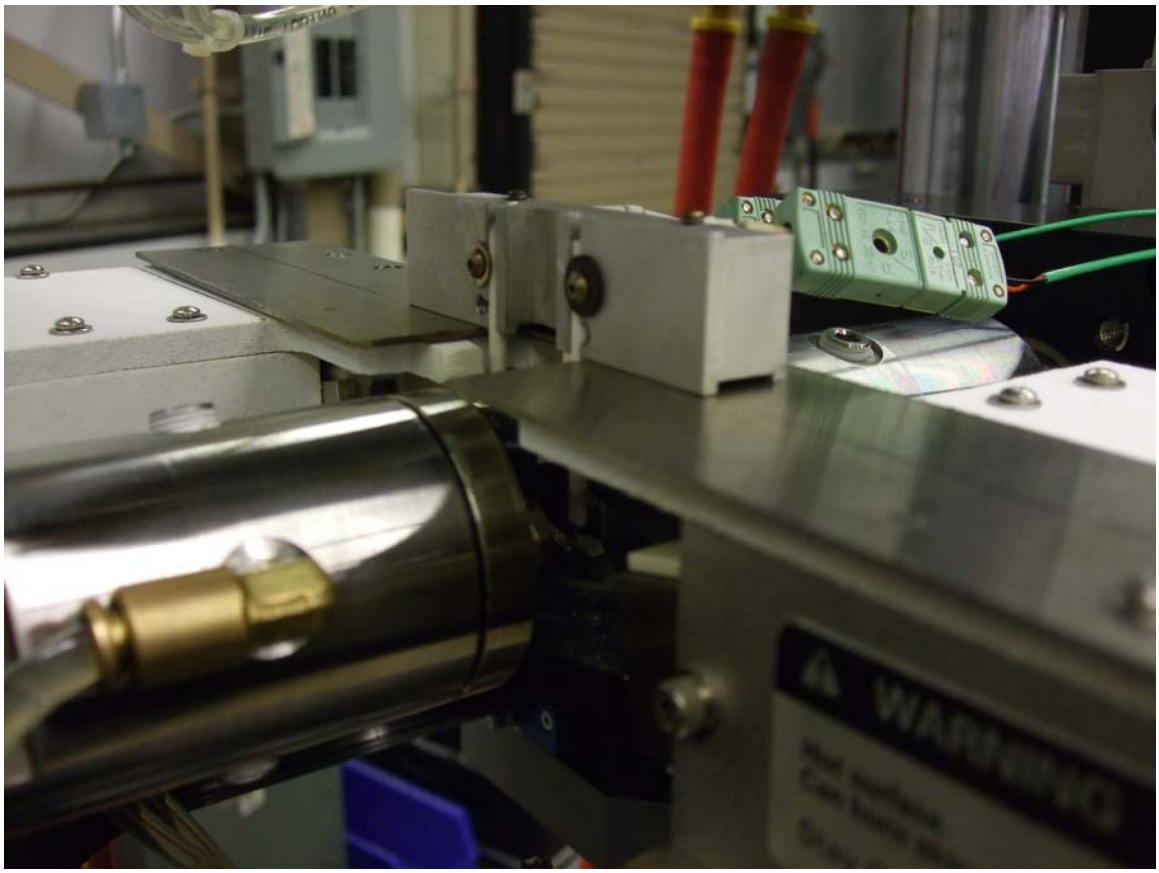

Figure 3.4 - Thermocouple apparatus as placed in normal test position

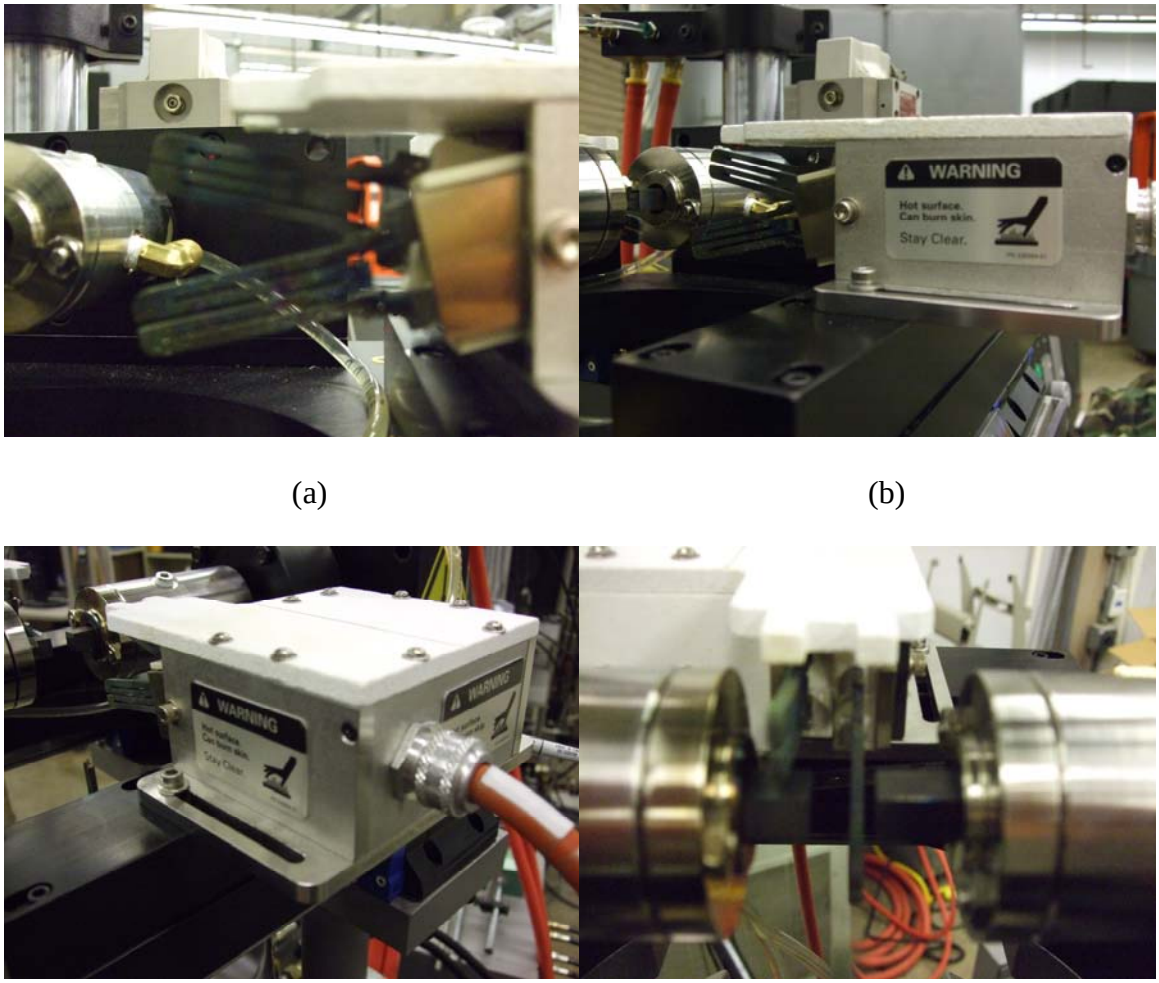

(a) (b)

(c) (d)

Figure 3.5 - Heating elements and heater boxes

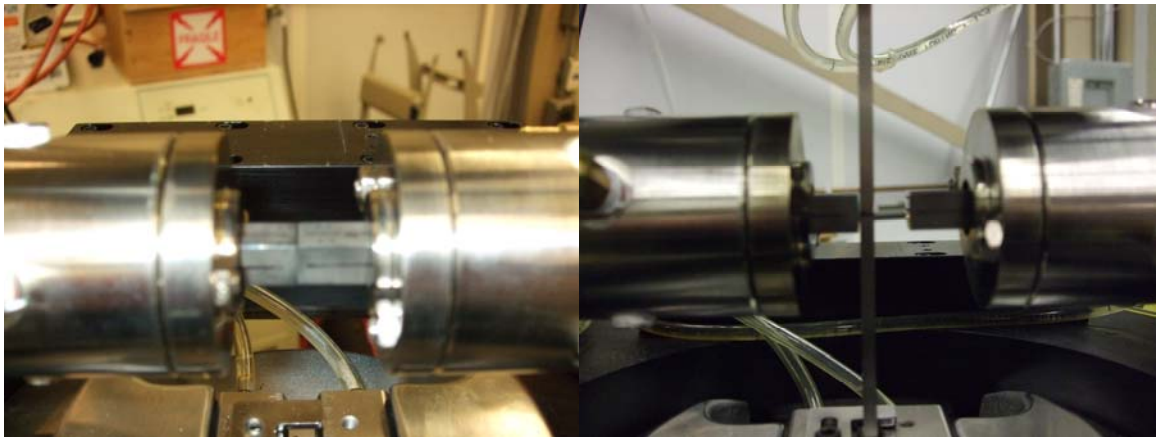

(a) (b)

Figure 3.6 - Guideline markings on fretting pads and specimen

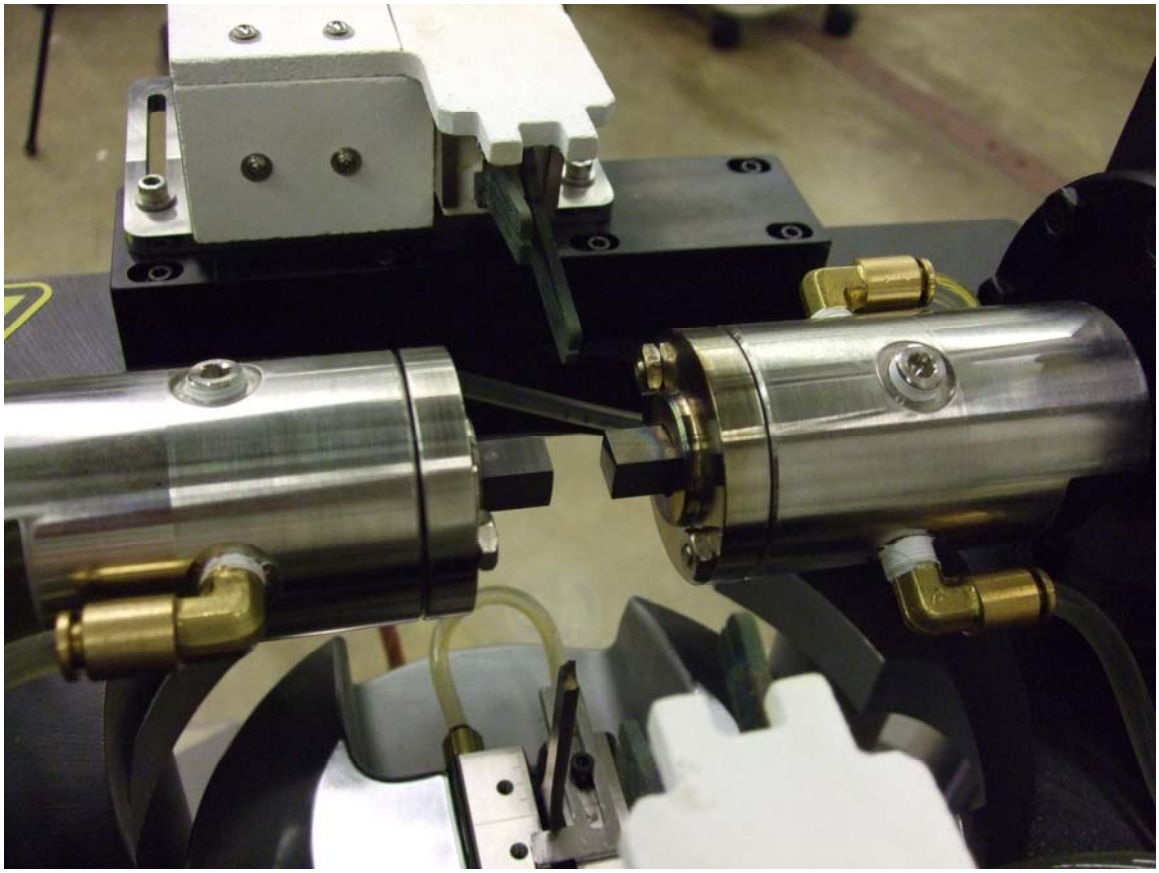

(a)

(b) (c) (d)

Figure 3.7 - Fretting pad holders

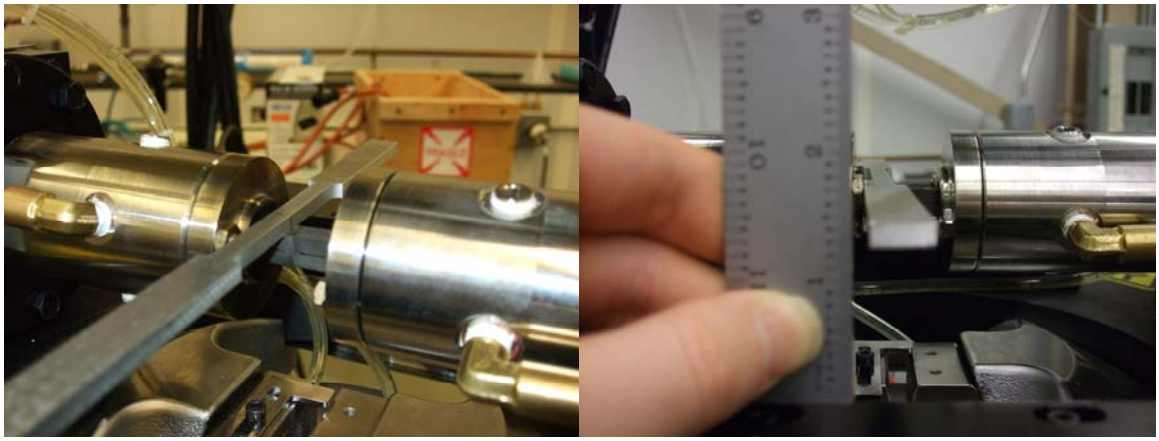

(a) (b)

Figure 3.8 - Leveling technique

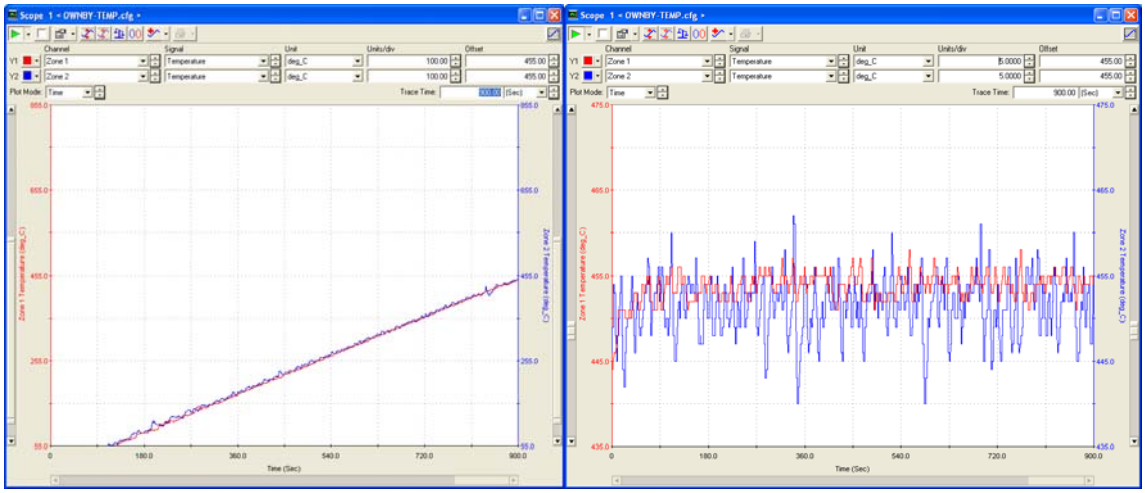

(a) (b)

Figure 3.9 - Temperature ramp up period and temperature stabilization period

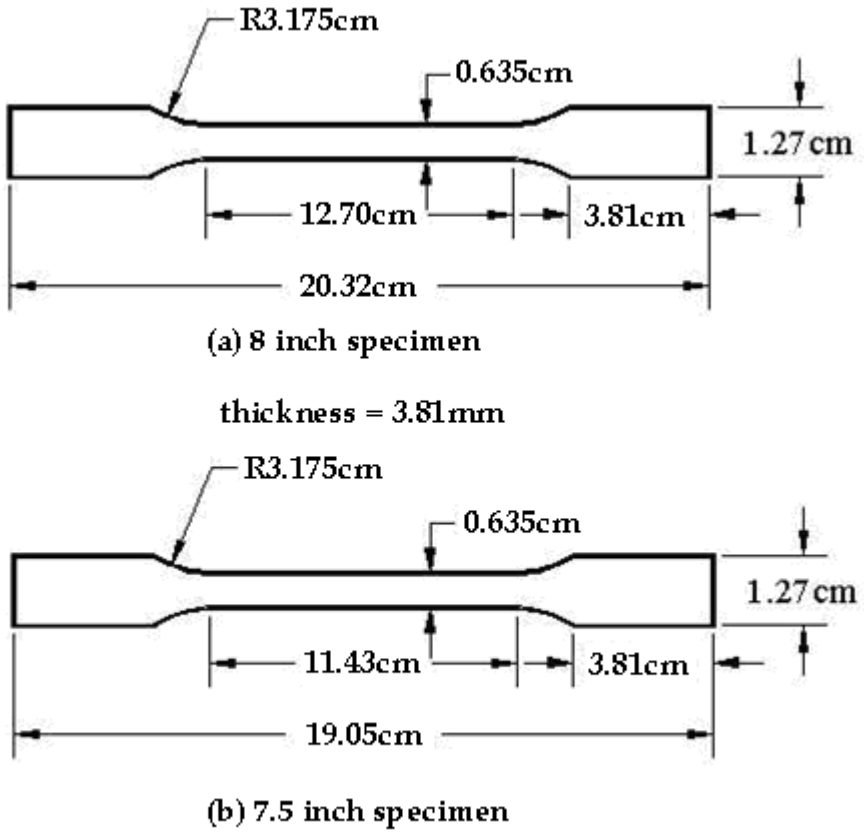

Figure 3.10 - Dog bone dimensions (a) 8 inch specimen (b) 7.5 inch specimen

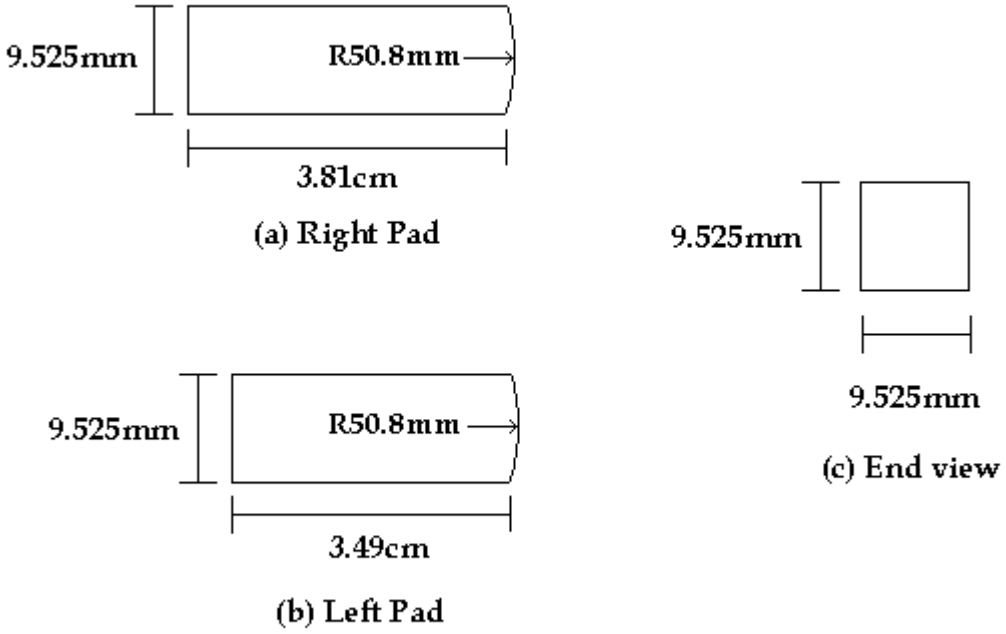

Figure 3.11 - Fretting pad dimensions (a) right pad (b) left pad (c) end view

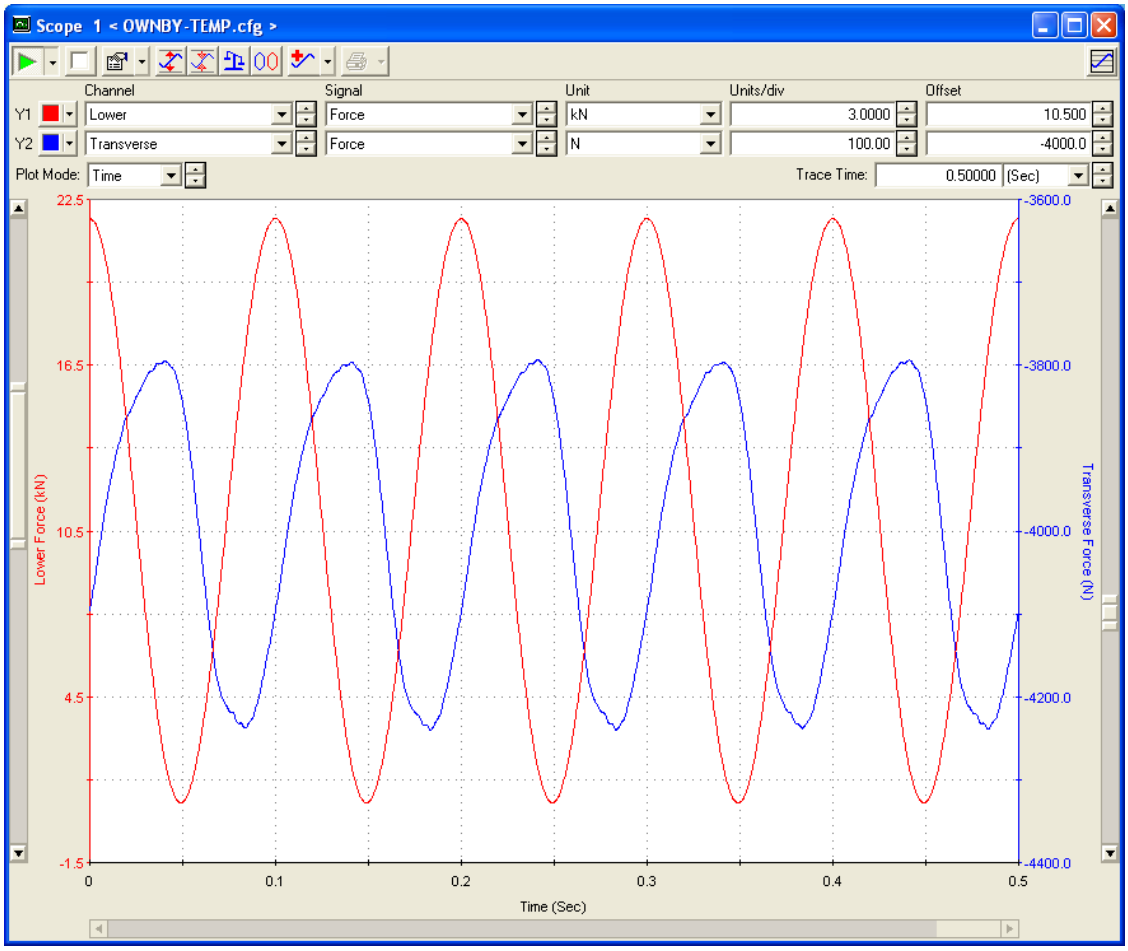

Figure 3.12 - MTS screen capture of observed axial and fretting loads from test #7

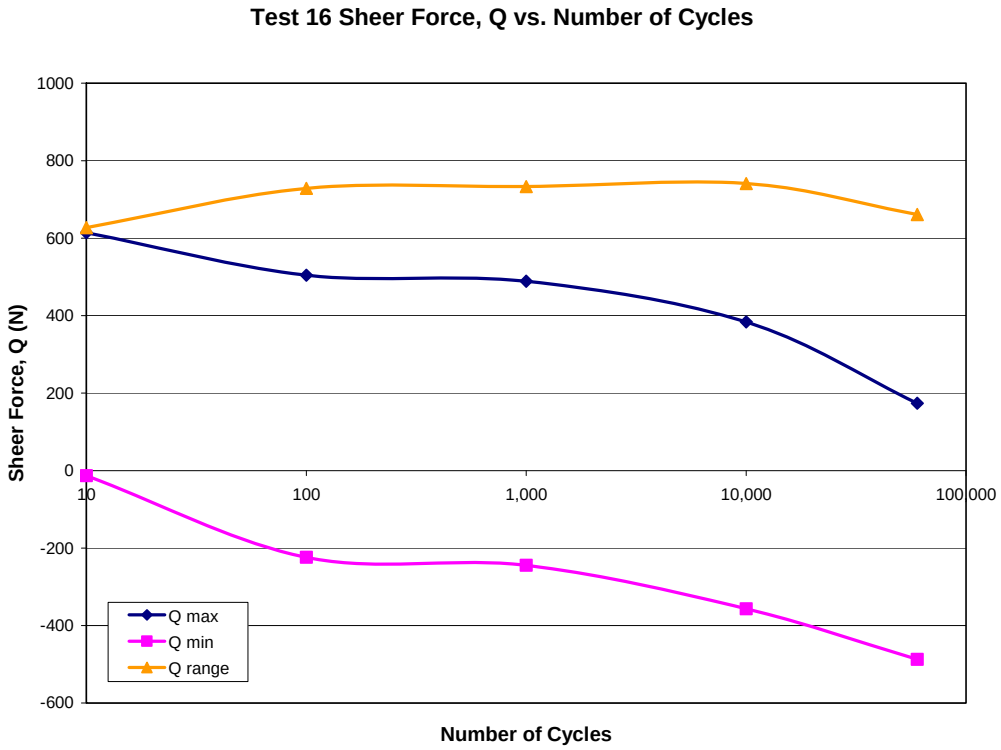

Figure 3.13 - Shear stress range plot (Q vs N) for test #16

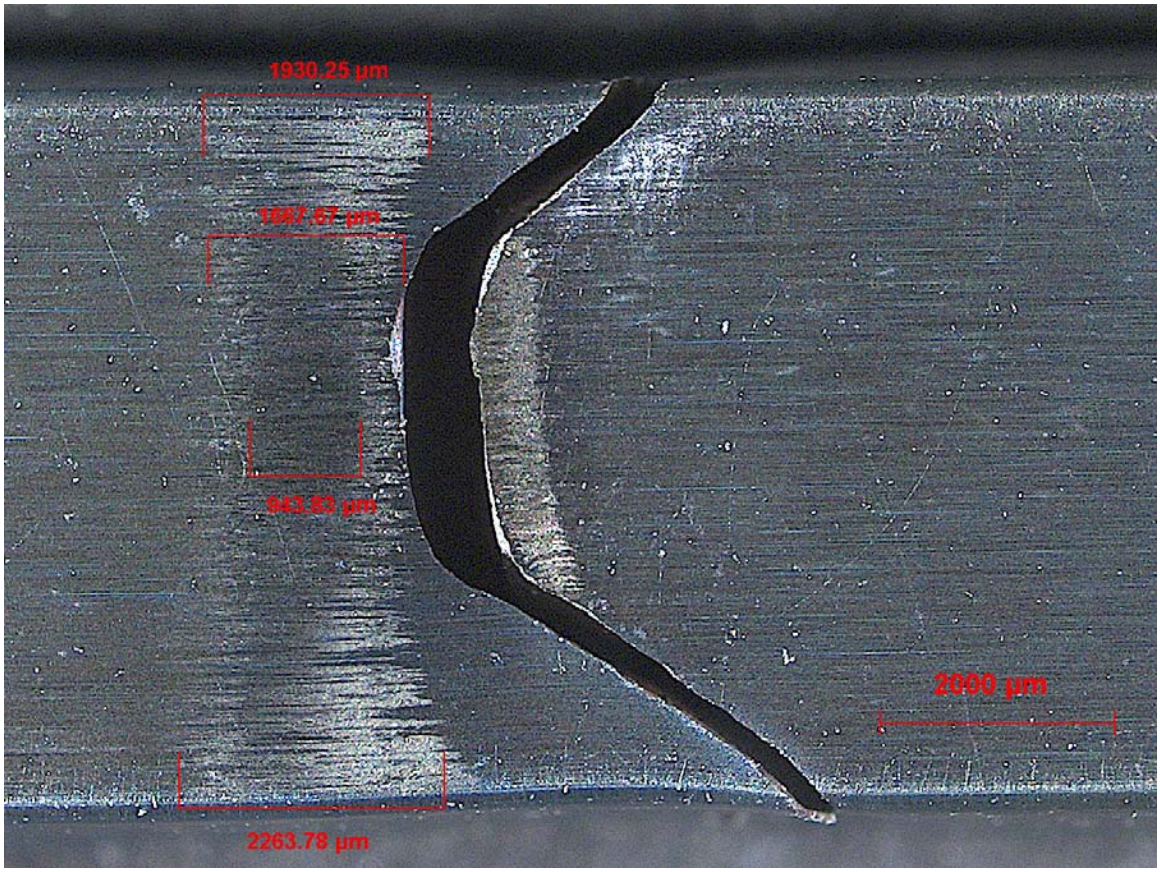

Figure 3.14 - Fretting scar on specimen used in test #5 (right side pictured)

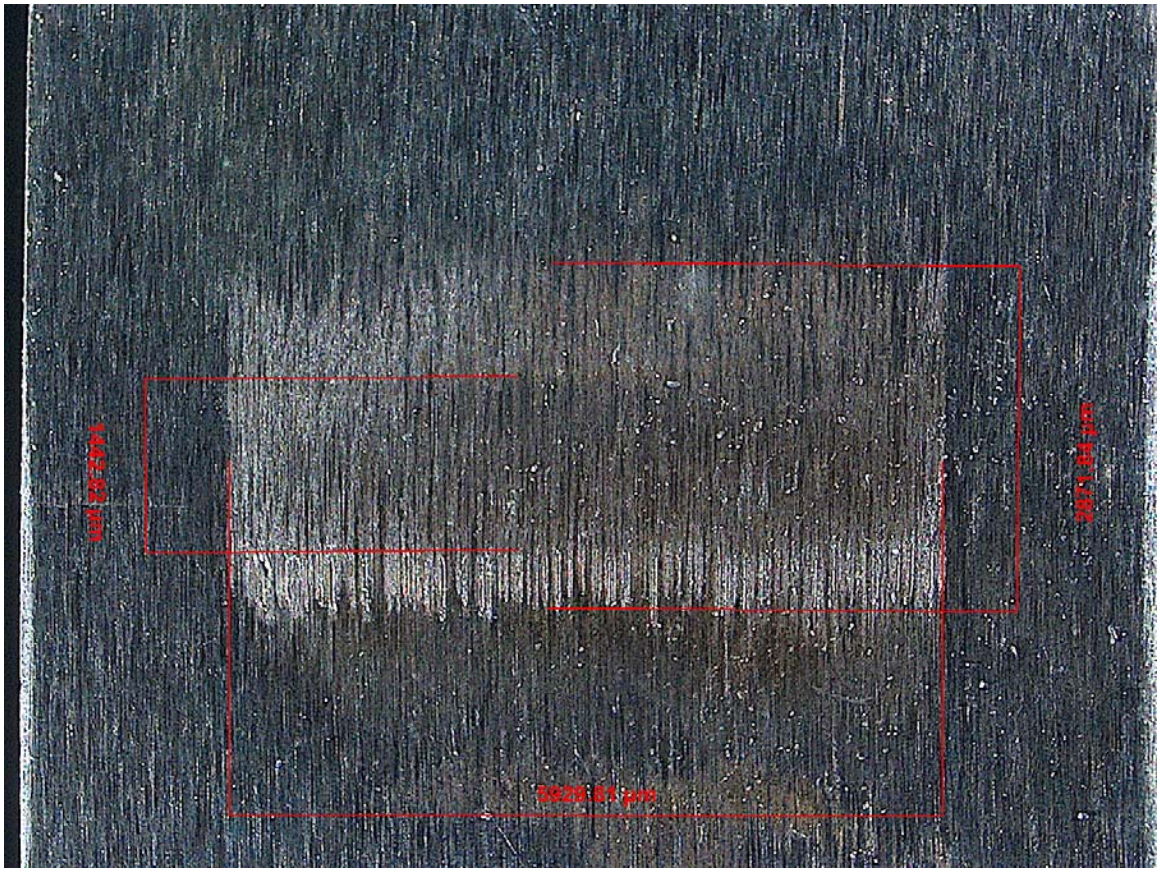

Figure 3.15 - Fretting scar on test #5 left fretting pad

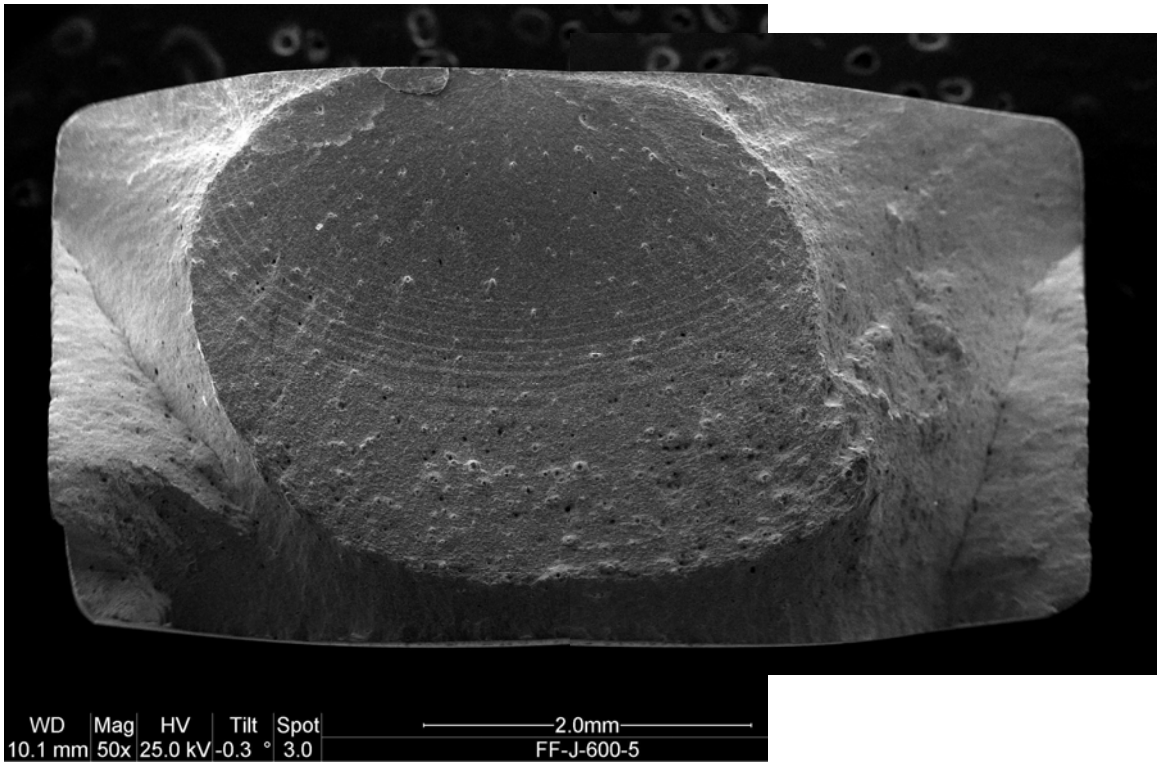

Figure 3.16 - Fracture surface of test #5 taken with SEM

IV. Results and Discussion

This chapter will present the experimental data beginning with an evaluation of the various aspects of the fretting condition such as partial slip, contact width, the fracture surface and crack initiation locations and progression. This is followed by a comparison of the data from room temperature and high temperature experiments under both plain and fretting fatigue conditions. Finally comparisons are made between the results of this study and other published high temperature studies of both titanium and nickel based alloys to establish the relevance of this study's conclusions.

4.1 Experimental Results

This study undertook a total of 17 independent tests; nine high temperature fretting fatigue tests, five high temperature plain fatigue tests and three room temperature fretting fatigue tests (Table 4.1). As mentioned in Chapter III, all axial loads for both fretting and plain fatigue tests had a constant stress ratio, R, of 0.03. All fretting fatigue tests were conducted with the same pad geometry and under the same contact loading conditions.

The applied stress range vs. number of cycles to failure curves, or S-N curves for all of these tests are plotted in Figure 4.1. Two tests, #1 and #6, were completely discarded because of experimental set up problems. Of the remaining 15 tests, all were executed under unique loading conditions except for test #9 which repeated the same testing conditions of test #7. The specimen associated with tests #2, #3, and #8 all failed outside of the fretting area. Specimen #3 failed in the transition region from the grip section to the gage section at the point where the radius of curvature ends. Test #8 failed below the fretting region but still inside of the gage section. Tests #2 and #10 both failed due to internal flaws in the specimens. Test #10 actually failed in the grip section of the

specimen (Figure 4.2). Test #11 failed very early in the low cycle region, much lower than expected thus this data point's validity is treated with some skepticism as a statistical outlier. Test #12 failed in the bottom portion of the gage section of the specimen and is believed to have failed at the point of greatest temperature gradient from the high temperature zone to the much cooler region below the lowest point of the heating elements. All of the data points correlated with these tests: #2, #3, #8, #10 and #12; have been labeled with an asterisk next to the number indicating that had they been permitted to fail under ideal conditions the number of cycles to failure would have been higher than indicated on the S-N curve.

4.1.1 Evaluation of Fretting Fatigue Conditions

Several different criteria are applied to ensure that the fretting condition was met for each fretting test. Crucial to establishing a test as a valid fretting test is confirming that it achieved the micro slip (i.e. partial slip) condition. Unfortunately there is no direct way of verifying this condition either during or after a test is complete; however it can be indirectly inferred from the data collected. As described in section 3.4, the calculated shear force, Q, can be plotted against the applied axial stress, σ_a, to create a hysteresis plot. These plots indicate how well the fretting condition was met for each test and how quickly it was achieved. Once the hysteresis plot collapses to a line then it is clear that the micro slip and therefore the fretting condition has been reached. Typically the fretting condition should be reached within the first 1000 cycles of the test.

Unfortunately the data from each of the fretting tests in this study did not initially indicate an ideal fretting condition. This was a significant concern throughout most of the testing and remained a mystery until it was determined that the peak axial stress and

peak shear force were only slightly out of phase with one another when they should have occurred at the same time. When the data is corrected for this small phase differential the hysteresis plots collapse to form a line as originally expected. The following section describes this technique in more detail.

4.1.2 Establishment of Partial Slip Condition Using Phase Analysis

The contact load, P, was commanded to be constant value of 4003N for all of the fretting tests at both high and room temperature. Although the contact load was intended to be a constant value it did however appear to exhibit a sinusoidal waveform that was slightly out of phase with the axial loading (see Figure 3.13). This was mentioned in section 3.4. The observed amplitude of the contact load was relatively similar for all fretting tests and the mean contact load was always approximately 4003N thus it is assumed that this contact load was sufficiently similar for all of the fretting tests and therefore not a significant source of variation form test to test. Because of this issue it became necessary to correct the observed data to cancel out the imposed phasing on the tangential loads.

In order to correct for this phasing first the axial loading must be compared with the calculated tangential loading. Figure 4.3 depicts the sinusoidal waveforms of both the applied axial loads and the calculated tangential load over time for test #8 at the 10,000th cycle. Notice that the magnitudes of the waveforms have been normalized to make for a clear comparison. From this it is clear that there is a slight phase difference equal to approximately 17.5 degrees. The phase difference was found to be constant over the entire range of loading profiles and did not change with respect to temperature. Figure

4.4 shows the same phase variance at the 100,000th cycle for test #8 and Figure 4.5 shows the same phase variance at the 10,000th for test #15.

Once this phase variance was isolated the original data was corrected for each fretting test and the new hysteresis plots were created. Figure 4.6 shows the difference between an uncorrected hysteresis loop and a corrected one. Once the correction is applied the corrected hysteresis loop immediately collapses to the line that is expecting indicating that the ideal fretting condition has been achieved.

4.1.3 Half Contact Width

One of the other characteristics of a fretting fatigue test is the contact region. The contact half-width, a, can be analytically calculated as well as directly observed after each experiment. Each fretting fatigue specimen was analyzed after it had failed under an optical microscope. Several images of each specimen's fretting scars on both the left and right side of the specimen were taken. The optical microscope also had the capability to measure the distances from point to point on each specimen. This technique was used to measure the contact widths of the fretting scars on each specimen. Table 4.2 lists the contact widths for most of the fretting fatigue tests conducted in this study. The values from each of these tests are consistent with one another as would be expected given the contact width is a function of the contact load, contact geometry and the material properties of the contact bodies. Since all of those values were essentially the same for each test they all have the same approximate analytical or expected value of 1.22 mm or 1220 micrometers. It is important to note that none of the fretting contact width in this study exactly matched the analytical value but several were close. There are any number of issues that could perturb the observed values. One in particular with regards to this

study is the previously mention variation in the applied contact load. Also it is possible that early in the fretting experiment gross slippage created some obscurities that make it harder to accurately distinguish the true contact region from the surrounding areas. At any rate, Figures 4.7, 4.8 and 4.9 are images from the optical microscope of the fretting scars from tests # 16, 4 and 9 respectively.

4.1.4 Crack Initiation Location

Theoretically the cracks should always initiate at the point where the combined stress conditions, particularly the shear stresses, are the greatest. As discussed in section 2.5.1, the location of maximum shear stress lies on the critical plane which is at angle in between the contact surface and the contact load. This plane also tends to run through the line that forms the boundary of the contact region because it is expected that the state of stress is maximized at or very near this location. While it is very difficult to actively monitor crack initiation in real time during an experiment, it is possible to analyze each specimen after it has failed for evidence of crack initiation. As mentioned in the previous section, every specimen was observed under an optical microscope and images were captured. These images were then analyzed for comparison of the experimental crack initiation locations to the analytically expected locations.

Figure 4.10 is an image of a specimen from test #4 and it clearly depicts the fretting fatigue crack originating at the edge of the contact region as expected by the analytical predictions. Figure 4.11 is another image from the optical microscope of the specimen used in test #7 also clearly showing the fretting fatigue crack initiation at the edge of the contact region. These two figures are typical of the optical microscope images of the fretting scars on most of the ten fretting fatigue specimens in this study;

seven at high temperature and three at room temperature. In seven of the ten fretting fatigue specimens, the fretting fatigue cracks initiated at or very close to the edges of the contact region. The exceptions were the specimens from tests #2, 3 and 8 which, as mentioned earlier in this chapter, failed well outside the fretting region due to other defects or flaws. In conclusion, in each of the seven fretting fatigue tests that failed due to fretting fatigue, the fretting cracks initiated at or very near the edges of the contact region as expected. This further supports the assertion that these tests were valid fretting fatigue tests and the data from these tests is suitable as such.

4.1.5 Fracture Surface Area

The facture surface is the exposed portion of the specimen after it has failed. Analyzing the fracture surface is an important technique for understanding what physically occurred during the test. There are always two fracture surfaces created when a specimen fails; one from the top portion of the specimen and one from the lower portion. Each surface is the reciprocal of the other and consequently a feature found on one surface should be equally evident on the other. In this study the fracture surfaces of the lower portions were typically the ones analyzed because the nature of the test procedures. Unfortunately in each high temperature test after the specimen broke, the test procedure software would leave the electric heaters operating. The top portion of the specimen would still be in nearly the same position as during the test therefore it remained in the hot zone after the test was complete, sometimes for several hours, and was over exposed to the high temperature environment. This exposure leads to oxidation that alters the surface making it difficult to analyze. Several attempts were made over the

course of this study to modify the test procedures to prevent this from occurring but none ever met with success.

From studying the fracture surface one can observe where the crack initiated as well as the different regions of the crack's growth. Recall that there are four stages of crack development in fretting fatigue: initiation, propagation due to bulk and contact stresses, propagation due to just bulk stresses and finally fracture. Figure 4.12 is a Scanning Electron Microscope (SEM) micrograph of the fracture surface from the specimen in test #5. Dashed lines have been added as well as text labels to highlight the different regions each labeled with a roman numeral, I - IV, associating it with the particular stage of crack development of that region. Also labeled is the point determined to be the origin of the crack. Figures 4.13 and 4.14 are also SEM micrographs from test #4 and test #7 respectively.

Notice the relative sizes of each of the four crack regions. The crack initiation region is the smallest area with each successive stage generally being larger than the previous stages. This is to be expected as the crack is growing faster with each stage. One might think that the relative areas of each stage represent the relative time spent in each stage but this is certainly not the case. The time spent in the final stage, stage IV, is infinitesimally small as once the crack has grown large enough such that the combination of crack geometry and applied loading is equivalent to the critical stress intensity factor, K_{Ic}, fracture occurs instantly. Conversely, as was stated earlier in chapter II, the crack initiation stage is the stage in which the longest amount of time is spent yet it represents the smallest area. The relative time spent in each stage varies inversely with the total area of each stage. This draws attention to the rate at which the crack must be in

advancing in each stage; how slowly it advances in the earliest stage and how rapidly it advances towards the end.

Another general relationship can be inferred from comparing the relative sizes of the areas associated with same stages from different specimens and the relationship of the applied loads from those stages. In comparing the areas from the second and third stages from tests #4 and #7 as shown in Figures 4.13 and 4.14, one notices that the areas in Figure 4.14 associated with test #7 are smaller than in test #4. This is most likely due to the fact that test #7 was subjected to a higher applied stress range, at 921.5 MPa, versus test #4 at 727.5 MPa. This relationship is a weak one however as it is dependent on crack geometry. Notice that test #5 was conducted at a stress range, 824.5 MPa, in between tests #4 and #7. If the areas of stages II and III from test #5 are compared to those from test #4 and #7 then it would seem that test #5 was conducted at much lower applied stress range than it actually was. The crack geometry is also no doubt ultimately dependent on where the crack initiated. This makes understanding crack initiation location all the more important as it clearly affects all of the other stages dramatically and ultimately influencing the total fatigue life.

4.2 High Temperature Effects on Plain and Fretting Fatigue

The ultimate purpose of this study is to determine what effect elevated temperature has on the fretting fatigue properties of IN-100. To properly determine the effects of temperature it is best to compare data from several different scenarios in order to isolate the characteristics that are different from those which are similar. Therefore it follows that these isolated characteristics or differences are what must be responsible for the change in behavior, if any, that is observed. This study utilizes the data provided

from Madhi's [11] (Table 4.3) and Saladin's [10] (Table 4.4) previous IN-100 studies as well as the experimental data that was introduced in the previous section.

4.2.1 Room Temperature Plain Fatigue vs. Fretting Fatigue

The conclusions reached by both Mahdi [11] and Saladin [10] confirm that fretting fatigue life is less than plain fatigue life under identical stress ranges. This is the same conclusion reached by every other fretting fatigue study of which this author is aware. The extent to which the fretting fatigue condition reduced the fatigue life at room temperature has been determined to be on the order of 30% to 35% less than plain fatigue conditions. This is an important relationship to consider when characterizing the effects of elevated temperature.

4.2.2 High Temperature Plain Fatigue vs. Fretting Fatigue

As with the room temperature studies, the premise holds that the fretting condition reduces the life of IN-100 as compared to the plain fatigue condition for identical stress ranges. Unfortunately, the data gathered by this study is not sufficient to reliably characterize how much fretting reduces the number of cycles to failure for the same stress ranges but it does appear to be greater than the 30% to 35% reduction observed at room temperature. Table 4.5 provides a short list of the comparisons between high temperature plain and fretting fatigue. The most valid comparison can be made between test #12 and test #9 which yields a reduction in life by 56.5%. The comparison between test #10 and test #3 is skewed by the fact that both tests failed earlier than they should have yet this still indicates a substantial reduction in life of 91.8%. A comparison of test #10 to test #5 is a little better despite the fact that test #5 was tested at a slightly higher stress range, yet it still indicates a reduction in life of 83.1%. Clearly the

fretting condition in the elevated temperature environment has a much more noticeable effect on the fatigue life of IN-100 than the room temperature environment.

4.2.3 High Temperature vs. Room Temperature Plain Fatigue

The high temperature plain fatigue life exceeded the room temperature plain fatigue life of all of Saladin's experiments except test #11 which failed much sooner than expected and consequently is regarded as a statistical outlier. Figure 4.15 is a plot of the S-N data points from the high temperature plain fatigue tests from this study and the plain fatigue S-N data points from Saladin's room temperature plain fatigue tests. Also, the extent to which the fatigue life is extended seems to be related to the applied stress level in each test case. Table 4.6 provides a short list of the following comparisons and the apparent increase in fretting life for each applied stress range.

The lower the applied stress, the greater the high temperature environment increases the number of cycles to failure while in the higher applied stress tests the temperature effect was not as great. This is consistent with the findings of Kawagoishi et al. [21] in Inconel 718, another nickel-based super alloy, in which the fatigue life increases with temperature except in the short life region. Kawagoishi also noted that the fatigue life was especially longer at high temperatures when compared to testing done at room temperature.

4.2.4 High Temperature vs. Room Temperature Fretting Fatigue

The high temperature fretting tests also exhibited an increase in the number of cycles to failure when compared to identical applied stress conditions at room temperature. The data indicates that higher temperature increases fretting fatigue life as compared to room temperature fretting just as was observed in the plain fatigue tests.

Figure 4.16 is a plot of the S-N data points from the high temperature fretting fatigue tests from this study and the fretting fatigue S-N data points from this study's and Saladin's room temperature fretting fatigue tests. Table 4.7 provides a list of the following comparisons of fretting fatigue life at various applied stress ranges.

The most striking comparison is between test #8 and test #15, both at the 630.5 MPa stress range, which indicates an increase in life of more than an entire order of magnitude (12.8X increase). When test #8 is compared to Saladin's test #3, also at 630.5 MPa stress range, the life increase is still very dramatic (6.4X increase). Test #8 does not appear as remarkable when compared to Madhi's test #1 (also at 630.5 MPa stress range) which was a declared a run out at 5,900,000 cycles compared to 5,565,917 cycles from test #8 yielding an actual reduction in life of 5.7%; however, recall that test #8 failed prematurely as it failed outside of the fretting region and so this comparison can not be entirely trusted.

At the 727.5 MPa stress range, the comparison of the data from test #4 to Madhi's test #2 yields an increase in life of 62.6%. Comparisons at the 776 MPa stress range are hindered by the fact that test #3 failed prematurely but if the data from test #5 (which was at a slightly higher stress range) is compared to Saladin's test #5 and Madhi's test #3 results in an increase in life of 69.8% and 44.1% respectively. At the 824.5 MPa stress range the comparison of the data from test #5 again to Madhi's test #4 yields an increase in life of 163.3%.

This clear increase in life does not span the entire scope of testing however as once the stress range is increased to 921.5 MPa the data from tests #7 and #9 fall very close together with Saladin's test #6 and Madhi's test #5. In fact, it appears that all of these data points lie within the expected scatter bands of each other. Still, it seems clear

that the high temperature environment does have a beneficial effect on the fretting fatigue life and that benefit is noticeably greater at lower stress ranges.

Figure 4.17 shows the high temperature trends from this study next to the room temperature trends from Saladin's study. Whereas the room temperature data lines show the plain fatigue curve with a nearly constant bias, as plotted on a logarithmic scale, the high temperature trend lines indicate a wider bias at the lower stress ranges. To be certain, more data points would be necessary to improve the accuracy of the slopes of the high temperature trend lines, especially the plain fatigue trend line, but the data does appear to support this assertion at this time.

Figure 4.18 is a plot of the shear force range vs cycles to failure from all of the test in this study as well as Saladin's and Madhi's tests on IN-100. At first glance the data on this plot is not very conclusive, but after some study a few observations can be made. First, it is clear that the shear force range from the tests conducted in this study were consistently lower than the shear force ranges of the other studies' tests. Second, the other studies data points indicate that higher shear force ranges tend to decrease fretting fatigue life more than lower shear force ranges. Third, this trend between higher shear force range and lower fatigue life is curiously absent from the high temperature data. Perhaps this has something to do with the high temperature environment or perhaps it is just something peculiar about the fretting apparatus used in this study compared to the previous studies.

4.3 Relevance to Other High Temperature Fretting Studies

This section focuses on the comparison of this study's results with other high temperature studies. Comparisons are drawn from high temperature examinations of

titanium alloys, especially Ti-6Al-4V, and high temperature studies of other nickel-based super alloys, some which have even included IN-100. The similarities and differences of each study's testing materials and conditions are discussed as well as the similarities and differences of their conclusions of the effect of high temperatures.

4.3.1 Comparison to High Temperature Titanium Alloy Fretting

In section 2.6.2 several studies were introduced that each had studied the affect of elevated temperature on the fretting fatigue of titanium alloys. Each of those studies concluded that elevated temperatures had an adverse impact, though not necessarily a dramatic one, on fatigue life. The results from this study however clearly indicate that IN-100 does not behave the same way as titanium based alloys in the elevated temperature environment. It should be noted however that the temperatures utilized in most of the elevated temperature studies of titanium alloys (200 to 300 C) were well below the elevated temperature of this study (600 C). Although it is possible that the results could vary if titanium alloys were studied at 600 C, it is doubtful that their fretting fatigue lives would increase. The author of this study believes that no comparisons can be successfully drawn from fretting fatigue behavior of titanium alloys elevated temperature and nickel-based alloys fretting fatigue behavior at elevated temperature.

4.3.2 Comparison to High Temperature Nickel-based Super Alloy Fretting

In section 2.6.4 several studies were introduced regarding the previous efforts known to this author on the high temperature fatigue and fretting fatigue behavior of nickel based super alloys. Of these several studies presented, three in particular provide an excellent basis of comparison for the results of this study.

The results of Shyam et al. [43] demonstrated that the effects of elevated temperature (593 C) and at relatively low frequency (10 Hz) lead to an increase in fatigue life in Rene' 88 DT, a nickel based superalloy. Shyam did not provide many details as to how much the fatigue life increased compared to room temperature (20 C) but from analyzing the data from one figure it appears to have been an entire order of magnitude to perhaps two orders of magnitude increase at lower applied stresses.

Hamdy and Waterhouse's [45] earlier fatigue study of Inconel 718 at temperatures up to 540 C also indicated that the fatigue life increased noticeably with increasing temperatures. The increase they measured was as much as 130%. Kawagoishi's [21] results from studying Inconel 718 at 300 C, 500 C and 600 C (Figure 4.19) show a trend toward increased life in the high cycle fatigue region but not in the low cycle fatigue region. Furthermore, his results indicate that the fatigue limit tends to increase with the increase in temperature except that at higher stress levels the fatigue life is subdued by the weakening of the material as it increases in temperature. The higher temperatures promote two phenomenon; the softening of the nickel matrix and the creation of oxide films. The oxide films are the chief reason for the increase in fatigue life because they promote crack closure. The softening of the material is detrimental to the static strength of the material but it is beneficial in that it can lead to plasticity induced crack closure.

Jha et al. [48] studied a P/M nickel-based superalloy under plain fatigue at a temperature of 650 C with a stress ratio of 0.05. Their findings also indicate an increase in fatigue life at elevated temperatures. Figure 4.20 shows the median trend line of the results from this study. Figure 4.21 shows the high temperature plain fatigue data from this study along with the high temperature fatigue data from the Jha [48] and Kawagoishi

[21] studies. From this figure it is clear the overall trend in high temperature fatigue in each study was similar. The vertical placement of the three curves is related to the stress ratio from each study with the highest ratio, 0.05, on top and the lowest ratio, -1, on bottom with the trend line from this study falling in between the two other lines as expected considering the stress ratio, 0.03, also fell in between these two studies. Ultimately, the high temperature fatigue behavior of nickel-based superalloys, whether IN-718 or IN-100, appear to be relatively similar to one another and exhibit increased fatigue life at elevated temperatures.

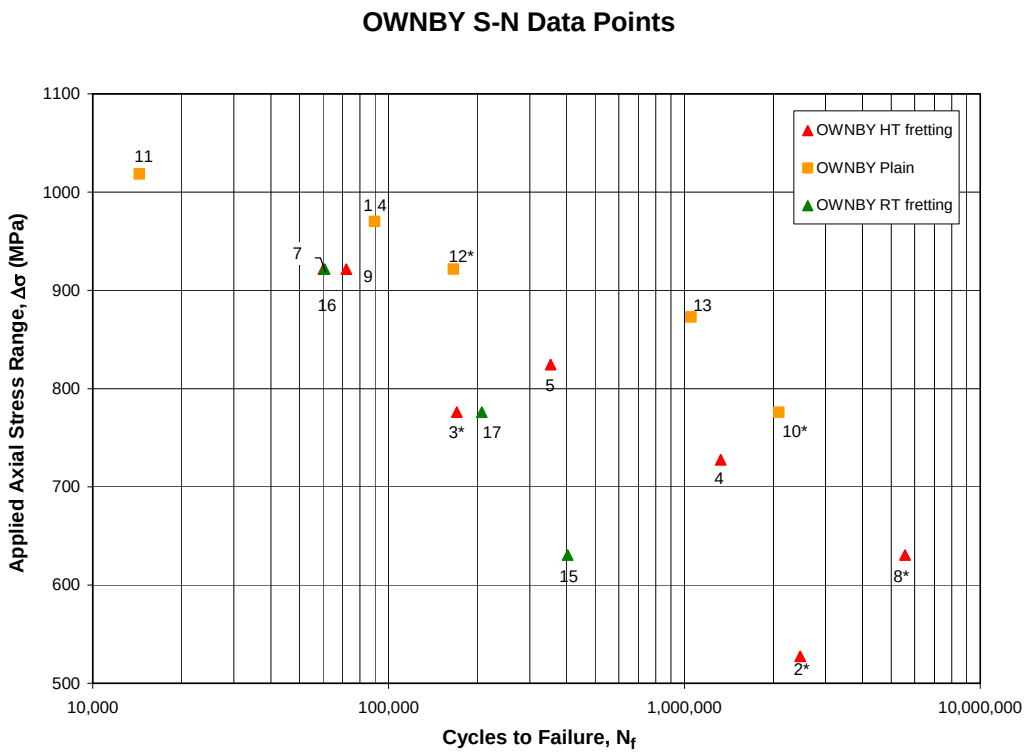

Figure 4.1 S-N data points for all tests in this study

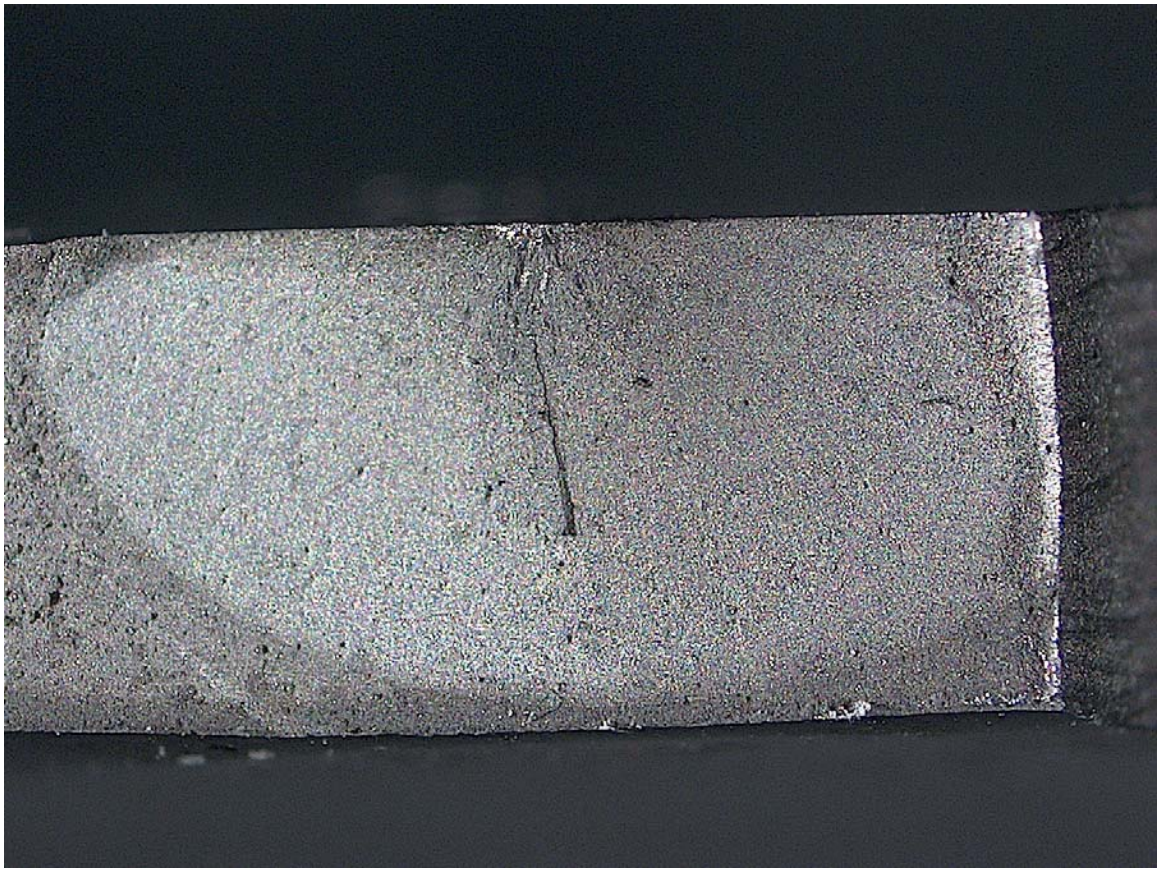

Figure 4.2 Optical Micrograph of internal flaw in specimen 10

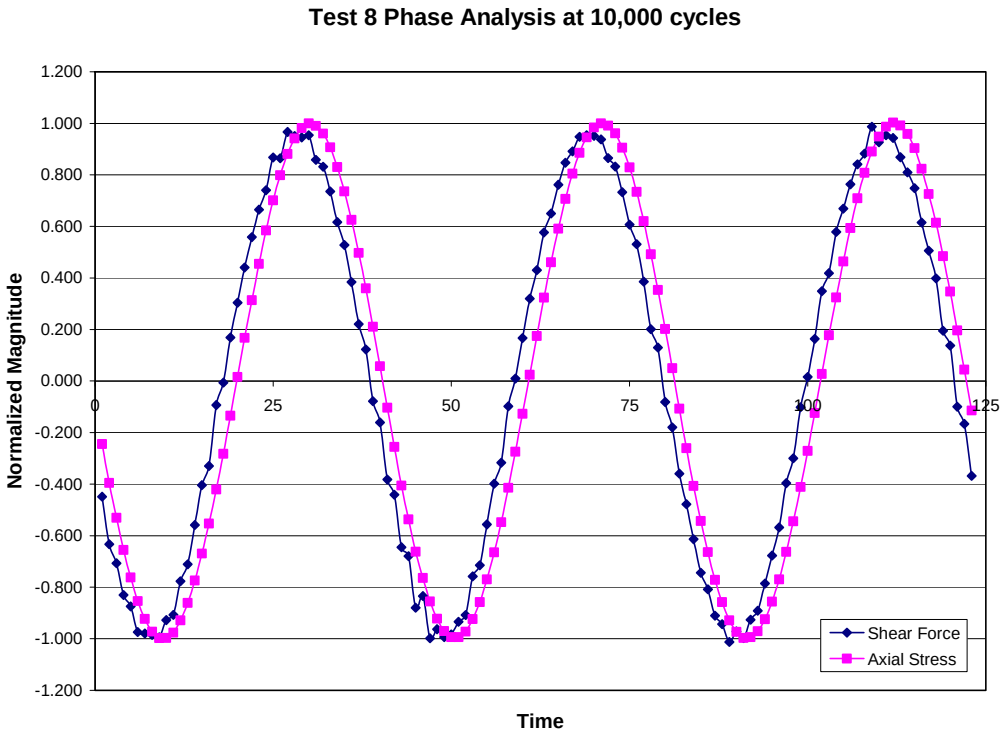

Figure 4.3 Phase of shear force and axial stress signals test #8 10,000th cycle

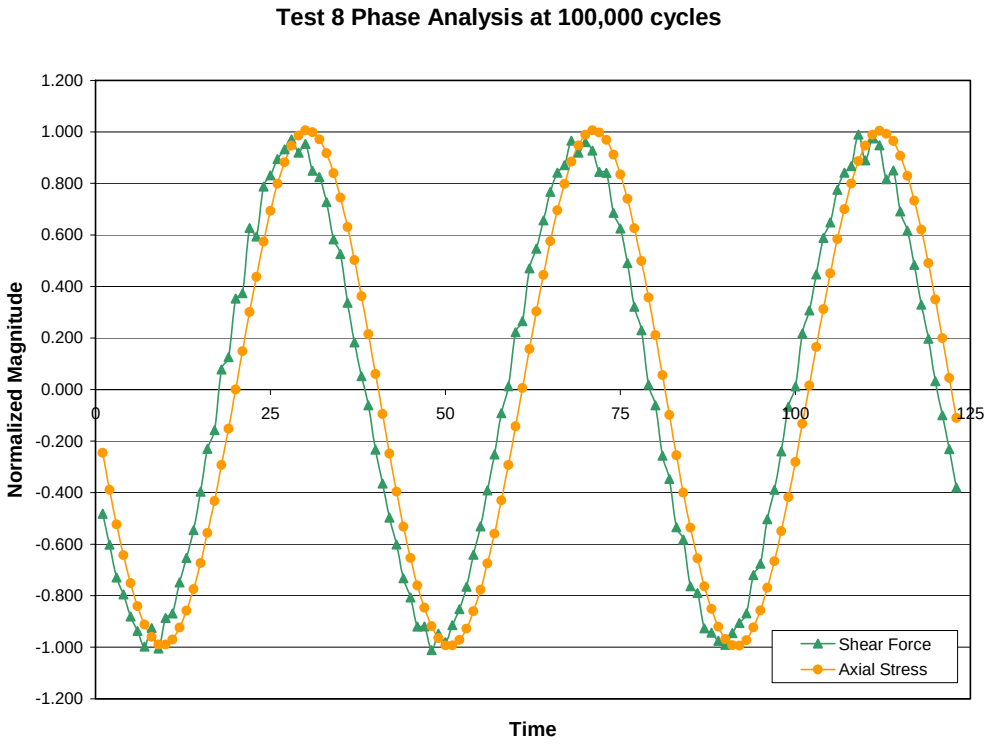

Figure 4.4 Phase of shear force and axial stress signals test #8 100,000th cycle

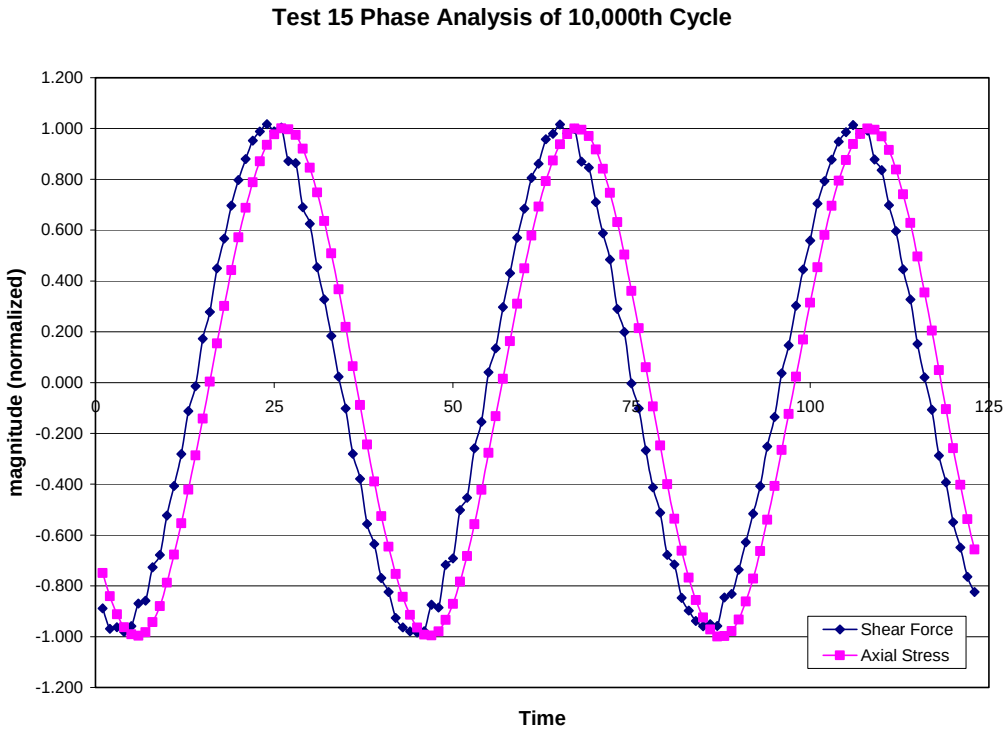

Figure 4.5 Phase of shear force and axial stress signals test #15 10,000th cycle

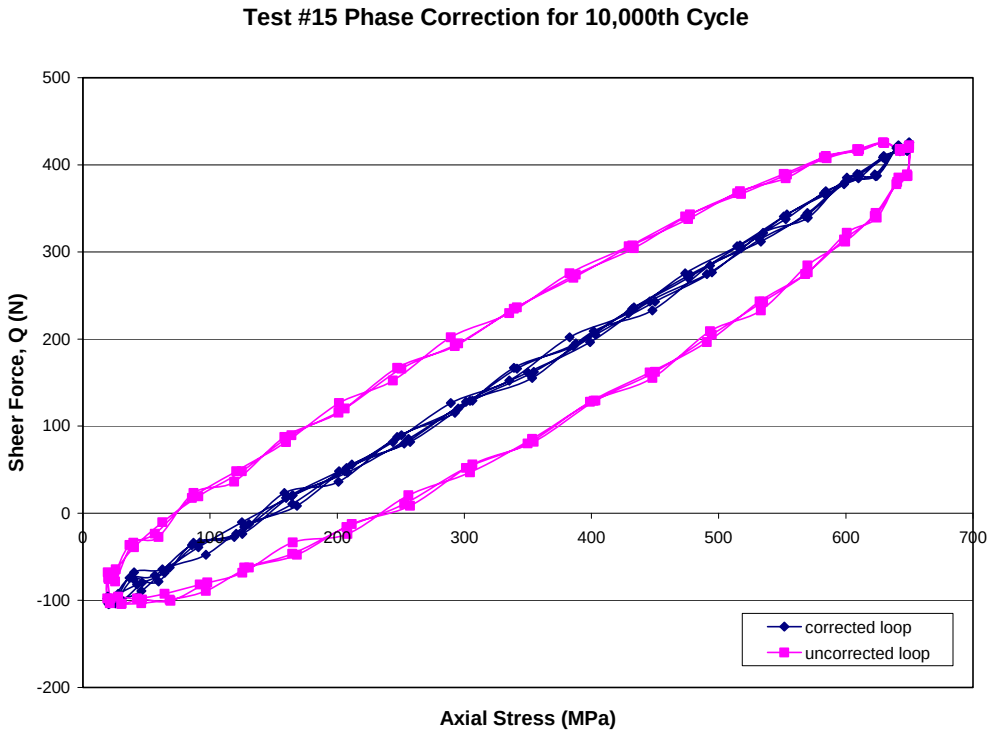

Figure 4.6 Hysteresis loops with and with out phase correction

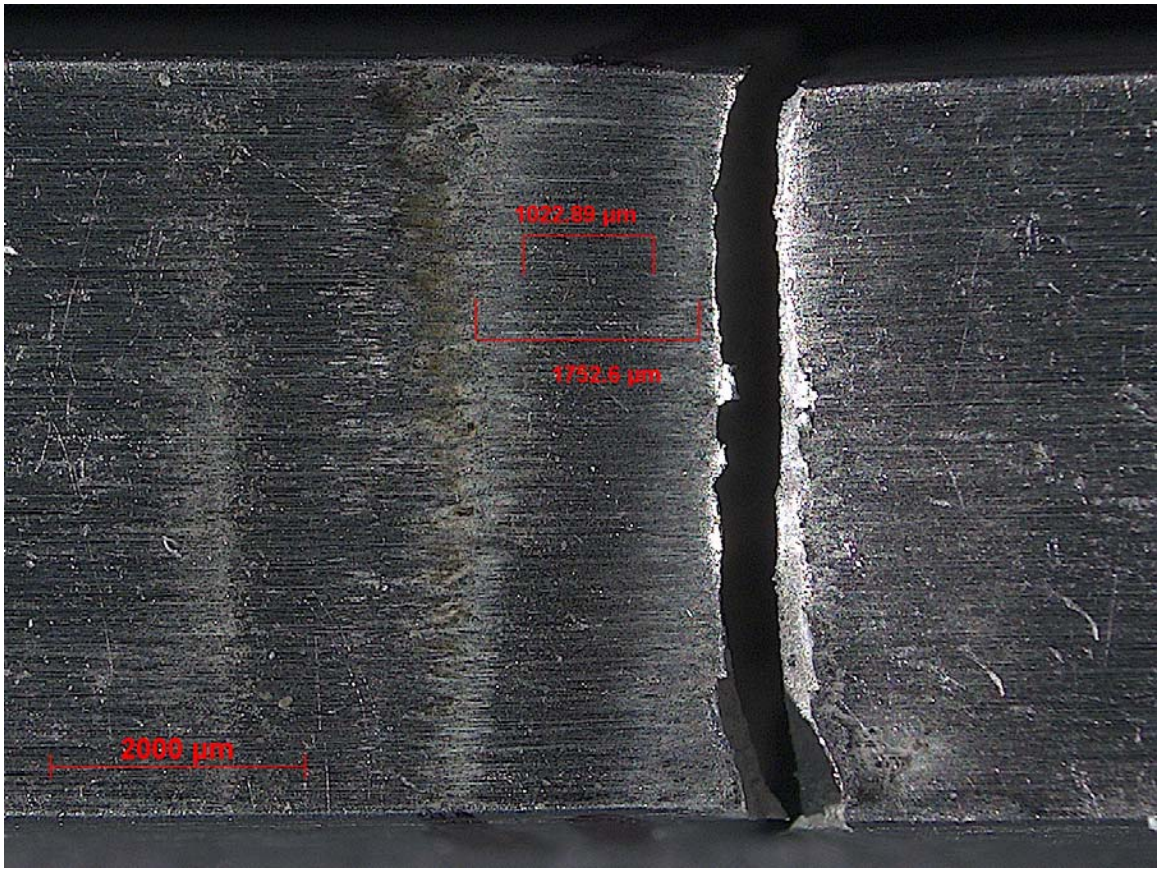

Figure 4.7 – Fretting scar from test #16

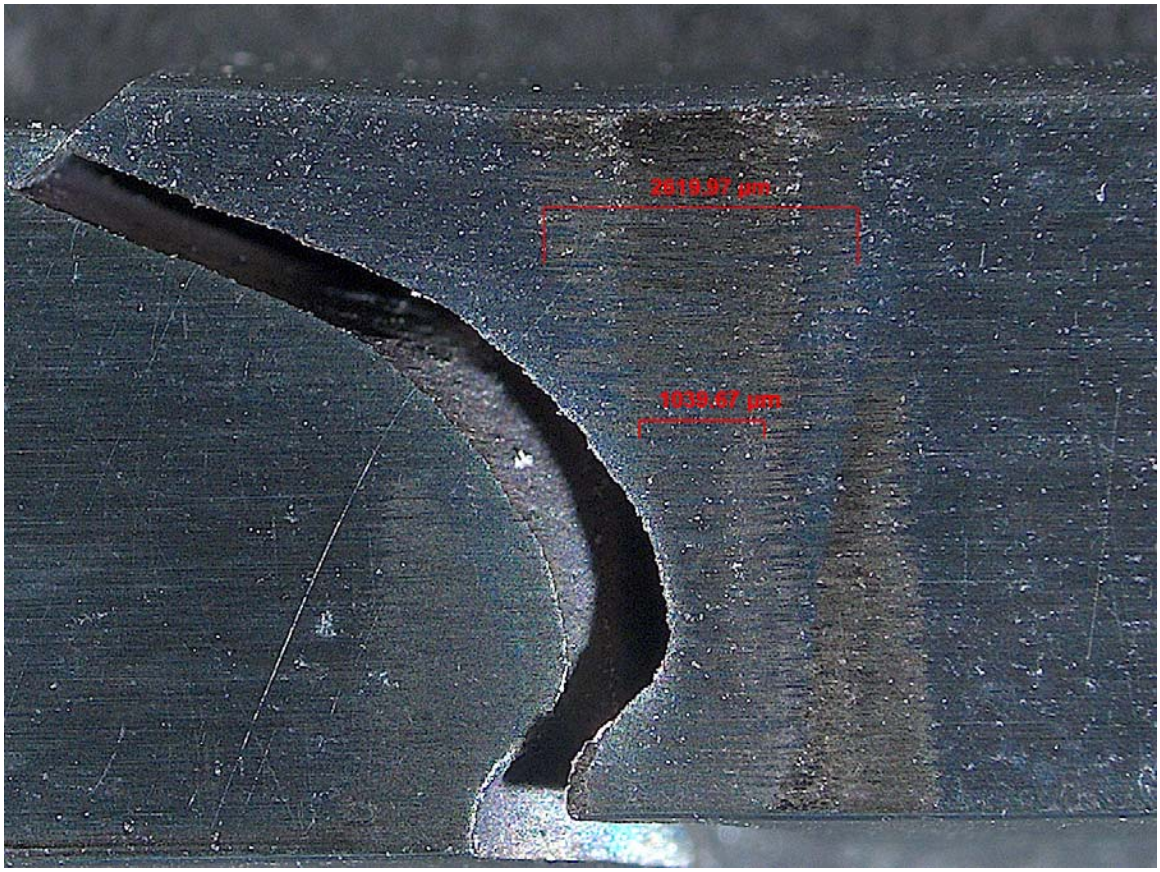

Figure 4.8 – Fretting scar from test #4

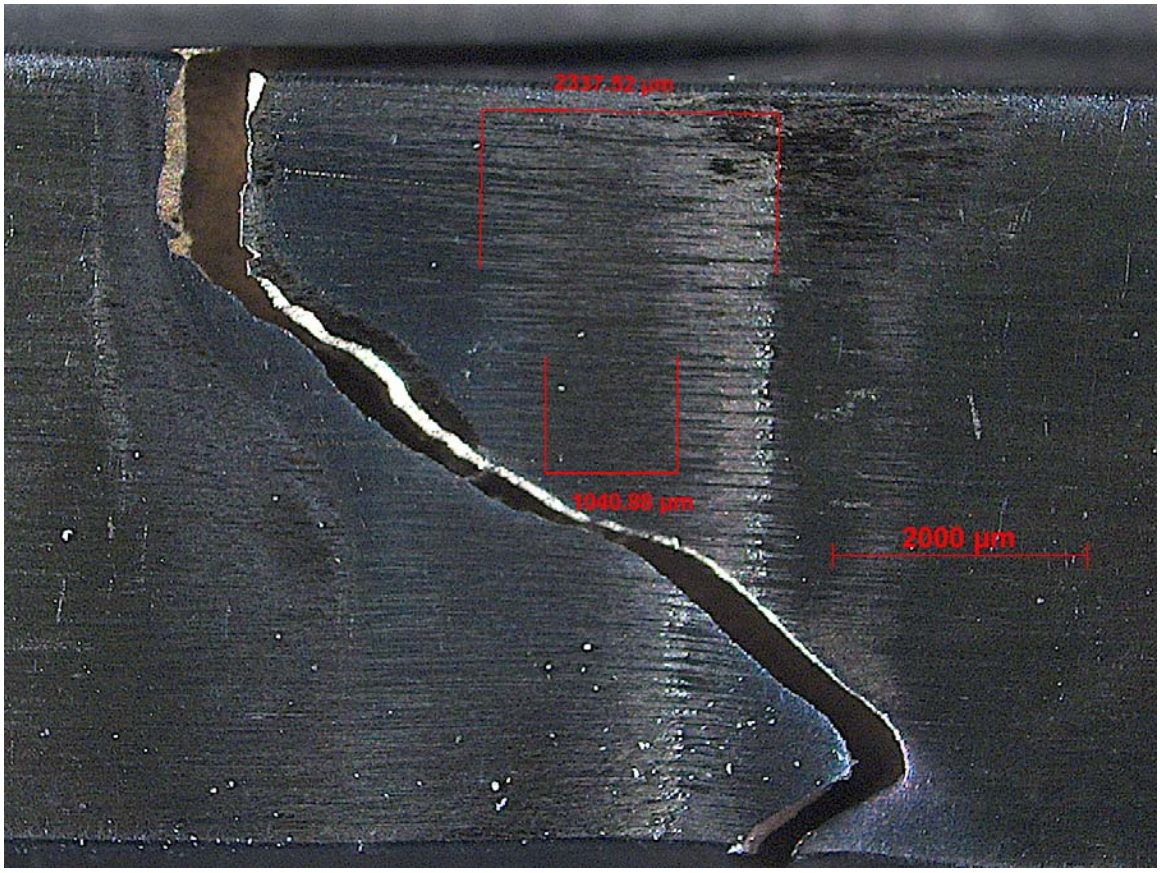

Figure 4.9 – Fretting scar from test #9

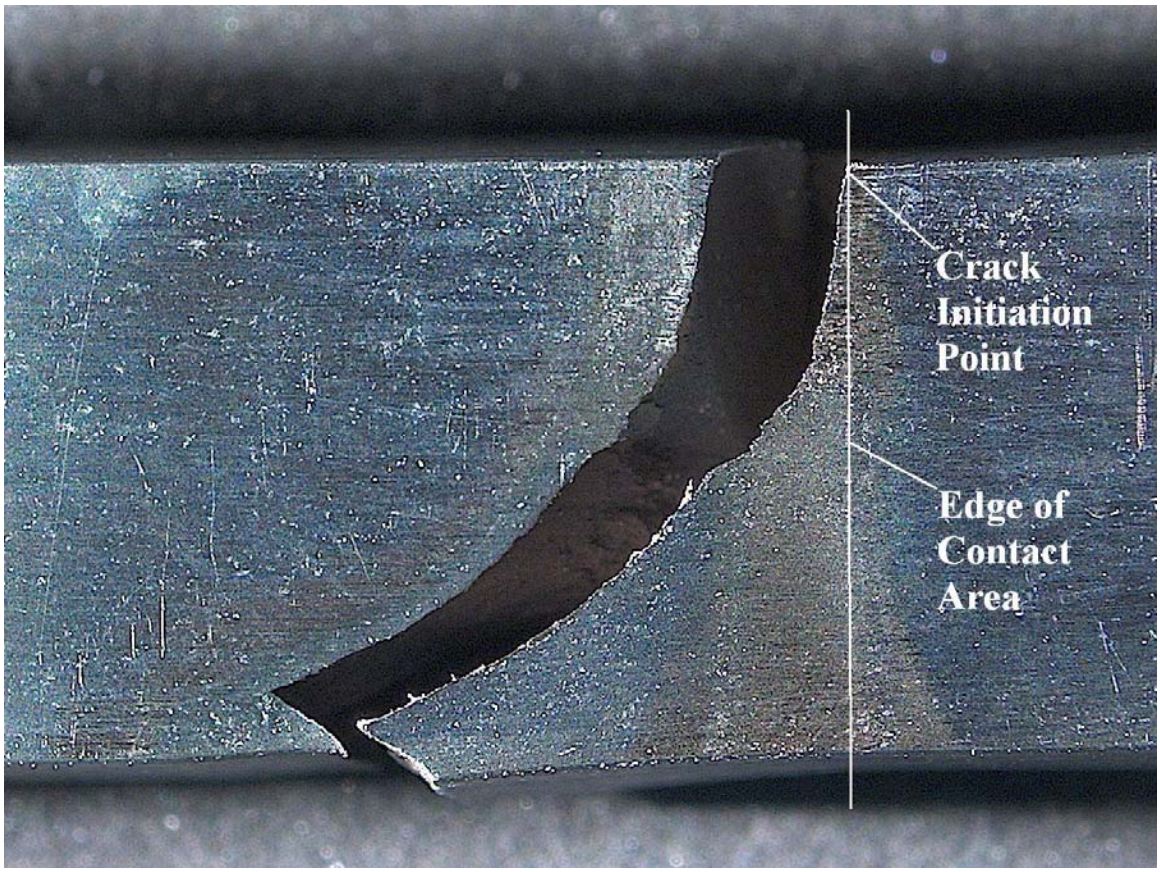

Figure 4.10 Optical microscope image of specimen from test #4

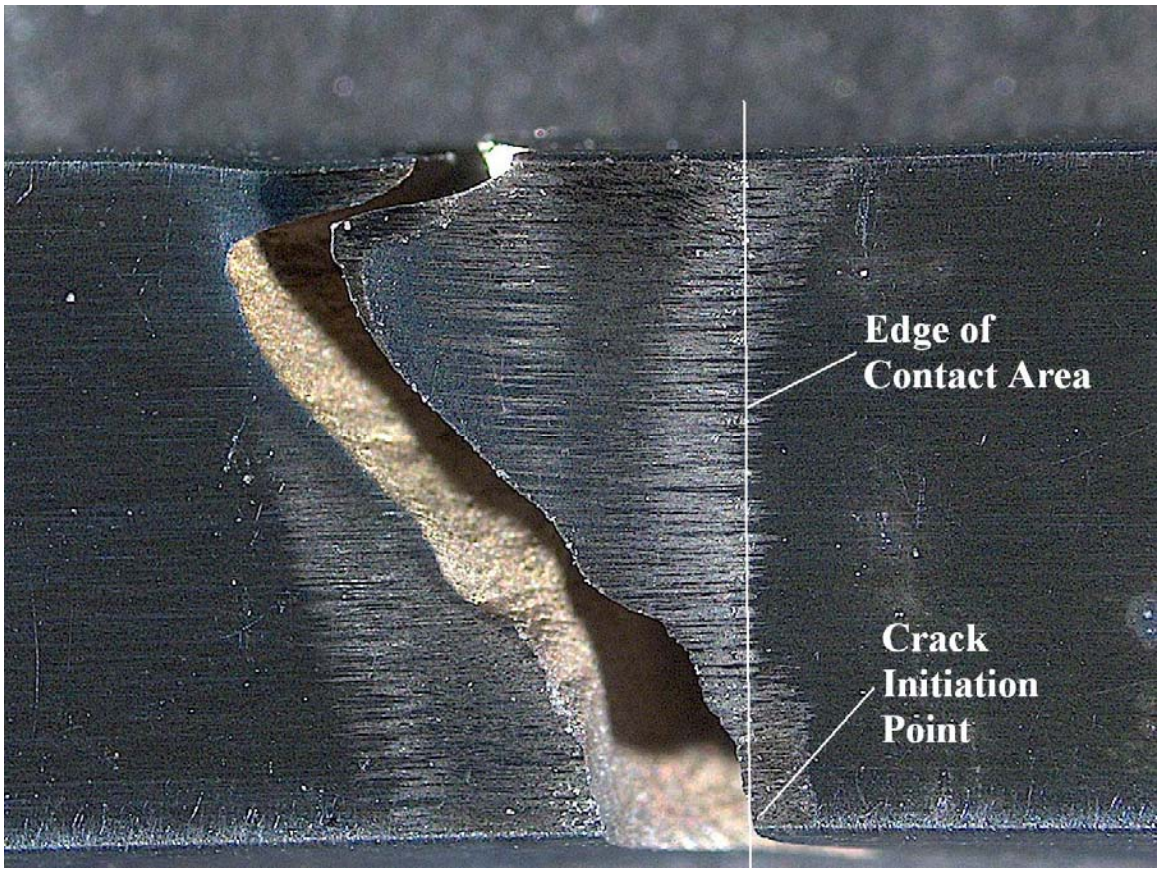

Figure 4.11 Optical microscope image of specimen from test #7

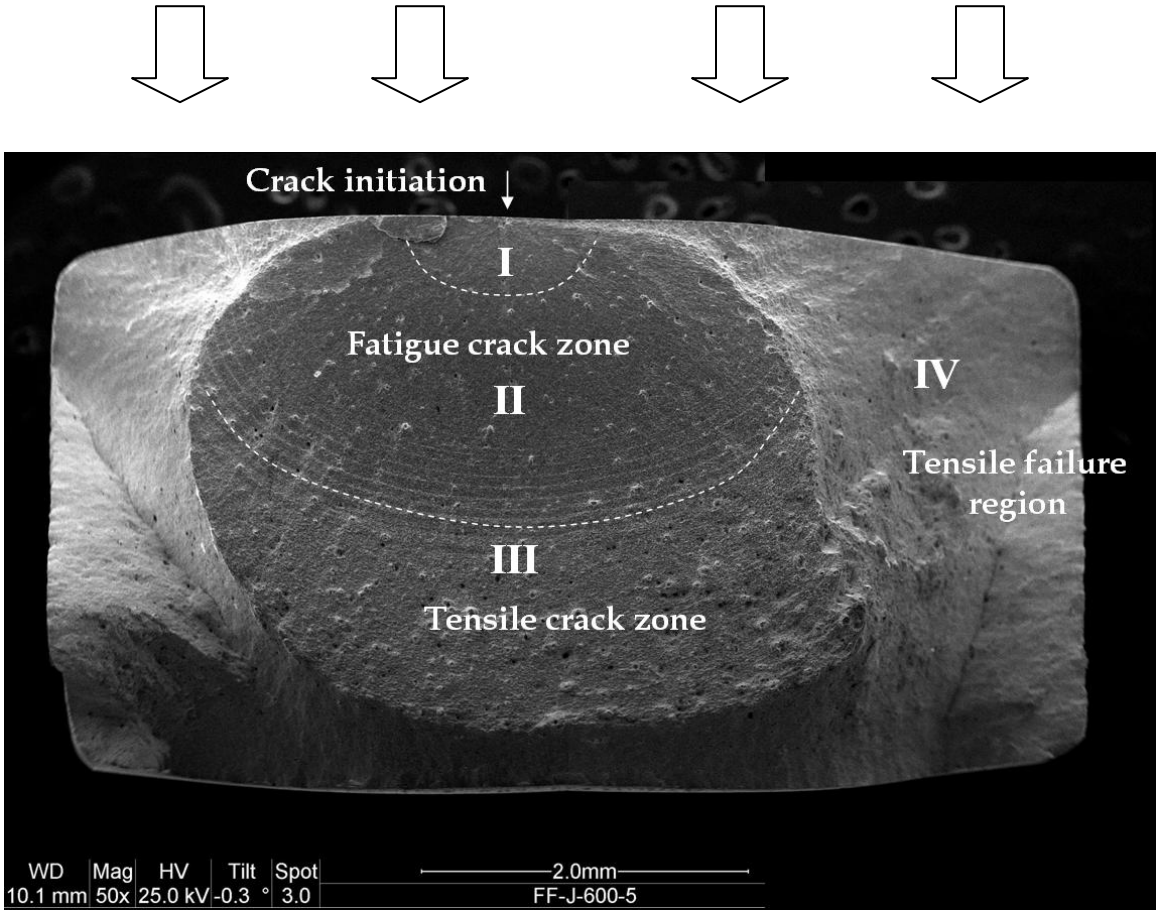

Figure 4.12 SEM micrograph of specimen from test #5

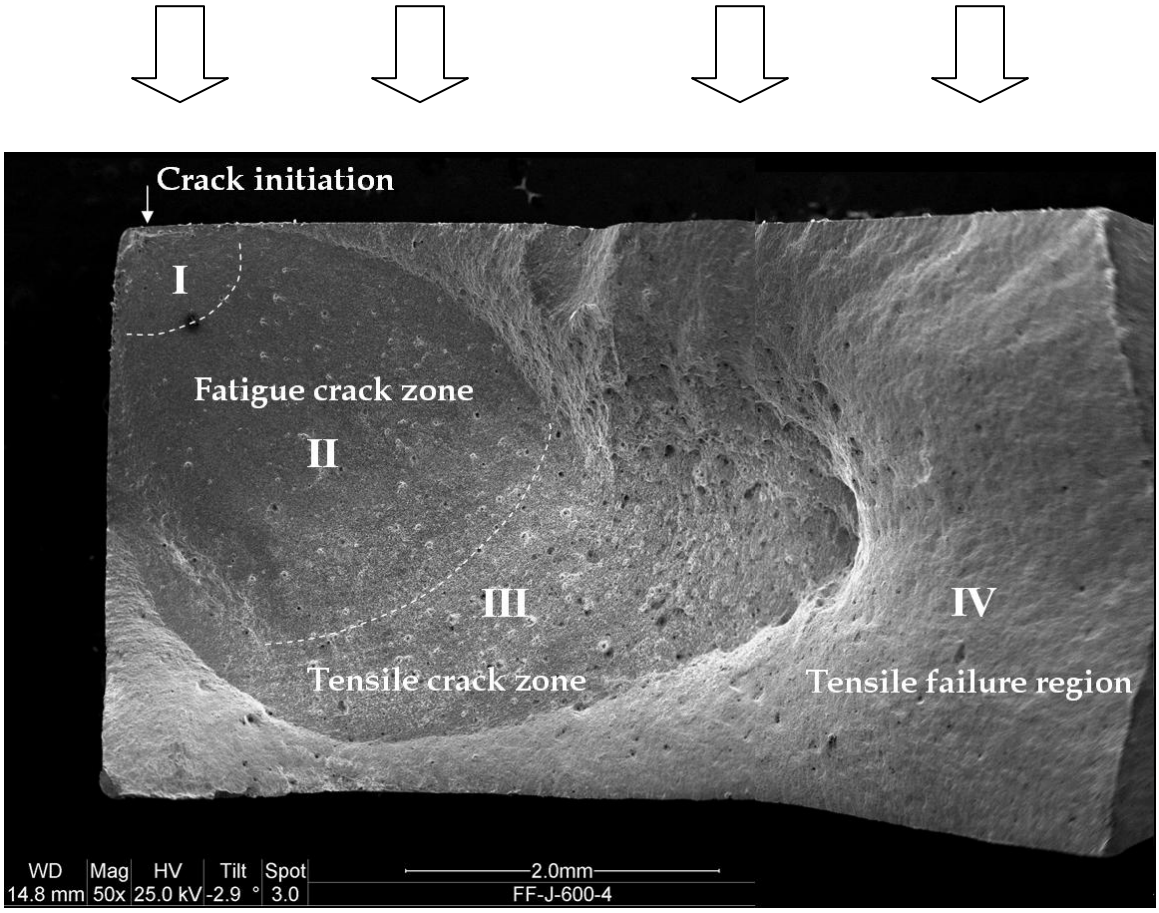

Figure 4.13 SEM micrograph of specimen from test #4

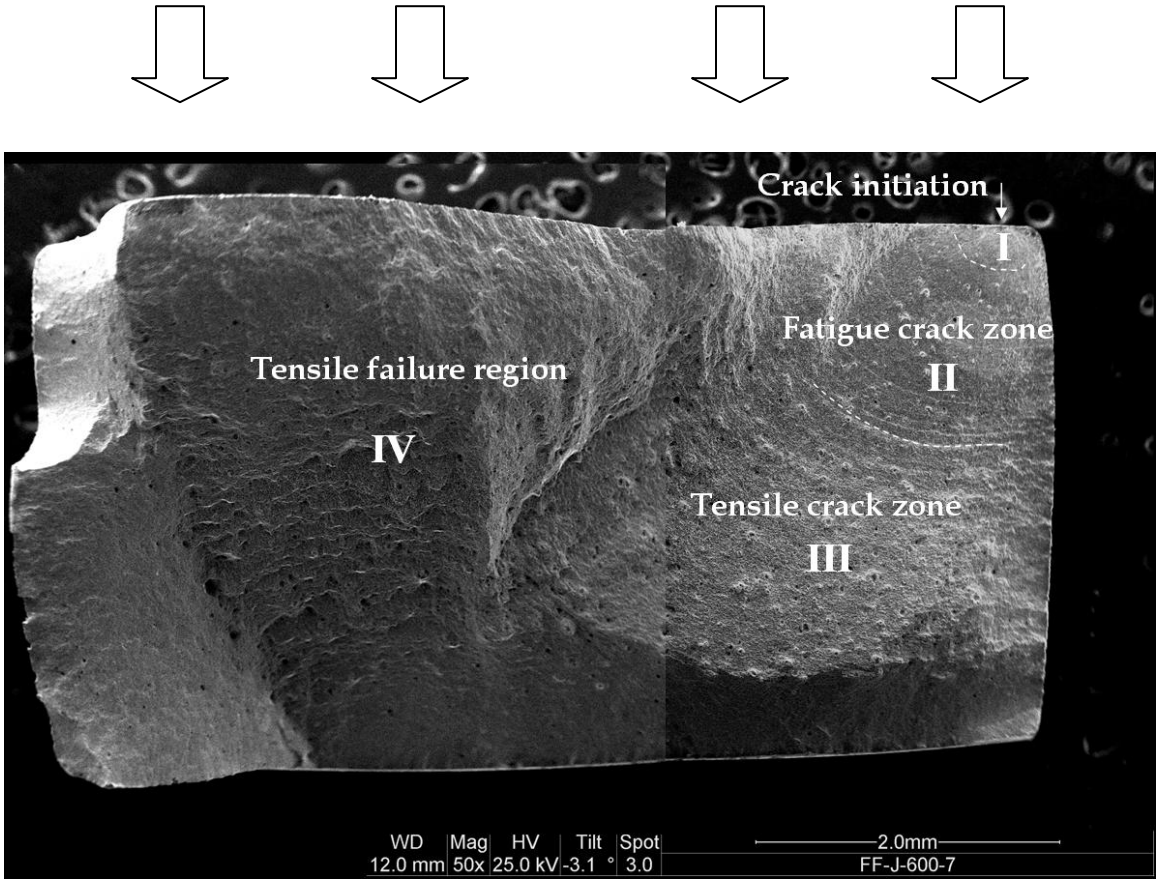

Figure 4.14 SEM micrograph of specimen from test #7

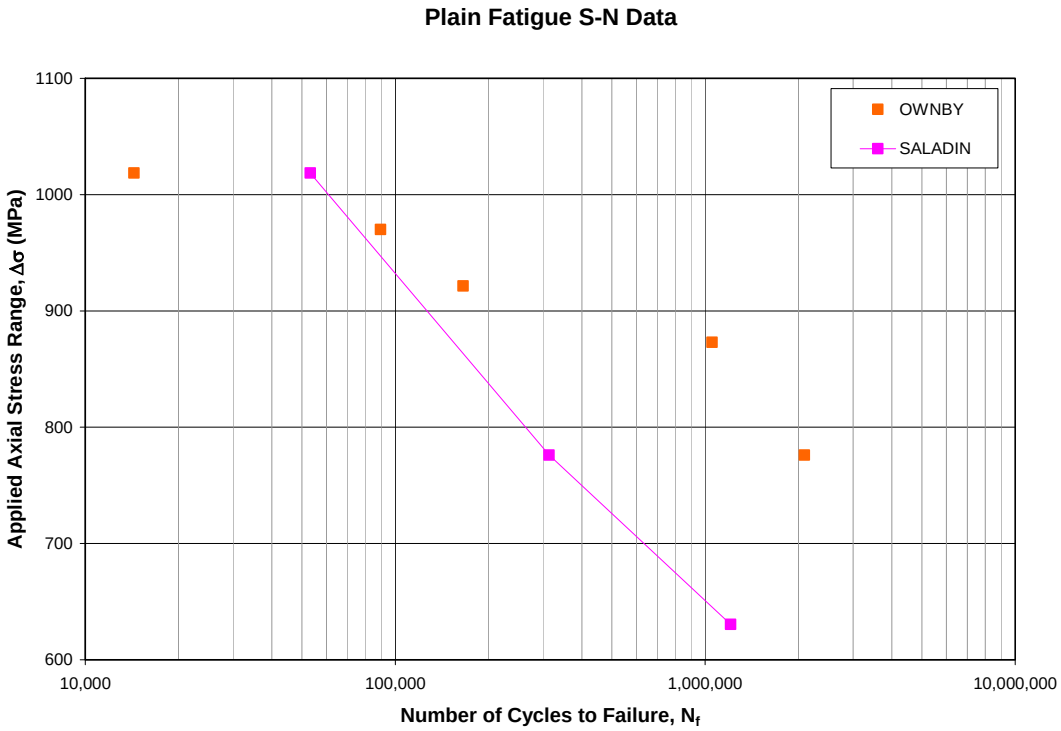

Figure 4.15 Comparison of Ownby and Saladin S-N data points for plain fatigue

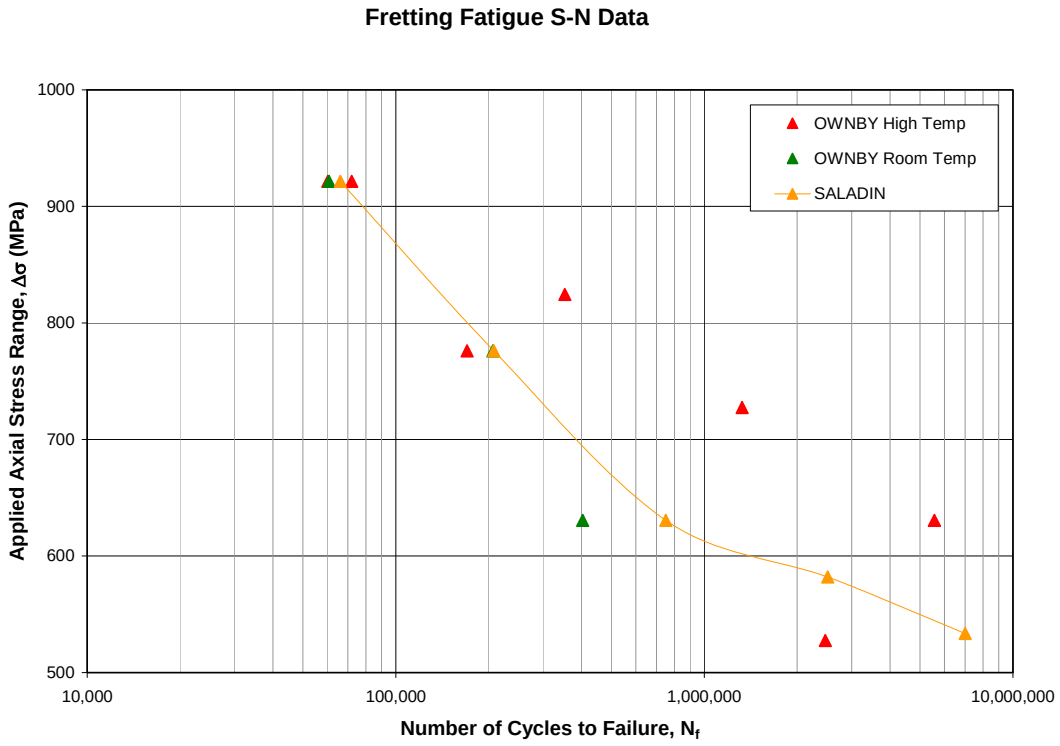

Figure 4.16 Comparison of Ownby and Saladin S-N data points for fretting fatigue

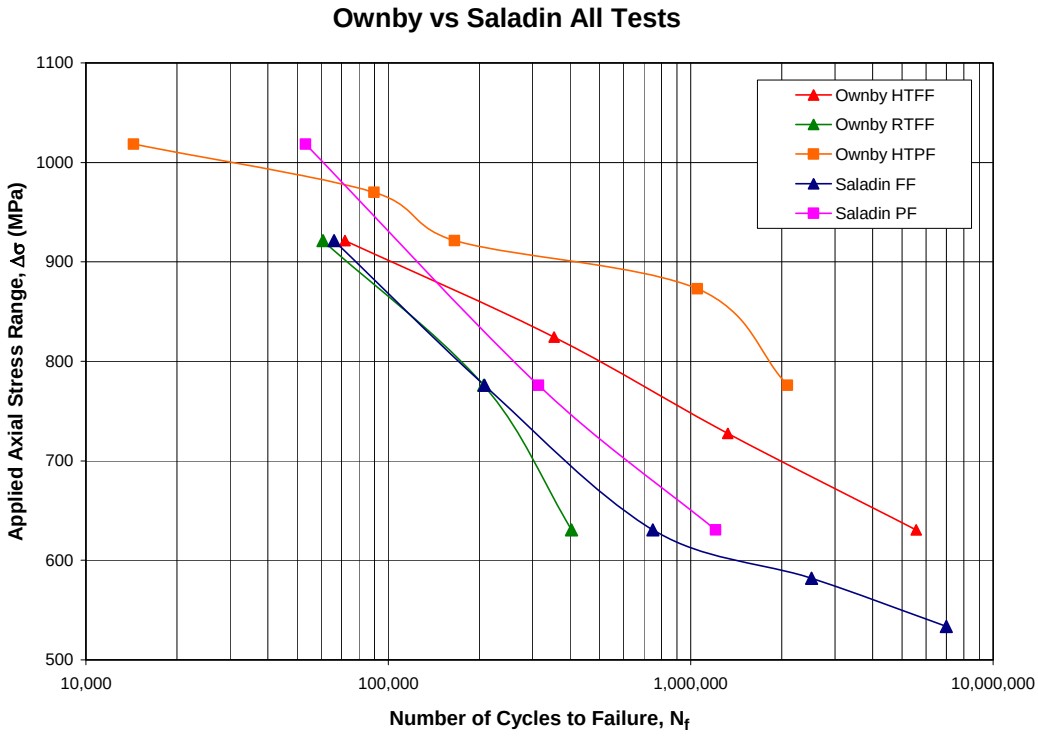

Figure 4.17 Comparison of Ownby and Saladin S-N data for all tests

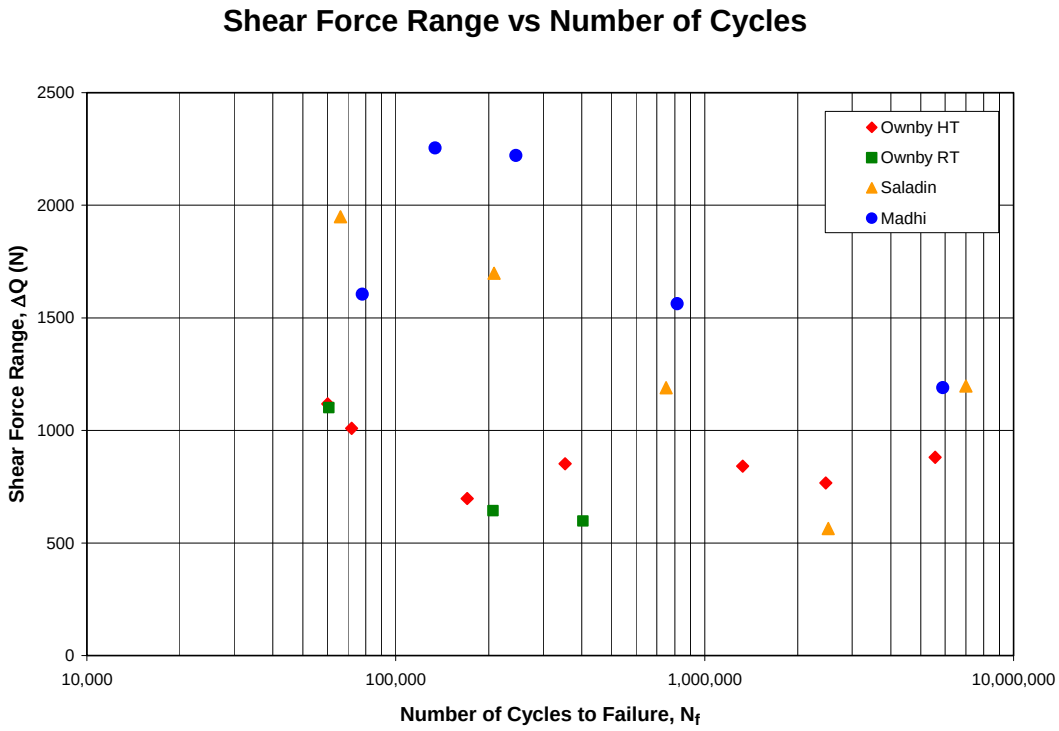

Figure 4.18 Plot comparing ΔQ vs N_f from Ownby, Saladin & Madhi data points

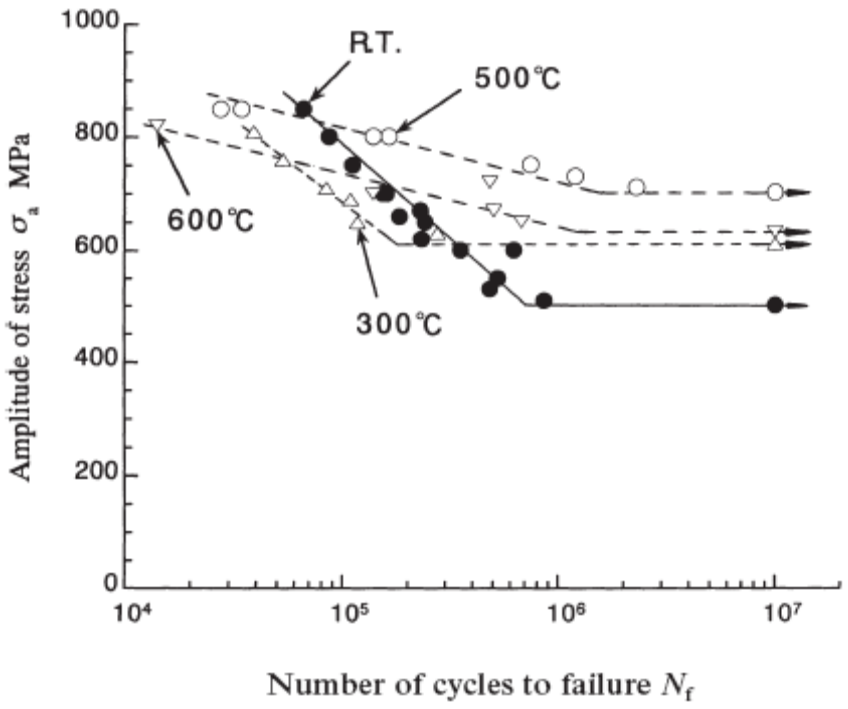

Figure 4.19 Plot from Kawagoishi et al. [21] of IN-718 at various temperatures, R= -1, ν= 55 Hz under rotary bending fatigue

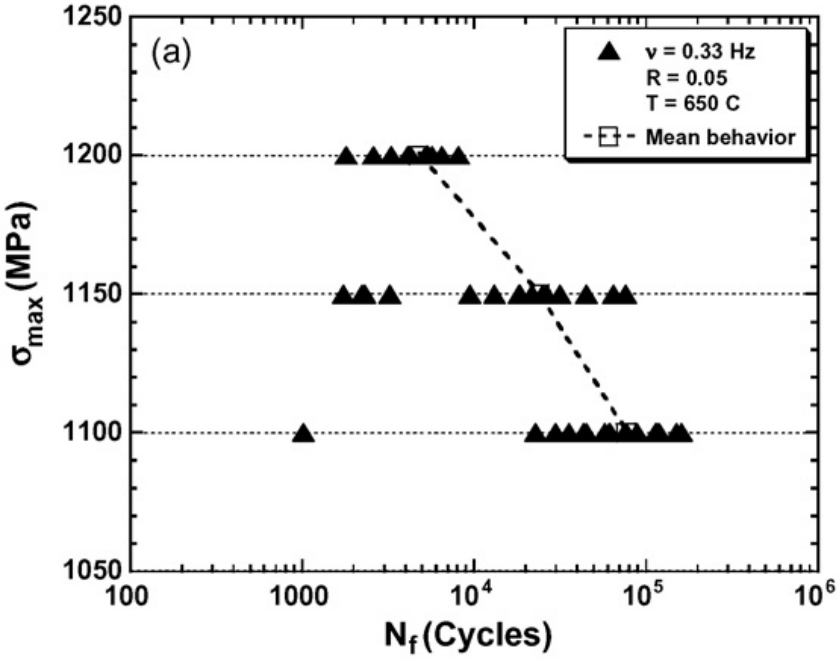

Figure 4.20 Plot from Jha et al [48] of P/M nickel-based alloy at 650 C, R=0.05 and ν = 0.33 Hz

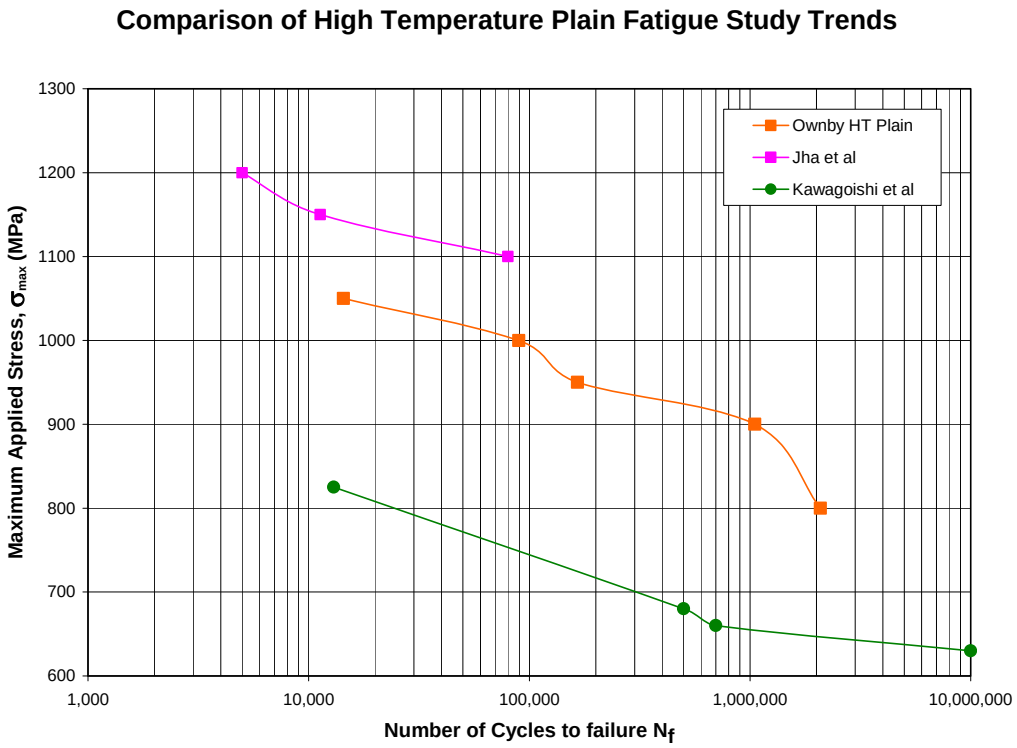

Notes: 1. Jha study was conducted at 650 C, R = 0.05 and ν = 0.33 Hz
2. Kawagoishi study was a rotary bending test at 600 C, R = -1, ν = 55 Hz

Figure 4.21 Plot of high temp plain fatigue data from this study with high temp data from Jha [48] and Kawagoishi [21] studies

Table 4.1 Testing conditions and cycles to failure from this study

Test #	Test Type	σ_{max} MPa	σ_{min} MPa	$\Delta\sigma$ MPa	σ_{eff} MPa	Q_{max} N	Q_{min} N	ΔQ N	Cycles to Failure
2	HT Fretting	650	122.5	527.5	641.15	1099.58	332.63	766.95	2,464,530
3	HT Fretting	800	24	776	789.11	698.14	1.06	697.08	170,160
4	HT Fretting	750	22.5	727.5	739.79	994.75	153.46	841.29	1,326,201
5	HT Fretting	850	25.5	824.5	838.43	1038.49	186.79	851.7	353,127
7	HT Fretting	950	28.5	921.5	937.07	876.64	-240.83	1117.47	60,232
8	HT Fretting	650	19.5	630.5	641.15	1021.88	141.39	880.49	5,565,917
9	HT Fretting	950	28.5	921.5	937.07	600.05	-409.44	1009.49	71,951
10	HT Plain	800	24	776	789.11				2,087,613
11	HT Plain	1050	31.5	1018.5	1035.71				14,370
12	HT Plain	950	28.5	921.5	937.07				165,509
13	HT Plain	900	27	873	887.75				1,052,188
14	HT Plain	1000	30	970	986.39				89,647
15	RT Fretting	650	19.5	630.5	641.15	472.49	-124.88	597.37	403,435
16	RT Fretting	950	28.5	921.5	937.07	614.18	-487.04	1101.22	60,765
17	RT Fretting	800	24	776	789.11			0	206,653

Note: HT indicates a high temperature test at 600 C and RT indicates a room temperature test at ~20 C

Table 4.2 Observed contacts width from each fretting fatigue test in this study

Fretting scar on specimen Total contact width = $2a_{exp}$		
Test #	Left side	Right side
	μm	μm
4	1040	1092
5	945	948
7	1229	993
9	1041	1244
15	1088	925
16	1023	978

Note: Analytical (expected) value 2a = 1220 μm

Table 4.3 Madhi fretting and plain fatigue testing data [11]

Test #	Test Type	σ_{max} MPa	σ_{min} MPa	$\Delta\sigma$ MPa	σ_{eff} MPa	Q_{max} N	Q_{min} N	ΔQ N	Cycles to Failure
1	Fretting	650	19.5	630.5	641.15	546.78	-643.44	1190.22	5,900,000
2	Fretting	750	22.5	727.5	739.79	788.98	-773.46	1562.44	815,449
3	Fretting	800	24	776	789.11	1139.75	-1081.7	2221.42	245,000
4	Fretting	850	25.5	824.5	838.43	1225.67	-1029	2254.63	134,103
5	Fretting	950	28.5	921.5	937.07	898.43	-706.73	1605.16	77,937
10	Plain	885	26.55	858.45	872.95				509,166
11	Plain	944	28.32	915.68	931.15				216,993
12	Plain	1062	31.86	1030.14	1047.54				95,671
13	Plain	1080	32.4	1047.6	1065.30				91,950

Table 4.4 Saladin fretting and plain fatigue testing data [10]

Test #	Test Type	σ_{max} MPa	σ_{min} MPa	$\Delta\sigma$ MPa	σ_{eff} MPa	Q_{max} N	Q_{min} N	ΔQ N	Cycles to Failure
1	Fretting	550	16.5	533.5	542.51	832	-365	1197	7,000,000
2	Fretting	600	18	582	591.83	471.5	-93	564.5	2,511,439
3	Fretting	650	19.5	630.5	641.15	478.2	-711.7	1189.9	750,028
4	Fretting	750	22.5	727.5	739.79	n/a	n/a	n/a	n/a
5	Fretting	800	24	776	789.11	598.3	-1100	1698.3	207,938
6	Fretting	950	28.5	921.5	937.07	844.7	-1104	1948.7	66,181
7	Plain	600	18	582	591.83				n/a
8	Plain	650	19.5	630.5	641.15				1,208,767
9	Plain	800	24	776	789.11				313,646
10	Plain	1050	31.5	1018.5	1035.71				53,210

Table 4.5 Comparison of cycles to failure at high temperature

High Temperature							
Fretting Fatigue			vs.	Plain Fatigue			
Test #	$\Delta\sigma$	N_f		Test #	$\Delta\sigma$	N_f	% Decrease
9	921.5	71,951		12	921.5	165,509	-56.5%
3	776	170,160		10	776	2,087,613	-91.8%
5	824.5	353,127		10	776	2,087,613	-83.1%

Table 4.6 Comparison of cycles to failure in plain fatigue

Plain Fatigue							
High Temperature			vs.	Room Temperature			
Test #	$\Delta\sigma$	N_f		Test #	$\Delta\sigma$	N_f	% Increase
Ownby 10	776	2,087,613		Saladin 9	776	313,646	565.6%
Ownby 13	873	1,052,188		Saladin 9	776	313,646	235.5%
Ownby 12	921.5	165,509		Madhi 11	915.68	216,993	-23.7%
Ownby 14	970	89,647		Saladin 10	1018.5	53,210	68.5%
Ownby 11	1018.5	14,370		Saladin 10	1018.5	53,210	-73.0%

Table 4.7 Comparison of cycles to failure in fretting fatigue

Fretting Fatigue							
High Temperature			vs.	Room Temperature			
Test #	$\Delta\sigma$	N_f		Test #	$\Delta\sigma$	N_f	% Increase
Ownby 8	630.5	5,565,917		Ownby 15	630.5	403,435	1279.6%
Ownby 8	630.5	5,565,917		Saladin 3	630.5	750,028	642.1%
Ownby 8	630.5	5,565,917		Madhi 1	630.5	5,900,000	-5.7%
Ownby 4	727.5	1,326,201		Madhi 2	727.5	815,449	62.6%
Ownby 5	824.5	353,127		Saladin 5	776	207,938	69.8%
Ownby 5	824.5	353,127		Madhi 3	776	245,000	44.1%
Ownby 5	824.5	353,127		Madhi 4	824.5	134,103	163.3%
Ownby 7	921.5	60,232		Saladin 6	921.5	66,181	-9.0%
Ownby 7	921.5	60,232		Madhi 5	921.5	77,937	-22.7%
Ownby 9	921.5	71,951		Saladin 6	921.5	66,181	8.7%
Ownby 9	921.5	71,951		Madhi 5	921.5	77,937	-7.7%

V. Conclusions and Recommendations

This chapter begins with a brief summary of the experiments conducted for this study and the analysis of their results. Next, the final conclusions of this study are presented and explained. Finally, potential topics for future study are suggested.

5.1 Summary

The main objective of this study was to determine what affect a high temperature environment of 600 C would have on the fretting fatigue behavior of IN-100. A total of 17 experiments were conducted for this study; nine high temperature fretting fatigue experiments, five high temperature plain fatigue experiments and three room temperature fretting fatigue experiments (Table 4.1). The test set up for these experiments was detailed in Chapter III. While the applied stress range was varied from 527.5 MPa to 921.5 MPa for fretting fatigue conditions and from 776 MPa to 1018.5 MPa for plain fatigue conditions, the stress ratio, applied contact load and fretting pad geometry were not varied from 0.03, 4003N and a cylindrical on flat condition with a radius of 50.8 mm, respectively. Of the 17 experiments attempted only 15 provided useful data. The data gathered from these experiments was then used to construct several S-N curves comparing the fretting fatigue life of IN-100 at 600 C to room temperatures (~20 C) over the range of applied stress conditions. In addition to analyzing the plain and fretting fatigue life of each experiment, the qualitative data from each experiment was also examined to validate the results from each test. The fretting condition was verified in all applicable cases by analysis of partial slip, contact width, crack initiation location and fracture surfaces.

5.2 Conclusions

This study supports the following conclusions. First, elevated temperature, up to 600 C, has a beneficial effect on plain and fretting fatigue life. The most likely reason for the increase in fatigue life is the oxidation of the high temperature environment and the promotion of crack closure that it provides.

Second, this effect is greatest at lower stress levels as was observed both in this study and in other studies of high temperature nickel-based alloy fatigue behavior. The crack closure mechanisms have a greater effect at these lower stress levels due to the slower crack growth rates associated with them thus enabling the closure mechanisms more time to take effect.

Third, it is a strong possibility that the fatigue limit of IN-100 increases with temperature as well. The data from this study suggests this relationship but more testing should be done to confirm this postulate.

5.3 Recommendations for Future Work

This study focused on the effect of just one major experimental factor, elevated temperature of 600 C, to determine its impact on the fretting fatigue life of IN-100. While this study has provided valuable data on this topic, it does not preclude further research into the effects of other temperatures, perhaps both higher and lower than 600 C, on the fretting fatigue behavior of IN-100. In addition it has been observed that the combination of elevated temperature with other factors, such as shot-peening and the frequency of applied bulk stress, can yield noticeably different results than when these factors are evaluated only at room temperature. With this in mind the author would like to suggest the following potential areas of study:

1. First, continued experimentation in the high temperature environment is needed. Testing at other temperatures between room temperature environment and 600 C would be useful. This study has hypothesized that the fatigue limit of IN-100 increases with temperature but to confirm this hypothesis several more tests at other temperatures are required. Further elevated temperature testing could establish the nature of the relationship between temperature and its affect on fretting fatigue life. Additionally testing at higher temperature more closely approaching the melting temperature of IN-100 would be useful in establishing the upper bounds of temperatures effect on fretting fatigue life. Once more data has been collected at multiple temperature levels it could be analyzed to see if temperatures effect could be characterized with a new set of parameters or perhaps to see how to modify existing parameters such as the MSSR to take temperature into account.

2. Second, aspects such as the combined effect of both elevated temperature and numerous other factors could be examined. For instance, it would be interesting to explore the combination of elevated temperature and the frequency of applied loads as has been done in a few other nickel based alloys to date. Another possible direction of study could be the combination of temperature and surface treatments such as shot-peening and other chemical treatments. Elevated temperature and differing pad geometries could be evaluated.

3. Third, while the elevated temperature aspect of the gas turbine engine was simulated in this study it still does not model the other aspects of the turbine engine environment. Perhaps further modifications could be made to simulate the atmospheric components of the turbine engine as well as the elevated temperature. Simply put, the

high temperature fretting fatigue of IN-100 in environments other than air to eliminate potential sources of oxidation of the crack surfaces and evaluate its impact on fatigue life.

Appendix A. Temperature Calibration

For the high temperature tests in this study it was necessary to calibrate the commanded temperature to accurately reach and maintain the desired temperature for each testing scenario. The commanded temperature was increased incrementally and then held constant until the observed temperatures were able to stabilize at each increment. The temperature calibration was performed twice, once on 6 Dec 07 and again on 30 Jan 08. The 6 Dec 07 data, represented in Figures A.1 and A.2, was the initial calibration of the high temperature controller. The 30 Jan 08 calibration, Figures A.3 and A.4, was required after all four heating elements were replaced.

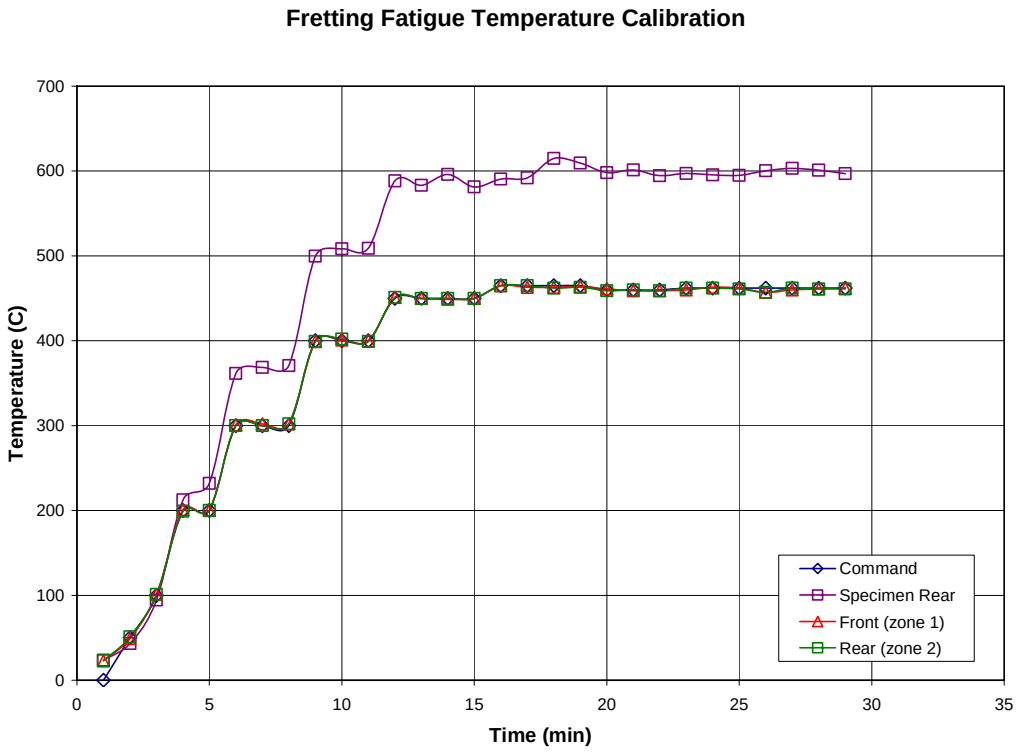

Figure A.1 Fretting fatigue condition calibration data from 6 Dec 07

Note the close correlation of the commanded temperature and the front and rear thermocouple observed temperatures thus indicating good control feedback.

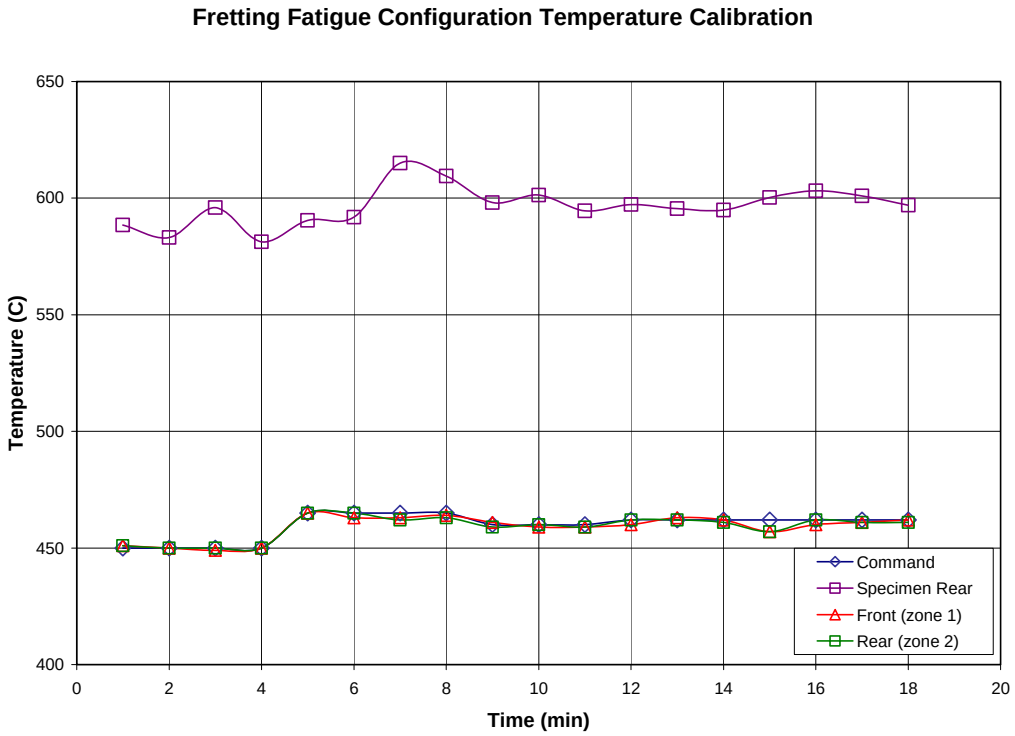

Figure A.2 Fretting fatigue condition calibration data from 6 Dec 07

In this figure the scale has been focused on the high temperature region. The specimen's observed temperature clearly stabilizes at the desired 600 C and maintains this temperature over time with a high degree of fidelity.

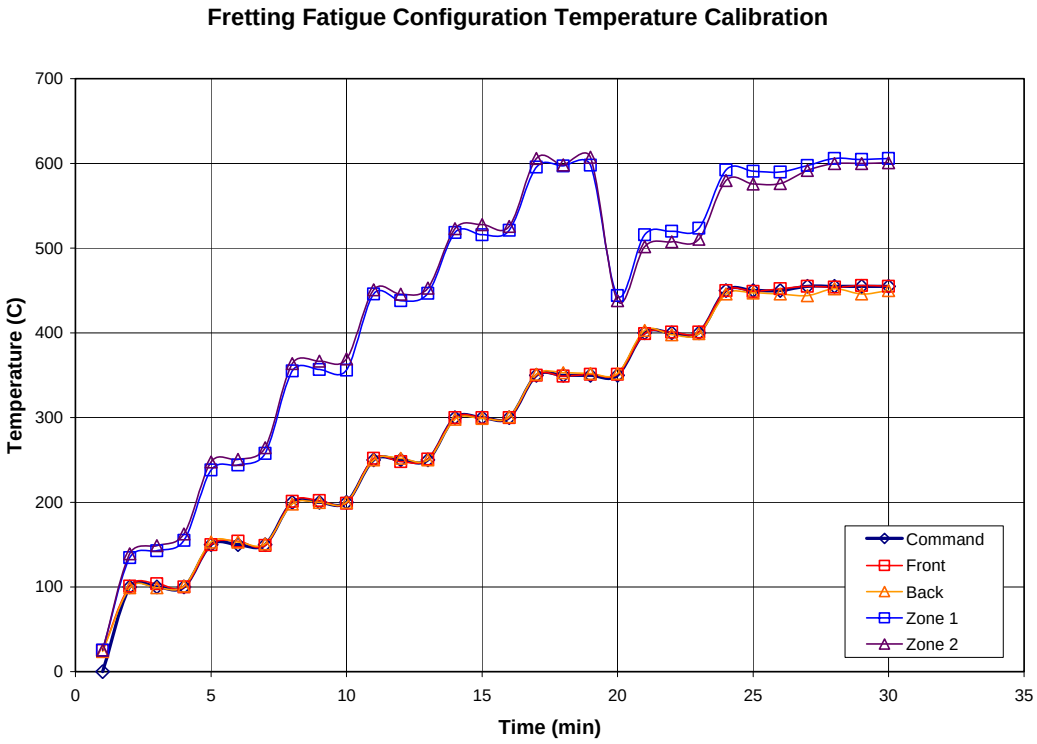

Figure A.3 Fretting fatigue condition calibration data from 30 Jan 08

Note the sudden change in observed temperature of the specimen, Zone 1 and Zone 2, in the 20th minute. This was due to the application of the fretting pads to the test specimen. This indicates the magnitude of the heat sink from the fretting pads.

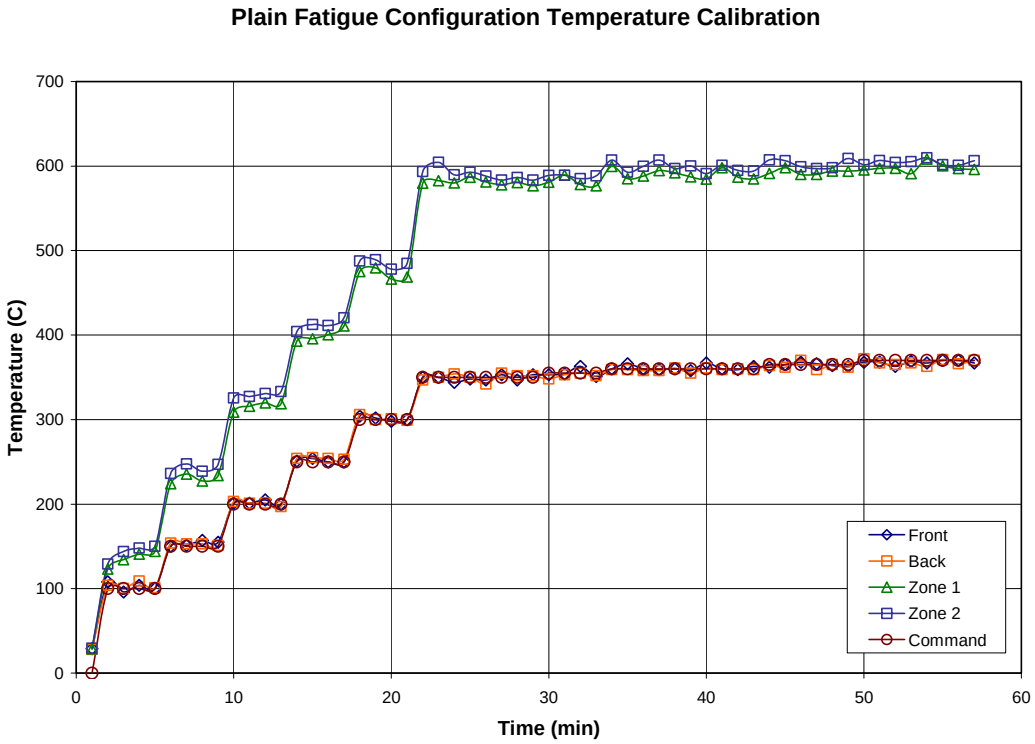

Figure A.4 Plain fatigue condition calibration data from 30 Jan 08

Notice that the commanded temperature for the plain fatigue configuration is much lower than in the fretting fatigue configuration. This difference is attributable to the heat sink from the fretting pads which are not applied in the plain fatigue configuration.

References

[1] D. A. Hills, D. Nowell and J. J. O'Connor, "On the mechanics of fretting fatigue," *Wear,* vol. 125, pp. 129-146, 7. 1988.

[2] D. Koshal, *Manufacturing Engineer's Reference Book.* Oxford, England: Butterworth-Heinemann Ltd, 1993,

[3] M. J. Donachie and S. J. Donachie, *Handbook of Materials and Selection.* New York, New York: John Wiley & Sons, Inc., 2002,

[4] S. Adibnazari and D. W. Hoeppner, "Study of fretting fatigue crack nucleation in 7075-T6 aluminum alloy," *Wear,* vol. 159, pp. 257-264, 12/1. 1992.

[5] C. D. Lykins, "An investigation of Fretting Fatigue Crack Initiation Behavior of the Titanium alloy Ti-6Al-4V," 2004.

[6] A. R. Kallmeyer, A. Krgo and P. Kurath, "Evaluation of multiaxial fatigue life prediction methodologies for Ti-6Al-4V," *J Eng Mater Technol Trans ASME,* vol. 124, pp. 229-237, 2002.

[7] S. A. NAMJOSHI, S. MALL, V. K. JAIN and O. JIN, "Fretting fatigue crack initiation mechanism in Ti–6Al–4V," *Fatigue & Fracture of Engineering Materials & Structures,* vol. 25, pp. 955-964, 10. 2002.

[8] H. I. Yuksel, "Effects of Shot-Peening on High Cycle Fretting Fatigue Behavior of Ti-6Al-4V," March 2002. 2002.

[9] S. Mall, S. A. Namjoshi and W. J. Porter, "Effects of microstructure on fretting fatigue crack initiation behavior of Ti-6Al-4V," *Materials Science and Engineering A,* vol. 383, pp. 334-340, 10/15. 2004.

[10] E. Saladin, "The Effect of Microstructure on Fretting Fatigue Behavior of Nickel Alloy IN-100," March 2007. 2007.

[11] E. Madhi, "Fretting Fatigue Behavior of Nickel Alloy IN-100," March 2006. 2006.

[12] R. S. Magaziner, "Examination of Contact Width on Fretting Fatigue," March 2002. 2002.

[13] D. Nowell and D. A. Hills, "Crack initiation criteria in fretting fatigue," *Wear,* vol. 136, pp. 329-343, 3. 1990.

[14] P. T. Rajeev, H. Murthy and T. N. Farris, "Load History Effects on Fretting Contacts of Isotropic Materials," *J. Eng. Gas Turbines Power,* vol. 126, pp. 385-390, April 2004. 2004.

[15] A. Sackfield, A. Mugadu and D. A. Hills, "The influence of an edge radius on the local stress field at the edge of a complete fretting contact," *International Journal of Solids and Structures,* vol. 39, pp. 4407-4420, 8. 2002.

[16] H. Murthy, D. B. Garcia, J. F. Matlik and T. N. Farris, "Fretting fatigue of single crystal/polycrystalline nickel subjected to blade/disk contact loading," *Acta Astronautica,* vol. 57, pp. 1-9, 7. 2005.

[17] A. Shyam and W. W. Milligan, "Effects of deformation behavior on fatigue fracture surface morphology in a nickel-base superalloy," *Acta Materialia,* vol. 52, pp. 1503-1513, 4/5. 2004.

[18] A. Shyam and W. W. Milligan, "A model for slip irreversibility, and its effect on the fatigue crack propagation threshold in a nickel-base superalloy," *Acta Materialia,* vol. 53, pp. 835-844, 2. 2005.

[19] J. S. Wan and Z. F. Yue, "A low-cycle fatigue life model of nickel-based single crystal superalloys under multiaxial stress state," *Materials Science and Engineering A,* vol. 392, pp. 145-149, 2/15. 2005.

[20] H. Murthy, G. Gao and T. N. Farris, "Fretting fatigue of single crystal nickel at 600 °C," *Tribology International,* vol. 39, pp. 1227-1240, 10. 2006.

[21] N. Kawagoishi, Q. Chen and H. Nisitani, "Fatigue strength of Inconel 718 at elevated temperatures," *Fatigue & Fracture of Engineering Materials & Structures,* vol. 23, pp. 209-16, 03. 2000.

[22] J. F. Matlik and T. N. Farris, "Fretting of single crystal/polycrystalline nickel contacts at elevated frequency and temperature," in *; 6th AIAA Non-Deterministic Approaches Forum; 5th AIAA Gossamer Spacecraft Forum,* 2004, pp. 451-460.

[23] S. Albinali, "Effects of Temperature and Shot-Peening Intensity on Fretting Fatigue Behavior of Titanium Alloy Ti-6Al-4V," March 2005. 2005.

[24] J. Kohout, "Temperature dependence of stress-lifetime fatigue curves," *Fatigue & Fracture of Engineering Materials & Structures,* vol. 23, pp. 969-77, 12. 2000.

[25] D. A. Hills and D. Nowell, *Mechanics of Fretting Fatigue.* ,1st ed.Dordrecht, The Netherlands: Kluwer Academic Publishers, 1994,

[26] L. J. Fellows, D. Nowell and D. A. Hills, "Contact stresses in a moderately thin strip (with particular reference to fretting experiments)," *Wear,* vol. 185, pp. 235-238, 6. 1995.

[27] K. Chan and Y. Lee, ""Ruiz Program"," 1998.

[28] G. Venkataraman, Y. Chung, Y. Nakasone and T. Mura, "Free energy formulation of fatigue crack initiation along persistent slip bands: calculation of S-N curves and crack depths," *Acta Metallurgica Et Materialia,* vol. 38, pp. 31-40, 1. 1990.

[29] M. P. Szolwinski and T. N. Farris, "Mechanics of fretting fatigue crack formation," *Wear,* vol. 198, pp. 93-107, 10. 1996.

[30] L. J. Fellows, D. Nowell and D. A. Hills, "On the initiation of fretting fatigue cracks," *Wear,* vol. 205, pp. 120-129, 4. 1997.

[31] T. Hattori and M. Nakamura, "Initiation and propagation behavior of fretting fatigue cracks," in *Proceedings of the 1997 3rd International Conference on Contact Mechanics,* 1997, pp. 183-192.

[32] K. Iyer and S. Mall, "Effects of cyclic frequency and contact pressure on fretting fatigue under two-level block loading," *Fatigue & Fracture of Engineering Materials & Structures,* vol. 23, pp. 335-346, 04. 2000.

[33] K. Walker, "The effect of stress relaxation during crack propagation ad fatigue for 2024-Y3 and7075-T6 aluminum," in *Subcommittee E-9 Winter Meeting,* 1969,

[34] C. D. Lykins, S. Mall and V. Jain, "A shear stress-based parameter for fretting fatigue crack initiation," *Fatigue & Fracture of Engineering Materials & Structures,* vol. 24, pp. 461-473, 07. 2001.

[35] V. Sabelkin, S. A. Martinez, S. Mall, S. Sathish and M. P. Blodgett, "Effects of shot-peening intensity on fretting fatigue crack-initiation behaviour of Ti–6Al–4V," *Fatigue & Fracture of Engineering Materials & Structures,* vol. 28, pp. 321-332, 03. 2005.

[36] M. M. Hamdy and R. B. Waterhouse, "The fretting fatigue behaviour of Ti-6A1-4V at temperatures up to 600 °C," *Wear,* vol. 56, pp. 1-8, 9. 1979.

[37] O. Jin, S. Mall and O. Sahan, "Fretting fatigue behavior of Ti–6Al–4V at elevated temperature," *International Journal of Fatigue,* vol. 27, pp. 395-401, 4. 2005.

[38] M. C. Gean and T. N. Farris, "Fretting fatigue testing of Ti-17 at elevated temperatures," in *47th AIAA/ASME/ASCE/AHS/ASC Structures, Structural Dynamics, and Materials Conference,* 2006,

[39] S. K. Sondhi, B. F. Dyson and M. McLean, "Tension–compression creep asymmetry in a turbine disc superalloy: roles of internal stress and thermal ageing," *Acta Materialia,* vol. 52, pp. 1761-1772, 4/19. 2004.

[40] V. Brien and B. Décamps, "Low cycle fatigue of a nickel based superalloy at high temperature: deformation microstructures," *Materials Science and Engineering A,* vol. 316, pp. 18-31, 11/15. 2001.

[41] V. Brien, L. P. Kubin and B. Decamps, "Low-cycle fatigue of a nickel-based superalloy at high temperature: Simplified micromechanical modelling," *Philosophical Magazine A,* vol. 81, pp. 2285, 2001.

[42] A. Piard, D. Gamby, C. Carbou and J. Mendez, "A numerical simulation of creep–fatigue crack growth in nickel-base superalloys," *Engineering Fracture Mechanics,* vol. 71, pp. 2299-2317, 11. 2004.

[43] A. Shyam, C. J. Torbet, S. K. Jha, J. M. Larsen, M. J. Caton, C. J. Szczepanski, T. M. Pollock and J. W. Jones, "Development of Ultrasonic Fatigue for Rapid, High Temperature Fatigue studies in Turbine Engine Materials," *Superalloys,* pp. 259-268, 2004.

[44] P. J. Golden, "Development of a Dovetail Fretting Fatigue Fixture for Turbine Engine Materials," 2007.

[45] M. M. Hamdy and R. B. Waterhouse, "The fretting-fatigue behavior of a nickel based alloy (Inconel 718) at elevated temperatures," *Wear,* pp. 351-355, 1979.

[46] H. Murthy and T. N. Farris, "Elevated temperature fretting of turbine materials subjected to engine type-loading," in *44th AIAA/ASME/ASCE/AHS/ASC Structures, Structural Dynamics, and Materials Conference,* 2003, pp. 1148-1158.

[47] H. Murthy, T. N. Farris and M. Okane, "Investigation of fretting characteristics of turbine materials at higher temperatures," in *43rd Structures, Structural Dynamics and Materials Conference,* 2002, pp. 2577-2585.

[48] S. K. Jha, M. J. Caton, and J. M. Larsen, "A new paradigm of fatigue variability behavior and implications for life prediction," in *Materials Science and Engineering A,* vol. 468, pp. 23-32, 2007.

REPORT DOCUMENTATION PAGE

Form Approved
OMB No. 074-0188

1. REPORT DATE *(DD-MM-YYYY)*	**2. REPORT TYPE**	**3. DATES COVERED** *(From – To)*
23-04-2008	Master's Thesis	14 Aug 2006 – 24 Apr 2008

4. TITLE AND SUBTITLE

The Effect of Elevated Temperature on the Fretting Fatigue Behavior of Nickel Alloy IN-100

5a. CONTRACT NUMBER

5b. GRANT NUMBER

5c. PROGRAM ELEMENT NUMBER

6. AUTHOR(S)

Ownby, John, F., Captain, USAF

5d. PROJECT NUMBER

5e. TASK NUMBER

5f. WORK UNIT NUMBER

7. PERFORMING ORGANIZATION NAMES(S) AND ADDRESS(S)

Air Force Institute of Technology
Graduate School of Engineering and Management (AFIT/EN)
2950 Hobson Way
WPAFB OH 45433-7765

8. PERFORMING ORGANIZATION REPORT NUMBER

AFIT/GA/ENY/08-M04

9. SPONSORING/MONITORING AGENCY NAME(S) AND ADDRESS(ES)

N/A

10. SPONSOR/MONITOR'S ACRONYM(S)

11. SPONSOR/MONITOR'S REPORT NUMBER(S)

12. DISTRIBUTION/AVAILABILITY STATEMENT

APPROVED FOR PUBLIC RELEASE; DISTRIBUTION UNLIMITED.

13. SUPPLEMENTARY NOTES

14. ABSTRACT

This thesis studied the effect of elevated temperature (600 C) on the fretting fatigue behavior of IN-100. First, fretting and plain fatigue S-N curves were determined over a large range of applied stress at an identical stress ratio of 0.03 at 600 C and for fretting tests, with a constant contact load. The partial slip condition was verified by using hysteresis between shear force and axial stress techniques. The contact width and the crack initiation location were observed for all of the fretting specimens. The contact widths were consistent with expected values and the crack initiation location was at the trailing edge of contact for all fretting specimens. This study compared its high temperature results to room temperature testing accomplished by this study as well as room temperature data from a previous study using IN-100 with an identical microstructure and another room temperature study of IN-100 with a coarser microstructure. It was found that fretting fatigue reduces the cycles to failure compared to plain fatigue at elevated temperature but a more pronounced reduction was noticed than with room temperature. It was also found that the elevated temperature environment increased the both the plain and fretting fatigue life as compared to similar stress levels at room temperature. The study found that elevated temperature does have an effect on crack initiation and crack propagation as compared to room temperature environment. The higher temperature allowed a longer initiation and crack propagation time which strongly suggests the fatigue life increases with temperature up to 600 C. The creation of oxide films and temperature induced softening or plasticity were both found to act as crack closure mechanisms in another nickel based superalloy, IN-718, when fatigued in the high temperature environment. It is therefore likely that these oxidation and plasticity crack closure mechanisms are the reasons for the improved performance at elevated temperatures. These findings were different than in titanium alloys, where elevated temperatures allowed a shorter crack initiation time by greater stress relaxation thus hastening crack development.

15. SUBJECT TERMS

Fretting Fatigue, Nickel-based Superalloys, IN-100, Elevated Temperature

16. SECURITY CLASSIFICATION OF:			**17. LIMITATION OF ABSTRACT**	**18. NUMBER OF PAGES**	**19a. NAME OF RESPONSIBLE PERSON**
REPORT	**ABSTRACT**	**c. THIS PAGE**			Dr. Shankar Mall
U	**U**	**U**	**UU**	122	**19b. TELEPHONE NUMBER** *(Include area code)* (937) 255-3636, ext 4587; e-mail: shankar.mall@afit.edu

Standard Form 298 (Rev: 8-98)
Prescribed by ANSI Std. Z39-18